Available online at www.sciencedirect.com
SCIENCE DIRECT®
Earth-Science Reviews 64 (2004) 189–241
EARTH-SCIENCE REVIEWS
www.elsevier.com/locate/earscirev

Optical properties of terrestrial clouds

A. Kokhanovsky*

Institute of Environmental Physics, University of Bremen, Otto Hahn Allee 1, D-28334 Bremen, Germany
Institute of Physics, 70 Skarina Avenue, Minsk 220072, Belarus

Received 18 January 2002; accepted 16 April 2003

Abstract

The aim of this review is to consider optical characteristics of terrestrial clouds. Both single and multiple light-scattering properties of water clouds are studied. The numerous results discussed can be used for solutions to both inverse and direct problems of cloud optics. An introduction to main microphysical characteristics of water and ice clouds, including the effective size, the liquid water content and path, the concentration of particles, is given. The refractive index of water and ice, which is of importance for optical waves propagation in clouds, is also considered. We consider extinction and absorption coefficients, phase functions, and asymmetry parameters of water and ice clouds and their relationships with the size, shape, and concentration of water droplets and ice crystals. Simple analytical results for absorption, reflection, and transmission characteristics of cloudy media are given. They are valid for optically thick clouds with optical thickness larger than 5. We have reviewed studies of polarization of solar light reflected from clouds. Image transfer problems have been considered as well. Modern methods of passive remote sensing of water and ice clouds are discussed. The review is finished by the discussion of optical properties of inhomogeneous clouds, which is a main topic of modern cloud optics research.

Keywords: Radiative transfer; Light scattering and propagation; Water and ice clouds

1. Introduction

Water, ice, and mixed clouds are major regulators of solar fluxes in the terrestrial atmosphere (Kondratyev and Binenko, 1984; Liou, 1992, 2002). They reflect a large portion of incoming visible radiation back to outer space. The light energy absorbed by water droplets and ice crystals leads to heating of atmospheric layers. Another important role of cloudy media is to serve as a blanket to protect the Earth's surface against cooling at night. This is due to the fact that the maximum of the terrestrial emission is in the far infrared, where water droplets are highly absorbing.

Clouds, mists, and fogs are very common. They reduce the visibility of objects in the atmosphere and limit capabilities of atmospheric vision, remote sensing, and detection systems (Zege et al., 1991). Thus, it is of a great importance to understand the peculiarities of light interaction with cloudy media, which can be considered as a huge "colloid", composed of liquid and solid water particles, dispersed in the air. It should be pointed out that water droplets and air around them can be contaminated by various fine particles (e.g., soot and dust particles). These aerosol particles influ-

* Institute of Environmental Physics, University of Bremen, P.O. Box 330440. Otto Hahn Allee 1, D-28334 Bremen, Germany. Tel.: +49-421-218-4475; fax: +49-421-218-4555.
E-mail address: alexk@florian.physik.uni-bremen.de (A. Kokhanovsky).

0012-8252/$ - see front matter © 2003 Elsevier B.V. All rights reserved.
doi:10.1016/S0012-8252(03)00042-4

ence both light-scattering and absorption properties of cloudy media, making the studies of light propagation in cloudy media even more difficult (Menon et al., 2002). The very existence of clouds is due to fine-aerosol particles, the so-called cloud nuclei (Twomey, 1977), with typical radii between 5 and 200 nm (Mason, 1975).

Studies of optical and microphysical properties of cloudy media have a long and fruitful history. The results of these investigations have been summarized in numerous books and papers (Kondratyev and Binenko, 1984; Zege et al., 1991; Liou, 1992, 2002; Kokhanovsky, 2001a). The main properties of cloudy media are well understood now, but unsolved problems remain. The most important of these include the accounting for the three-dimensional shape of clouds (Evans, 1998; Macke et al., 1999; Schreier, 2001; Schreier and Macke, 2001), and their inhomogenity in horizontal and vertical directions (Cahalan et al., 1994, 2001; Platnick, 2000, 2001). The influence of aerosols inside cloudy media, which can be one of explanations of the anomalous absorption paradox (Danielson et al., 1969; Rozenberg et al., 1978; Stephens and Tsay, 1990), also should be clarified.

Another current issue is the characterization of optical properties of ice clouds, which have extremely complex microstructure (Liou, 1992, 2002; Liou and Takano, 1994; Macke et al., 1996; Yang and Liou, 1998; Kokhanovsky and Macke, 1999; Yang et al., 2000, 2001) and appear almost with the same frequency as water clouds. One rarely finds two identical crystals in ice clouds because preferential shapes vary with temperature and pressure (Mason, 1975), which vary across cloudy media (Yang et al., 2001). It should be stressed that optical properties of a single particle and, as a result, optical properties of a cloud as a whole are highly influenced by particles' shapes (Mishchenko et al., 1995, 1996, 1999, 2000).

A complete review across all fields of cloud optics, which is in a state of a rapid transition, would be difficult within a single book, not to mention in a single article. Thus, I will concentrate mostly on analytical results, which can be used for cloud optical properties studies. The formulae presented can be applied for rapid estimations of light fluxes in cloudy atmosphere and will assist understanding the information content of transmitted and reflection functions of cloudy media in respect to microphysical characteristics of clouds.

2. Microphysical characteristics

2.1. Water clouds

2.1.1. Particle-size distributions

Water clouds consist of small liquid droplets that generally have the spherical shape although particles of other shapes can exist due to different external influences. For instance, the deformation of large particles due to the gravitation force is of importance for raining clouds with particles having radii 1 mm and larger (Macke and Grossklaus, 1998). The average radius of droplets in nonraining water clouds is usually around 10 μm and the approximation of spherical particles works quite well. Natural clouds with droplets of uniform size throughout never occur due to the variability of physical properties of air both in space and time domains (Twomey, 1977). Thus, one can consider a radius of a droplet, a, as a random value, which is characterized by the distribution function $f(a)$. This function is normalized by the following condition:

$$\int_0^\infty f(a)\mathrm{d}a = 1. \tag{2.1}$$

The integral

$$F(a) = \int_{a_1}^{a_2} f(a)\mathrm{d}a \tag{2.2}$$

gives the fraction of particles with radii between a_1 and a_2 in a unit volume of a cloud. The distribution function $f(a)$ can be represented as a histogram, graphically or in a tabular form (Ayvazian, 1991). However, it is the most common to use an analytical form of this function, involving only two or three parameters (Deirmendjian, 1969). Of course, this is a great simplification of real situations occurring in natural clouds, but most optical characteristics of a cloud as a whole practically do not depend on the fine structures of particle-size distributions (PSD) $f(a)$ (Hansen and Travis, 1974). McGraw et al. (1998) found that the local optical properties of polydispersions can be modelled with high accuracy by just the first six moments of the particle-size distribution, and the use of certain combinations of moments can reduce the number of parameters even further.

In most cases, the function $f(a)$ can be represented by the gamma distribution (Deirmendjian, 1969):

$$f(a) = \mathbb{N} a^{\mu} \mathrm{e}^{-\mu \frac{a}{a_0}}, \tag{2.3}$$

where

$$\mathbb{N} = \frac{\mu^{\mu+1}}{\Gamma(\mu+1) a_0^{\mu+1}} \tag{2.4}$$

is the normalization constant and $\Gamma(\mu+1)$ is the Gamma function. It follows that the first derivative $f'(a_0)=0$ and the second derivative $f''(a_0)<0$ (see Eq. (2.3)). Thus, the function (Eq. (2.3)) has the maximum at $a=a_0$. Note that Eq. (2.4) follows from Eq. (2.1) and the definition of the Gamma function:

$$\Gamma(\mu) = \int_0^{\infty} x^{\mu-1} \mathrm{e}^{-x} \mathrm{d}x. \tag{2.5}$$

One can see that the parameter μ characterizes the width of the particle-size distribution $f(a)$, being smaller for wider distributions. Moments

$$\langle a^n \rangle = \int_0^{\infty} a^n f(a) \mathrm{d}a \tag{2.6}$$

of the distribution (Eq. (2.3)) are calculated from the following simple analytical equation

$$\langle a^n \rangle = \left(\frac{a_0}{\mu} \right)^n \frac{\Gamma(\mu+n+1)}{\Gamma(\mu+1)}. \tag{2.7}$$

Eq. (2.7) can be used to find the average volume of particles

$$\langle V \rangle = \frac{4\pi}{3} \int_0^{\infty} a^3 f(a) \mathrm{d}a, \tag{2.8}$$

the average surface area

$$\langle \Sigma \rangle = 4\pi \int_0^{\infty} a^2 f(a) \mathrm{d}a, \tag{2.9}$$

and the average mass of droplets

$$\langle W \rangle = \rho \langle V \rangle, \tag{2.10}$$

where $\rho = 1$ g/cm^3 is the density of water. It follows that

$$\langle V \rangle = \frac{\Gamma(\mu+4)}{\mu^3 \Gamma(\mu+1)} v_0, \tag{2.11}$$

$$\langle \Sigma \rangle = \frac{\Gamma(\mu+3)}{\mu^2 \Gamma(\mu+1)} s_0, \tag{2.12}$$

$$\langle W \rangle = \frac{\Gamma(\mu+4)}{\mu^3 \Gamma(\mu+1)} w_0, \tag{2.13}$$

where

$$v_0 = \frac{4\pi a_0^3}{3}, \quad s_0 = 4\pi a_0^2, \quad w_0 = \rho v_0 \tag{2.14}$$

are corresponding parameters for monodispersed particles with radii a_0. One can obtain in the case of the most often employed cloud model with $a_0 = 4$ μm and $\mu = 6$ (Cloud C.1 model of Deirmendjian, 1969):

$$\langle V \rangle = \frac{7}{3} v_0, \quad \langle \Sigma \rangle = \frac{14}{9} s_0, \quad \langle W \rangle = \frac{7}{3} w_0, \tag{2.15}$$

where $v_0 \approx 2.7 \times 10^{-16}$ m^3, $s_0 \approx 2 \times 10^{-12}$ m^2, $w_0 \approx 2.7 \times 10^{-10}$ g. Although parameters (Eq. (2.14)) are small, the very large numbers of cloud droplets (typically, 100 particles in cm^3) create important factors for atmospheric processes (see next section).

Eq. (2.3) allows to characterize the cloud droplet distribution only by two parameters: a_0 and μ. However, it should be remembered that neither is constant and can vary inside the body of a cloud. Thus, their values depend on the averaging scale, with large averaging scales producing more broad particle-size distributions with smaller values of μ. The value of $\mu = 2$ was found to be rather representative (Khrgian and Mazin, 1952) and is advised to be used in low-resolution cloud satellite retrieval algorithms. The parameter $\mu = 6$ (Deirmendjian, 1969), used in the derivation of Eq. (2.15), is typical only for small averaging scales (Fomin and Mazin, 1998). General features of the droplet spectra in water clouds were studied in a great detail by, e.g., Warner (1973).

Parameters a_0 and μ are defined in terms of the specific unimodal cloud droplet distribution (Eq. (2.3)). It is of an advantage to characterize cloud particle-size distributions by their moments. Moments can be retrieved from optical measurements without reference to specific distribution laws (McGraw et al., 1998).

Hansen and Travis (1974) found that the effective radius

$$a_{\mathrm{ef}} = \frac{\langle a^3 \rangle}{\langle a^2 \rangle} \tag{2.16}$$

is one of the most important parameters of any particle-size distribution. It is proportional to the average volume/surface ratio of droplets. The parameter (Eq. (2.16)) can be also defined for nonspherical particles as we will see later. The coefficient of variance (CV) of the particle-size distribution

$$\Delta = \frac{s}{\langle a \rangle} \tag{2.17}$$

where

$$s = \sqrt{\int_0^\infty (a - \langle a \rangle)^2 f(a) \mathrm{d}a}, \tag{2.18}$$

is also of importance, especially for narrow droplet distributions. The value of s is called the standard deviation. The CV, which is equal to the ratio of the standard deviation to the mean radius $\langle a \rangle$, is often expressed in percent.

It follows for the PSD (Eq. (2.3)):

$$a_{\mathrm{ef}} = a_0 \left(1 + \frac{3}{\mu}\right), \qquad \Delta = \frac{1}{\sqrt{1+\mu}} \tag{2.19}$$

and, therefore,

$$\mu = \frac{1}{\Delta^2} - 1, \quad a_0 = \frac{1-\Delta^2}{1+2\Delta^2} a_{\mathrm{ef}}. \tag{2.20}$$

For instance, we obtain at $\mu = 3$: $a_{\mathrm{ef}} = 2a_0$, $\Delta = 0.5$, $s = \langle a \rangle / 2$. The effective radius, a_{ef}, is always larger than the mode radius, a_0.

Eq. (2.20) gives the meaning of the parameter μ in the PSD (Eq. (2.3)). In situ measurements show that the value of a_0 often varies from 4 to 20 μm (Mason, 1975) and $\mu \in [2,8]$ in most of cases. It should be pointed out that clouds with smaller droplets are not stable due to the coagulation and condensation processes (Twomey, 1977). Particles with a large radius cannot reside in atmosphere for a long time due to the gravitation force. Thus, several physical processes lead to the existence of the most frequent mode radius range. One can obtain from Eq. (2.19) and inequality $2 \le \mu \le 8$ that the value of $\Delta \in [0.3, 0.6]$. Thus, it follows that the standard deviation of the radius of particles in water droplets is from 30% to 60% of an average radius in most cases. Smaller and larger values of Δ do occur, but values of Δ smaller than 0.1 were never observed (Twomey, 1977). Larger values of Δ may indicate the presence of the second mode in the range of large particles (Ayvazian, 1991).

Eq. (2.19) and the results for a_0 and μ just reported lead to the effective radius, a_{ef}, of water droplets being in the range from 5 to 50 μm, depending on the cloud type. Near-global survey of the value of a_{ef} using satellite data shows that typically $5\,\mu\mathrm{m} \le a_{\mathrm{ef}} \le 15\ \mu\mathrm{m}$ (Han et al., 1994). We see that water clouds with $a_{\mathrm{ef}} > 15$ μm are rare. This can be used to discriminate satellite pixels with ice crystals even at wavelengths where ice and water absorption coefficients are almost equal. Such a possibility of discrimination is due to much larger (e.g., in 5–10 times) effective sizes of ice crystals as compared to droplets. The large size of ice crystals will reduce the reflection function in near infrared considerably as compared to droplets. This reduction can be easily detected. Note that clouds with $a_{\mathrm{ef}} > 15$ μm are often raining (Masunaga et al., 2002). Pinsky and Khain (2002) showed that the threshold of the occurrence of drizzle is around $a_{\mathrm{ef}} = 15$ μm. Then strong collisions of droplets start.

Some authors prefer to use the representation of the particle-size distribution by the following analytical form (Ayvazian, 1991):

$$f(a) = \frac{1}{\sqrt{2\pi}\sigma a} \exp\left(-\frac{\ln^2 \frac{a}{a_m}}{2\sigma^2}\right), \tag{2.21}$$

which is called the lognormal distribution. The relations between the values of a_{ef}, $\langle a \rangle$, Δ and the parameters of the gamma and the lognormal particle-size distributions are presented in Table 1. The value of Δ_{ef} in this table represents the effective variance defined as

$$\Delta_{\mathrm{ef}} = \frac{\int_0^\infty (a - a_{\mathrm{ef}})^2 a^2 f(a) \mathrm{d}a}{a_{\mathrm{ef}}^2 \int_0^\infty a^2 f(a) \mathrm{d}a}.$$

This value is often used instead of the coefficient of variance, Δ, (Hansen and Travis, 1974) because of a special importance attached to the value of the effective radius of droplets, a_{ef}, in a cloudy medium as compared to the average radius, $\langle a \rangle$, of droplets. For instance, light extinction in clouds is governed mostly by values of a_{ef} and liquid water content independently on the particle-size distribution (Kokhanovsky, 2001a).

Table 1
Droplet-size distributions

$f(a)$	B	$\langle a\rangle$	a_{ef}	Δ	Δ_{ef}	$\langle a^n\rangle$
Gamma distribution $Ba^{\mu}e^{-\mu\frac{a}{a_0}}$	$\frac{\mu^{\mu+1}}{a_0^{\mu+1}\Gamma(\mu+1)}$	$a_0(1+(1/\mu))$	$a_0(1+(3/\mu))$	$\sqrt{(1/\mu+1)}$	$1/(\mu+3)$	$\left(\frac{a_0}{\mu}\right)^n\frac{\Gamma(1+\mu+n)}{\Gamma(1+\mu)}$
Lognormal distribution $\frac{B}{a}\exp\left(-\frac{\ln^2\frac{a}{a_m}}{2\sigma^2}\right)$	$\frac{1}{\sqrt{2\pi}\sigma}$	$a_m e^{0.5\sigma^2}$	$a_m e^{2.5\sigma^2}$	$\sqrt{e^{\sigma^2}-1}$	$e^{\sigma^2}-1$	$a_m^n e^{\frac{n^2\sigma^2}{2}}$

2.1.2. The concentration of droplets

The number concentration of particles, N, in addition to size and shape of particles, is of importance for the optical waves propagation, scattering, and extinction in cloudy media. The concentration of droplets depends on the concentration C_N of atmospheric condensation nuclei. The value of C_N is smaller over oceans than over continents; thus, the concentration of droplets in marine clouds is on average smaller than over continents. Generally, the smaller concentration of droplets over oceans means that they can grow larger, producing clouds with larger droplets over oceans, which is confirmed by the analysis of the satellite optical imagery as well (Han et al., 1994). This influences the occurrence and the rate of precipitation.

Swensmark and Friis-Christensen (1997) and Marsh and Swensmark (2000) have speculated that cosmic ray ionization could influence the production of condensation nucleii and, therefore, cloud properties. This is of importance for climate change problems as well (Swensmark, 1998).

The dimensionless volumetric concentration of droplets $C_v = N\langle V\rangle$ and the liquid water content (LWC) $C_w = \rho C_v$ or (see Eq. (2.10)) $C_w = N\langle W\rangle$ are often used in cloud studies as well.

The typical variability of N, C_v, and C_w in water clouds is presented in Table 2 (Mason, 1975; Fomin and Mazin, 1998). Numbers in Table 2 are representative, but it should be remembered that these values can change in broader range in real situations. The liquid water content is not constant throughout a cloud, but has larger values near the top of a cloud (Feigelson, 1981; Paul, 2000; Yum and Hudson, 2001).

The liquid water path (LWP), w, is defined as

$$w = \int_{z_1}^{z_2} C_w(z)\mathrm{d}z, \tag{2.22}$$

where $l = z_2 - z_1$ is the geometrical thickness of a cloud. If $C_w = \text{const}$,

$$w = C_w l. \tag{2.23}$$

The geometrical thickness of clouds varies, depending on the cloud type (Landolt-Bernstein, 1988). It usually is in the range 500–1000 m for stratocumulus clouds. Near-global data obtained by Han et al. (1994) from satellite measurements show that the liquid water path is typically in the range 50–150 g/m^2. The annual mean is equal to 86 g/m^2 (Han et al., 1994).

Cloud systems can easily cover area $S \approx 10^3$ km^2 (Kondratyev and Binenko, 1984); thus, the total amount of water $W = wS$ (for idealized clouds having the same liquid water path for the whole cloudy area) stored in such a water cloud system is equal approximately to 10^8 kg, if we assume that $w = 100$ g/m^2, which is a typical value (Han et al., 1994). This underlines the importance of clouds both for climate problems and human activity (e.g., crops production, etc.).

2.2. Ice clouds

Microphysical properties of ice clouds cannot be characterized by a single particle-size distribution curve as is the case for liquid clouds even if one considers relatively small volumes of a cloudy medium. This is due to extremely complex shapes of ice particles in crystalline clouds. Major shapes of ice crystals are plates, columns, needles, dendrites, stellars, and bullets (Mason, 1975; Volkovitsky et al., 1984; Takano and Liou, 1989, 1995; Liou, 1992, 2002; Yang et al., 2001). Combinations of bullets

Table 2
Typical range of values N, C_v, and C_w in water clouds

N (cm^{-3})	C_v	C_w (g/m^3)
20–1000	10^{-7}–10^{-6}	0.01–1

and needles are also common. The Magano–Lee classification of natural crystals includes 80 shapes (Magano and Lee, 1966), ranging from the elementary needle (the classification index N1a) to the irregular germ (the classification index G6).

The concentration of crystals, N, varies with height, often in the range 50–50,000 crystals per cubic meter. The ice water content

$$C_{\mathrm{i}} = N\langle W\rangle, \tag{2.24}$$

where $\langle W\rangle$ is average mass of crystals, usually in the range 10^{-4}–10^{-1} g/m^3. Thus, the average mass of a crystal is in the range 2×10^{-3}–2×10^{-9} g. Crystals have a bulk density, ρ, less than that of the bulk ice ($\rho=0.3$–0.9 g/cm^3) due to the presence of impurities and bubbles inside ice particles (Landolt-Bernstein, 1988). The size of crystals is usually characterized by their maximal dimension, D, which is related to the effective size (Yang et al., 2000). D is usually in the range 0.1–6 mm for single crystals and 1–15 mm for snow crystal aggregates. Smaller crystals (e.g., with maximal sizes around 20 μm) also are present in ice clouds (Yang et al., 2001). The mode D_0 of size distribution curves $f(D)$ depends on the shape of crystals, with characteristic values of D_0 being 0.5 mm for plates and columns, 1 mm for needles, sheaths, and stellars, and 2 mm for dendrites. Distribution curves can be modelled by gamma distributions with half-widths of distributions, $\Delta_{1/2}$, being larger for larger values of D. Frequently, $\Delta_{1/2}\approx\bar{D}$, where $\bar{D}$ is the average size of crystals.

Simple shapes of ice crystals (e.g., hexagonal prisms) can be characterized by two dimensions: the length of the prism, L, and the diameter, $D=a\sqrt{3}$, where a is the side of a hexagonal cross section. Even in this most simple case, two-dimensional distribution functions, $f(D,L)$, should be used. Note that $f(D,L)$ can be approximately reduced to one-dimensional functions, $f(D)$, due to the existence of empirical relationships between the length of crystals and their diameter in natural clouds (Auer and Veal, 1970). For instance, for hexagonal columns with the semiwidth, ζ, and the length, L, (Mitchell and Arnott, 1994), $\zeta=0.35L$ at $L<100$ μm and $\zeta=3.48\sqrt{L}$ otherwise. Pruppacher and Klett (1978) give the following empirical relationship for plates: $L=2.4483\zeta^{0.474}$ at $\zeta\in$[5 μm, 1500 μm]. Similar relationships can be obtained for other shapes (Mitchell and Arnott, 1994).

It should be pointed out, however, that the whole concept of a single-distribution function breaks down for ice clouds. Recall that the microphysical properties of most water clouds (as far as their optical properties are concerned) can be characterized by just three numbers (e.g., the effective radius of droplets, the coefficient of variance of the droplet distribution function $f(a)$, and the concentration of droplets) (Deirmendjian, 1969).

By contrast, at least 80 multidimensional particle-size distributions are needed if one would like to use the classification of crystals developed by Magano and Lee (1966). This calls for the introduction of a new way for particle characterization in the case of complex particulate systems such as ice clouds. The same problem arises in the optics of mineral aerosol, blown from the Earth's surface to atmosphere (Volten et al., 2001; Mishchenko et al., 2002).

One of the possible solutions of the problem lies in the characterization of ice crystals in an elementary volume of a cloudy medium by the function

$$f(\vec{a},\vec{b}) = \sum_{r=1}^{N} c_r f_r(\vec{a}) + \sum_{i=1}^{M} c_i f_i(\vec{b}), \tag{2.25}$$

where $f_r(\vec{a})$ is the size distribution of particles of a regular shape (e.g., hexagonal plates or columns), $f_i(\vec{b})$ is the statistical distribution of particles with random surfaces or the so-called irregularly shaped particles. Note that instead of single variables (e.g., the radius of particles a), we need to introduce vector parameters $\vec{a}$ and $\vec{b}$ in the case of crystalline clouds. In particular, we have for the components of the two-dimensional vector parameter, $\vec{a}$, with coordinates a_1, a_2 in the case of an idealized cloud with hexagonal columns: $a_1=D$, $a_2=L$.

Functions $f_i(\vec{b})$ present statistical distributions of some statistical characteristics of particles (e.g., average radii, correlation lengths, etc.). Values of c_i and c_r give concentrations of different crystal habits. Clearly, the simplest case is to consider the function $f(\vec{a},\vec{b})$ as a sum of two functions:

$$f(\vec{a},\vec{b}) = c_1 f_1(\vec{a}) + c_2 f_2(\vec{b}), \tag{2.26}$$

where function $f_1(\vec{a})$ represents particles of a regular shape (say, hexagonal cylinders) and the function $f_2(\vec{b})$ represents statistical parameters of a single particle of irregular shape.

This irregularly shaped particle can be presented, e.g., as a fractal (Macke and Tzschichholz, 1992; Macke et al., 1996; Kokhanovsky, 2003a). It should be pointed out that the function $f_2(\vec{b})$ in this case represents "fictive" particles (Kokhanovsky, 2001a) which do not exist in a cloud at all. However, ice cloud optical characteristics, calculated using $f_2(\vec{b})$, indeed represent quite well the optical characteristics of particles with extremely diverse shapes (Macke et al., 1996; Kokhanovsky, 2003a).

A similar approach to optical characterization of irregularly shaped particles was developed by Peltoniemi et al. (1989), Peltoniemi (1993), and Muinonen et al. (1996). It is based on Monte-Carlo calculations of light scattering by a large particle with a rough surface. The model of spheres with rough surfaces was successfully applied to the optical characterization of irregularly shaped aerosol particles (Volten et al., 2001). This model presumably can be extended for the case of ice clouds as well. For this, the parameters of the irregularity of the so-called fictive particle (Kokhanovsky, 2001a) should be changed accordingly. This is due to different morphology of ice crystals (Magano and Lee, 1966) as compared to mineral aerosol (Okada et al., 2001). Also note that the refractive index of aerosol in visible is larger than that for ice.

2.3. Refractive index of liquid water and ice

The complex refractive index of particles suspended in the atmosphere is another important parameter in atmospheric optics studies (Liou, 1992). This is due to the fact that not only the size, shape, and concentration of particles influence the light propagation in atmosphere. The chemical composition, thermodynamic phase, and temperature of particles are of importance as well. The refractive index of water droplets and ice crystals varies with the temperature and has been tabulated by many authors (see, e.g., Hale and Querry, 1973 for liquid water and Warren, 1984 for ice).

Spectral dependencies of real and imaginary parts of the complex refractive index of water and ice are presented in Figs. 1 and 2. The differences in light absorption by liquid and solid water are considerable, a fact that can be used for the retrieval of the cloud thermodynamic phase (liquid, ice, or mixed-phase clouds) from ground (Dvoryashin, 2002) and satellite (Knap et al., 2002) measurements. In particular, we see that the absorption band around the wavelength,

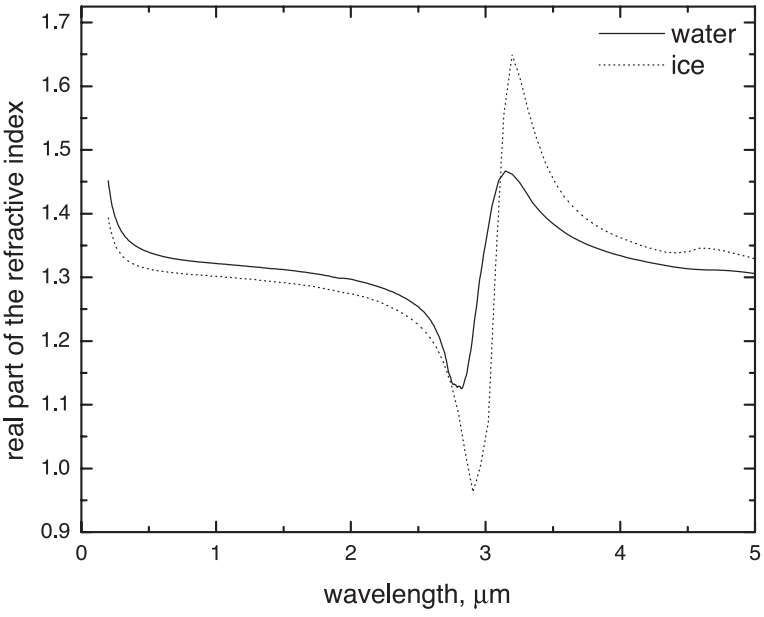

Fig. 1. Real part of the refractive index of water and ice.

$\lambda = 1.55$ μm, for ice is shifted to larger wavelengths as compared to liquid water. This shift in the absorption band position can be easily detected with the use of modern spectrometers (see, e.g., Bovensmann et al., 1999).

The real part of the refractive indices of water, n_w, and ice, n_i, do not vary considerably in the visible and near-infrared regions of electromagnetic spectra. Generally, $n_i(\lambda) < n_w(\lambda)$, with n_w in the range 1.33–1.34 for $\lambda = 0.4$–1 μm and n_i in the range 1.30–1.32 within the same spectral band. Somewhat larger values of refractive indices occur at shorter wavelengths.

The spectral variability of the imaginary part of the refractive index of water, which is responsible for the level of absorption of solar radiation by clouds, is much higher (see Fig. 2). It changes six orders of magnitude in the spectral range 0.4–2 μm both for liquid water and ice.

Different impurities in water droplets (mainly soot (Markel, 2002) and various aerosol particles (Twomey, 1977)) can change the imaginary part of the refractive index of droplets (especially in visible, where water is almost transparent). This may influence the accuracy of modern cloud remote-sensing techniques (Nakajima et al., 1991; Zege et al., 1998c; Schuller et al., 2000; Asano et al., 2001). Note that Asano et al. (2001) found that the temperature dependence (Kuo et al., 1993) of liquid water absorption can also influence the cloud droplets' size retrievals.

3. Local optical characteristics

3.1. Water clouds

3.1.1. Extinction coefficient

The information presented in Section 2 can be used as an input for studies of light interaction with cloudy media on a global or local scale. In particular, the attenuation of a direct light beam with the intensity, I_0, in a cloudy medium is governed by the following equation:

$$I = I_0 \exp(-\tau/\cos\vartheta_0), \tag{3.1}$$

where I_0 is the intensity of an incident light, I is the intensity of the transmitted direct light, and ϑ_0 is the solar zenith angle,

$$\tau = \int_0^H \sigma_{ext}(z)\mathrm{d}z \tag{3.2}$$

is the optical distance in a cloud, H is the geometrical distance, and σ_{ext} is the extinction coefficient. It is assumed that the cloud can be represented by a

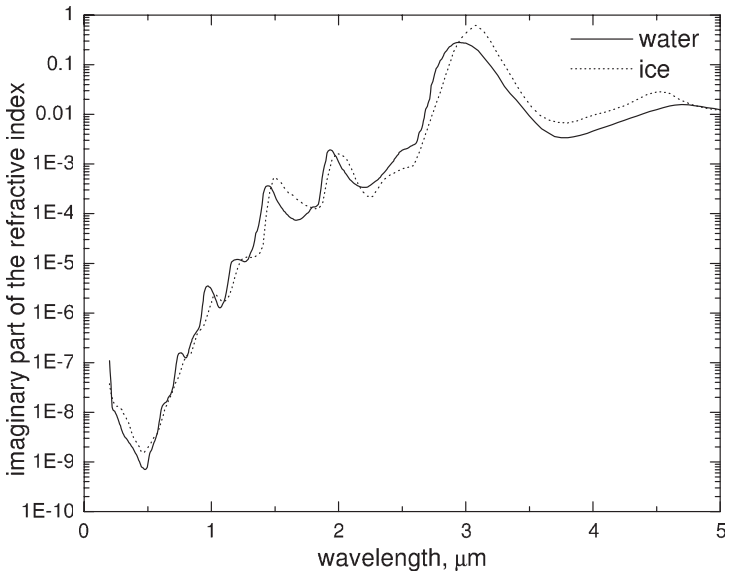

Fig. 2. Imaginary part of the refractive index of water and ice.

horizontally infinite homogeneous plane-parallel layer, which is, of course, a great simplification of a real cloud field (Cahalan et al., 1994, 2001). The value $l=1/\sigma_{ext}$ is called the photon-free path length and gives the average distance between photon-scattering events in a cloud. Knowing the average number of scattering events, $\bar{n}$, it is easy to find the average distance, $L=\bar{n}l$, which photon travels in the medium before it escapes out of the scattering layer. We have for the average total time, which photon spends in a cloud: $t=L/c$, where c is the group light speed.

The value of l is often in the range 10–200 m for water clouds; thus, the value of σ_{ext} is in the range 0.005–0.1 m^{-1}, depending on the cloud type, and perhaps even larger for dense fogs and mists. The extinction coefficient, σ_{ext}, determines the meteorological range of visibility (Zege et al., 1991; Liou, 1992), which is defined as $S_m=3.91/\sigma_{ext}$. In particular, we have at $\sigma_{ext}=0.1$ m^{-1}: $S_m=39.1$ m. In a cloudless atmosphere, this number is approximately 1000 times larger.

A more advanced understanding of the image reduction by cloudy media can be achieved on the base of the image transfer theory (Zege et al., 1991; Zege and Kokhanovsky, 1994, 1995; Barun, 1995, 2000; Zuev et al., 1997; Katsev et al., 1998). This theory treats a cloud as a high-frequency spatial filter. The cloud greatly reduces high spatial frequencies of observed objects, causing fine features of objects to be lost due to multiple light scattering and photon direction randomization process. Clouds with larger particles have "better" optical transfer functions (higher values) as compared to clouds with very fine droplets, a fact that can be used for cloud microphysical parameters monitoring purposes (Zege and Kokhanovsky, 1992; Zuev et al., 1997).

The extinction coefficient varies with height in a cloud (see Eq. (3.2)) and, for a given value of the vertical coordinate, z, is given by

$$\sigma_{ext}=N\int_0^{\infty} f(a)C_{ext}\mathrm{d}a, \tag{3.3}$$

where N is the number concentration of particles. The value of the extinction cross section, C_{ext}, is obtained from Mie theory valid for spherical droplets (Shifrin, 1951; Van de Hulst, 1957; Kerker, 1969; Bohren and Huffman, 1983; Kokhanovsky, 2003b). It is known that (Shifrin, 1951)

$$C_{ext}=\Sigma/2 \tag{3.4}$$

in a good approximation for water droplets in the visible range of the electromagnetic spectrum. Here Σ is the surface area of a droplet. From Eqs. (3.3) and (3.4)~

$$\sigma_{ext}=\frac{N\langle\Sigma\rangle}{2}. \tag{3.5}$$

Thus, the extinction coefficient depends on the product of the number concentration of particles and their average surface area. By use of

$$N=\frac{C_v}{\langle V\rangle}, \tag{3.6}$$

where $\langle V\rangle$ is the average volume of particles (see Eq. (2.8)) and C_v is the volumetric concentration of particles, we get from Eq. (3.5)

$$\sigma_{ext}=\frac{3C_v}{2a_{ef}}, \tag{3.7}$$

where we introduced the effective radius

$$a_{ef}=\frac{3\langle V\rangle}{\langle\Sigma\rangle}. \tag{3.8}$$

The extinction coefficient decreases with the size of particles at $C_v=\mathrm{const}$.

For constant C_v, the value of σ_{ext} can be expressed via the liquid water content, C_w, which is often measured in cloudy media:

$$\sigma_{ext}=\frac{3C_w}{2\rho a_{ef}}, \tag{3.9}$$

where $\rho=1$ g/cm^3 is the density of water. It follows for typical values $a_{ef}=6$ μm and $C_w=0.4$ g/m^3 that $\sigma_{ext}=0.1$ m^{-1}. This is rather dense cloud with the ratio $I_0/I=e$ at the distance 10 m for light incident perpendicular to a cloud layer (see Eq. (3.1)).

We should underline two peculiarities of water clouds, which follow from Eq. (3.9). First of all, the extinction does not depend on the wavelength, λ, and, second, it depends only on the ratio of liquid water content to the effective radius, a_{ef}. The first point leads to the conclusion that clouds do not change the spectral composition of a direct light beam in visible. Thus, spectral transmittance methods of particulate media

microstructure determination (Shifrin and Tonna, 1993) cannot be applied in cloud optics. Another important property, which follows from Eq. (3.9), is independence of the value of σ_{ext} on the type of particle-size distribution. Even the width of the PSD is of no importance at a given value of the effective radius of particles. This is the reason why the satellite methods of cloud microstructure determination (Arking and Childs, 1985; Nakajima and King, 1990; Han et al., 1994) are concerned mostly with the retrievals of a_{ef} values and the liquid water path (see Eqs. (2.23) and (3.9))

$$w = \frac{2}{3}\rho a_{ef}\tau \tag{3.10}$$

and not the droplet-size distribution itself.

The type of particle-size distribution in clouds is not possible to find from extinction measurements in the visible. On the other hand, there is an advantage in that one can calculate the extinction coefficient of cloudy media even with limited information on statistical properties of droplets and crystals. This is especially important for ice clouds as we will see later.

Eq. (3.9) is valid only in the visible range of the electromagnetic spectrum and for comparatively large droplets. Calculations for longer wavelengths should be performed with Mie theory although a simple correction to Eq. (3.9) allows for its use in the near-infrared region of the electromagnetic spectrum (Kokhanovsky and Zege, 1995, 1997a,b; Kokhanovsky, 2001a):

$$\sigma_{ext} = \frac{3C_w}{2\rho a_{ef}}\left\{1 + \frac{\upsilon}{(ka_{ef})^{2/3}}\right\}, \tag{3.11}$$

where $k = 2\pi/\lambda$ and υ is the parameter which only slightly depends on the dispersion of the particle-size distribution. It follows that for most typical widths of particle-size distributions in clouds $\upsilon = 1.1$ (Kokhanovsky and Zege, 1997b). We get from Eq. (3.11) that the extinction coefficient of cloudy media slightly increases with the wavelength in the visible and near infrared. The spectral dependence of σ_{ext} for the gamma PSD (Eq. (2.3)) at $a_{ef} = 4$ μm, $\mu = 6$ is presented in Fig. 3 for the spectral range 0.2–5 μm. The data were obtained with simple Eq. (3.11) and Mie theory, assuming that $C_w = 0.1$ g/m^3. The value of υ was equal to 1.1. The accuracy of Eq. (3.11) decreases with wavelength/size ratio, but the error is smaller than 5% at $\lambda < 2$ μm and $a_{ef} > 4$ μm. Smaller values of a_{ef} are of a rare occurrence in natural clouds (Han et al., 1994). Eq. (3.9) gives a constant value of 0.375 m^{-1} in the case, presented in Fig. 3. We see

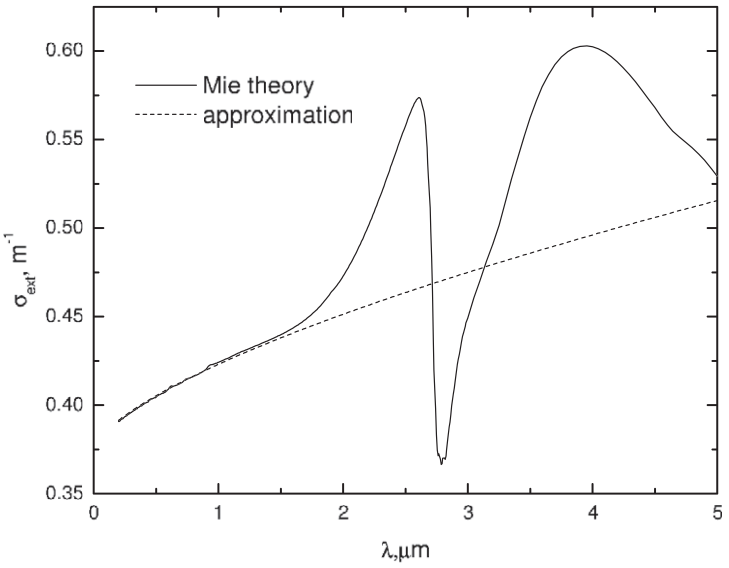

Fig. 3. Extinction coefficient of a cloudy medium with water droplets, characterized by the PSD (Eq. (2.3)) at $a_{ef} = 4$ μm, $\mu = 6$. The value of C_w is 0.1 g/m^3.

that Eq. (3.11) has a high accuracy and gives the correct spectral dependence the extinction coefficient (at least up to the wavelength equal to 1.5 μm).

The accuracy of Eq. (3.11) at larger wavelengths can be increased if one accounts for the dependence of the extinction cross section on the refractive index of particles, which could be done, for instance, in the framework of the Van de Hulst approximation (Ackerman and Stephens, 1987; Kokhanovsky, 2001a). Parameterizations developed by Mitchell (2000) and Harrington and Olsson (2001) can be used even outside the geometrical optics limit.

Clearly, the accuracy of Eq. (3.11) increases with a_{ef}. Thus, the case presented in Fig. 3 provides the maximal error of the approximation (3.11) for terrestrial clouds having $a_{ef} > 4$ μm. Typically, errors are even smaller.

3.1.2. Absorption coefficient

Clouds both scatter and absorb incident radiation. The probability of photon absorption, β, is defined by the following equation:

$$\beta = \frac{\sigma_{abs}}{\sigma_{ext}}, \tag{3.12}$$

where σ_{abs} is the absorption coefficient and σ_{ext} is the extinction coefficient (see, e.g., Eq. (3.11)). The value of β is close to zero in the visible and near infrared, which allows to obtain simple equations for reflection and transmission functions of cloudy media in terms of series $\beta^{j/2}$, where j is an integer number (Rozenberg, 1962, 1967; Van de Hulst, 1980; Minin, 1988; Kokhanovsky, 2002b).

The absorption coefficient is defined as:

$$\sigma_{abs} = N \int_0^\infty C_{abs} f(a) \mathrm{d}a, \tag{3.13}$$

where C_{abs} is the absorption cross section (Shifrin, 1951). It follows for the scattering coefficient, $\sigma_{sca} = \sigma_{ext} - \sigma_{abs}$. The absorption cross section can be calculated from Mie theory for spherical particles. Another way to calculate the absorption cross section, which is valid for nonspherical particles as well, is to use the exact integral (Kokhanovsky, 2001a; Markel, 2002):

$$C_{abs} = \frac{2k}{\left|\vec{E}_0\right|} \int_V n(\vec{r}) \chi(\vec{r}) \vec{E}(\vec{r}) \vec{E}^*(\vec{r}) \mathrm{d}^3\vec{r}, \tag{3.14}$$

where $\vec{E}_0$ is the electric field of an incident wave, $\vec{E}$ is the electric field inside a particle, $k = 2\pi/\lambda$ is the wave number, $m = n - i\chi$ is the refractive index, V is the volume of a droplet or crystal. The first coarse approximation is to assume that the value of

$$\vec{E}(\vec{r}) \vec{E}^*(\vec{r}) \approx B(n) E_0(\vec{r}) \vec{E}_0^*(\vec{r}) \tag{3.15}$$

due to the weakness of absorption. Thus, it follows in this case

$$C_{abs} = B(n) \alpha V, \tag{3.16}$$

where $\alpha = 4\pi\chi/\lambda$ and we assumed that a particle is uniform (n and χ do not depend on the radius vector $\vec{r}$). Clearly, we have that $B \to 1$ as $n \to 1$ for arbitrarily shaped particles (Kokhanovsky, 2001a). It follows from Eqs. (3.13) and (3.16):

$$\sigma_{abs} = B(n) \alpha N \langle V \rangle \tag{3.17}$$

or

$$\sigma_{abs} = B(n) \alpha C_v. \tag{3.18}$$

We have calculated the value $B = \sigma_{abs}/\alpha C_v$ for the PSD (Eq. (2.3)) with $\mu = 6$ and $a_{ef} = 4$ μm with Mie theory and presented it in Fig. 4 as the function of the wavelength. One can see that the value of B almost does not depend on the wavelength. This means that also there is only weak dependence of B on $n(\lambda)$, $\chi(\lambda)$, and $x_{ef} = ka_{ef}$ at $\lambda \leq 1.8$ μm. For larger values of λ, Eq. (3.15) becomes invalid due to higher absorption of light by droplets or crystals. We have from Fig. 4: $B \approx 5/3$.

The accuracy of approximation (3.18) at $B = 5/3$ is better than 5% below $\lambda = 1.8$ μm for values of a_{ef} in the range 4–6 μm. For larger particles, the accuracy reduces due to the neccesity to account for terms proportional to α^2 and higher. Then Eq. (3.18) should be modified (see, e.g., Kokhanovsky and Macke, 1997; Kokhanovsky, 2001a).

Eq. (3.18) can be written as

$$\sigma_{abs} = \frac{B(n) \alpha C_w}{\rho}, \tag{3.19}$$

where C_w is the liquid water content and ρ is the density of water. One can see that the spectral variation of the absorption coefficient of liquid clouds approximately coincides with the spectral dependence of the absorption coefficient of liquid water itself (see Fig. 2) at least

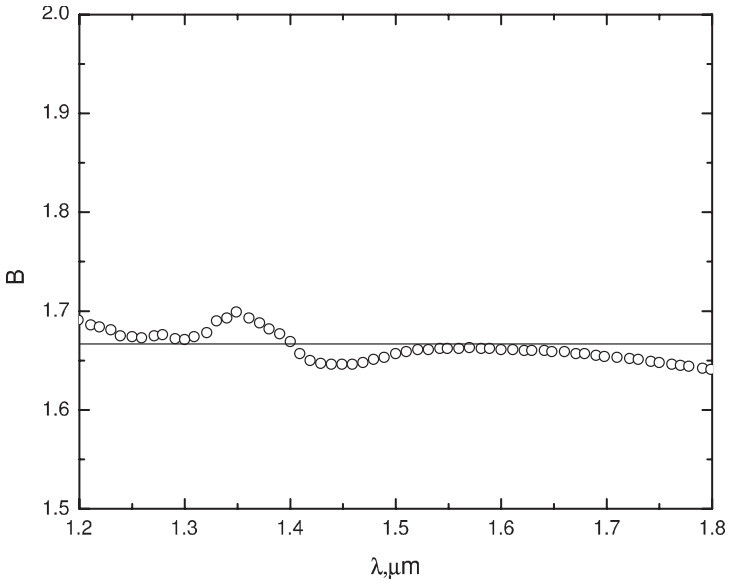

Fig. 4. Spectral dependence $B(\lambda)$, obtained for the same conditions as in Fig. 3.

up to 1.8 μm. The same applies to ice clouds, namely, $\sigma_{abs} \sim 4\pi\chi_i(\lambda)/\lambda$, where $\chi_i(\lambda)$ is the imaginary part of the refractive index of ice. This feature can be used for the cloud thermodynamic phase determination by remote-sensing techniques (see Fig. 2). Note that B in Eq. (3.19) depends on the shape of particles (Kokhanovsky and Macke, 1997).

It should be pointed out that water droplets can collect absorbing particles from surrounding air. Liquid aerosol particles penetrate into droplets. They dissolve and change the value of α in Eq. (3.18). Soot particles can form a discontinuous layer on the surface of a droplet. All these effects will produce an enhancement of the absorption coefficient as compared to simple Eq. (3.18) (Prishivalko et al., 1984; Kokhanovsky, 1989; Asano et al., 2001). Note that the effects of aerosol particles (e.g., soot) can be modelled by inserting into Eq. (3.18) the value of

$$\alpha = \alpha_w + \sum_{i=1}^{N} c_i \alpha_i, \tag{3.20}$$

where α_w and α_i are absorption coefficients of water and impurities, respectively, and c_i is the relative concentration of impurities. The problem of black carbon influence on the light absorption in cloud was studied in detail by Chylek et al. (1996) and Liu et al. (2002).

The parameter of considerable importance in the radiative transfer problems in clouds is not the absorption coefficient itself, but the ratio of the absorption and extinction coefficients. It follows from Eqs. (3.11) and (3.19) for this ratio

$$\beta = \tilde{B}\alpha a_{ef}, \tag{3.21}$$

where $\tilde{B}=(2/3)B(n)(1+\upsilon x_{ef}^{-2/3})^{-1}$ is close to 1. The value of β is obtained from the measurement of the reflection function of clouds in the infrared (Nakajima and King, 1990). Thus, Eq. (3.21) can be used to find the effective radius of droplets ($a_{ef} \approx \beta/\alpha$), which corresponds to a given value of β. The uncertainty in the value of α (see Eq. (3.20)) can introduce additional errors in the retrieved values of the effective radius of droplets (Asano et al., 2001).

Let us estimate this error, neglecting the term $\upsilon x_{ef}^{-2/3}$ for the sake of simplicity. Then it follows:

$$a_{ef} = \frac{3\beta}{2B\alpha} \tag{3.22}$$

and, therefore, $(\delta a_{ef}/a_{ef}) = (-\delta\alpha/\alpha)$. Aerosol particles trapped in droplets make the value of α larger. Thus, the effective radius, a_{ef}, of polluted clouds (as obtained from Eq. (3.22) without account for pollutants) appears to be smaller as compared to values

obtained from in situ measurements (e.g., using laser diffractometers (Kokhanovsky, 2001a)). This was found also experimentally (Nakajima et al., 1991). To correct this effect, one should use the value of α (Eq. (3.20)) in Eq. (3.22). The problem, however, is complicated by the fact that values of absorption coefficients and concentrations of impurities are not known a priori. On the other hand, one can formulate the inverse problem in such a way that they can be derived from measured spectral reflectances simultaneously with the value of the effective radius of droplets (Zege et al., 1998c).

Eq. (3.18) is limited to the case of weak absorption. It can be generalized to account for larger absorption of light by water droplets. We found, parameterizing Mie theory results, that

$$\sigma_{\mathrm{abs}} = B\alpha C_{\mathrm{v}}[1 - \alpha a_{\mathrm{ef}}]. \tag{3.23}$$

Eq. (3.23) transforms to Eq. (3.18) for small values of absorption ($\alpha a_{\mathrm{ef}} \to 0$).

In conclusion, we present the spectral dependence of the probability of photon absorption in Fig. 5. Data were obtained using Mie theory and approximate solution, given by Eq. (3.23) with account for Eqs. (3.11) and (3.12). The effective radii of particles were equal to 4 and 16 μm. The accuracy of the approximation is better than 10% at wavelengths smaller than 2 μm (see Fig. 6). They are typically smaller than 5% at $\lambda \leq 1.8$ μm.

3.1.3. Phase function

Until now, we have considered only the extinction and the absorption characteristics of cloudy media. However, clouds not only attenuate propagated signals and absorb light but also scatter incident light in all directions. Generally, the probability of photon scattering by a droplet depends on the size of the droplet and the energy of the incident photon (or the light wavelength).

Now we should characterize the probability of photon scattering in a given direction, specified by the scattering angle, θ ($\theta = 0$ corresponds to the forward scattering). It is known that the intensity of light scattered by water droplets is much larger in the forward hemisphere than it is in the backward directions (Deirmendjian, 1969; Kokhanovsky et al., 1998a).

Let us introduce the probability dP of light scattering in the direction, specified by the vector

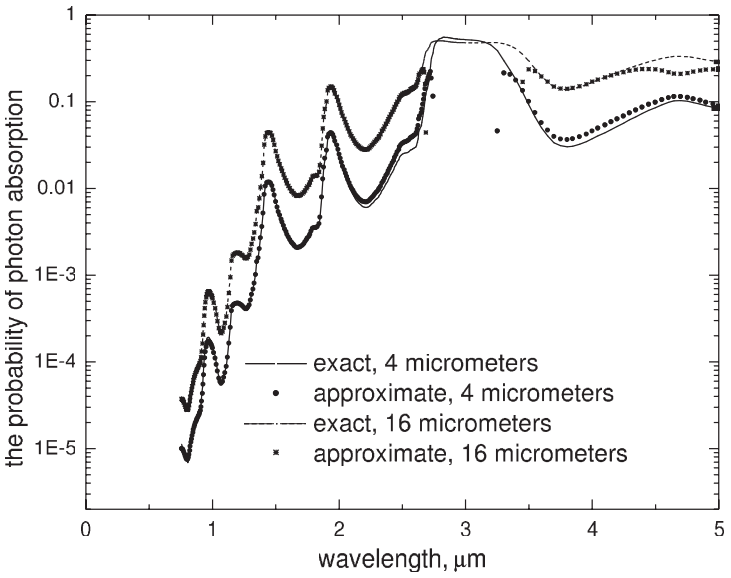

Fig. 5. Probability of photon absorption, obtained for the same conditions as in Fig. 3. Results for the effective radius, $a_{\mathrm{ef}} = 16$ μm are also shown.

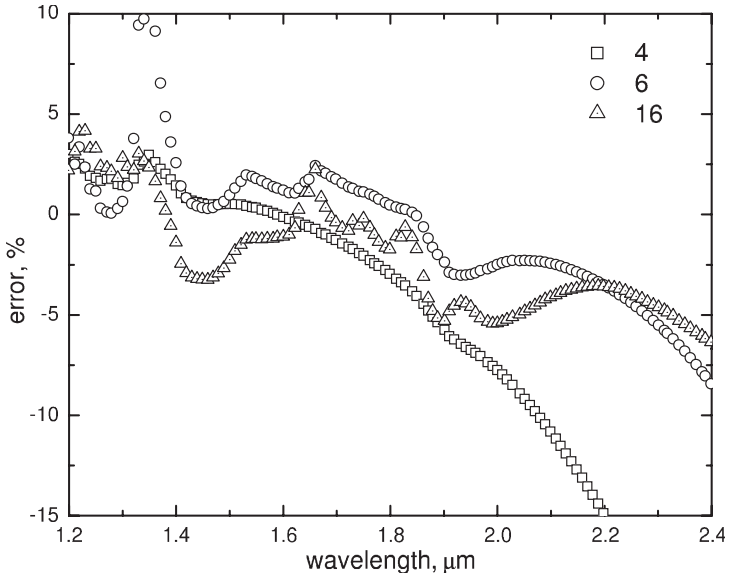

Fig. 6. Error of the geometrical optics approximation for the probability of photon absorption, obtained from data presented in Fig. 5 for effective radii 4 and 16 μm. Data for the effective radius 6 μm are also shown.

$\vec{\Omega}$ inside the solid angle $d\Omega$. This probability will be proportional to the value of $d\Omega/4\pi$. Namely, we have:

$$dP = x(\Omega)\frac{d\Omega}{4\pi}, \tag{3.24}$$

where $x(\Omega)$ is the coefficient of proportionality. It follows from Eq. (3.24):

$$\int_{4\pi} x(\Omega)\frac{d\Omega}{4\pi} = P. \tag{3.25}$$

The value of P represents the probability of photon survival in the scattering process. It is equal to 1 if there is no absorption of light by a particle and it is smaller than 1 if some photons are absorbed by a particle. Clearly, the probability of photon survival, P, is equal to the single-scattering albedo (Chandrasekhar, 1950):

$$w_0 = \frac{\sigma_{sca}}{\sigma_{ext}}. \tag{3.26}$$

It should be pointed out that $\beta = \sigma_{abs}/\sigma_{ext}$ is a small parameter for water clouds (see Fig. 5) in the visible and $P \equiv w_0 = 1 - \beta \approx 1$ in this case. The value $p(\Omega) = x(\Omega)/P$ is called the phase function. It is equal to one if the probability of light scattering does not depend on the angle (see Eq. (3.25)). Note that the value of $x(\Omega)$ is sometimes also called the phase function or the scattering indicatrix (Ishimaru, 1978; Van de Hulst, 1980).

Light scattering by water droplets is azimuthally symmetric due to their spherical shape, thus

$$\frac{1}{2}\int_0^{\pi} p(\theta)\sin\theta d\theta = 1. \tag{3.27}$$

The phase function $p(\theta)$ (or the scattering indicatrix) can be calculated from Mie theory (Shifrin, 1951). It does not depend on the concentration of particles, by the definition, but on their refractive index and size. Functions $p(\theta)$, obtained from Mie theory, for different particle-size distributions are presented in Fig. 7 at $\lambda = 0.65$ μm. Main features of phase functions of water clouds in visible are (see Fig. 7):

- sharp forward–backward asymmetry;
- weak dependence on the size of droplets in the range of scattering angles 20–60°;
- enhanced scattering near rainbow θ_r (approximately 138° for water droplets) and glory θ_g (180°) scattering angles (Tricker, 1970; Greenler, 1980; Konnen, 1985; Spinhirne and Nakajima, 1994);
- strong forward peak.

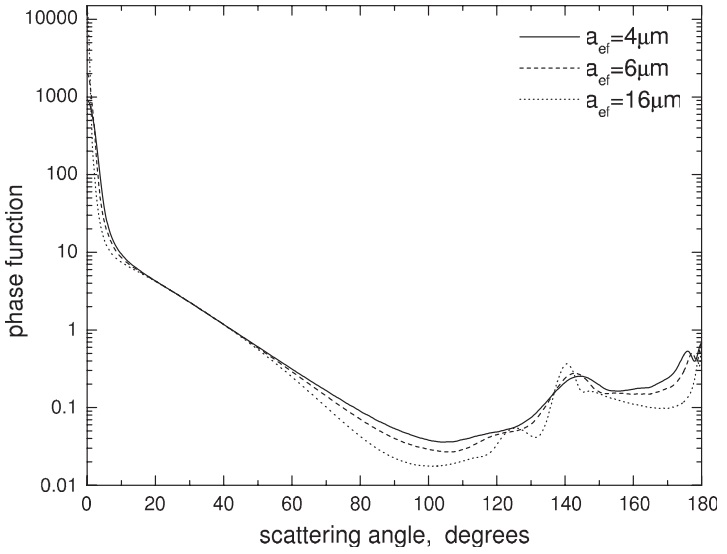

Fig. 7. Phase functions of water clouds obtained from Mie theory for the same conditions as in Fig. 3. Data for a_{ef} equal to 6 and 16 μm are also given for the comparison.

Amplitudes of peaks at angles $\theta=0$, θ_r, π can be used as indicators of the size of droplets (Van de Hulst, 1957; Shifrin and Tonna, 1993; Kokhanovsky and Zege, 1997b).

Approximate equations for the phase functions of water clouds, derived using the geometrical optics concept, have been presented by many authors (e.g., see Shifrin, 1951; Van de Hulst, 1957; Nussenzveig, 1992; Zege et al., 1993; Kokhanovsky and Zege, 1997b; Grandy, 2000). A detailed comparison of the geometrical optics and Mie theory was performed by Liou and Hansen (1971), who conclude that the ray optics results have a high accuracy for large droplets with size parameters larger than 400. For some angular regions, errors are small even for comparatively small droplets (see, e.g., the region 20–60° in Fig. 7). Geometrical optics equations are not very simple even for spherical droplets (Kokhanovsky, 2001a).

Thus, we found, parameterizing Mie theory results, that the phase function of a cloud can be presented approximately by the following equation:

$$p(\theta) = Q\exp(-\mathbb{C}\theta) + \sum_{i=1}^{5} b_i \exp[-\beta_i(\theta-\theta_i)^2],$$

where $Q=17.7$, $\mathbb{C}=3.9$, θ is given in radians and constants b_i, β_i, θ_i are given in Table 3. The shortcoming of this equation is that it does not account for the influence of the size of droplets on the phase function (see Fig. 7). However, it can be useful for general modelling of single and multiple light scattering in cloudy media (Zege et al., 1993, 1995; Katsev et al., 1998).

The solution of the radiative transfer equation, which describes the radiative transfer through cloudy media, is simplified if one uses the expansion of the phase function in series:

$$p(\theta) = \sum_{s=0}^{\infty} a_s P_s(\cos\theta). \tag{3.28}$$

Here $P_s(\cos\theta)$ is the Legendre polynomial. However, note that in practice, the number of coefficients, a_s, could be taken to be finite. It is approximately equal to $2kd$, where d is the average diameter of particles and k is the wave number (Kokhanovsky, 1997). The coef-

Table 3
Parameters b_i, β_i, and θ_i

i	b_i	β_i	θ_i
1	1744.0	1200.0	0.0
2	0.17	75.0	2.5
3	0.30	4826.0	π
4	0.20	50.0	π
5	0.15	1.0	π

ficients, a_s, for cloudy media calculated with Mie theory at $\lambda = 0.65$ μm for the PSD (Eq. (2.3)) with $\mu = 6$ are presented in Fig. 8. Approximate equation for a_s, based on the combination of the geometrical optics and the Fraunhofer diffraction, were obtained by Kokhanovsky (1997, 2001a). They can be used to avoid long numerical calculations with Mie theory as $x_{ef} \to \infty$.

We emphasize that both geometrical optics results (Kokhanovsky, 1997) and data presented in Fig. 8 show that the number s^{max}, which corresponds to the largest coefficient a_s^{max}, is equal approximately to $4x_{ef}/5$. Also we have approximately $s^{max}a_s^{max}=2$.

It follows from Eq. (3.28) using the orthogonality of Legandre polynomials

$$a_s = \frac{2s+1}{2}\int_0^{\pi} p(\theta)P_s(\cos\theta)\sin\theta d\theta. \quad (3.29)$$

In particular, we have $a_0 = 1$ (see Eq. (3.27)) and $a_1 = 3g$, where

$$g = \frac{1}{2}\int_0^{\pi} p(\theta)\sin\theta\cos\theta d\theta \quad (3.30)$$

is the so-called asymmetry parameter, giving the average cosine of the photon-scattering angle. Note that the value of g determines (together with the extinction coefficient) the coefficient of photon diffusion, $D=[3\sigma_{ext}(1-g)]^{-1}$, in a cloudy medium.

We stress that it is the value of integral (Eq. (3.30)) (and not the phase function itself), which determines a number of important radiative characteristics of clouds (Zege et al., 1991). For instance, we have for the value of the total cloud reflectance or the spherical albedo in the case of a semiinfinite cloud (Zege et al., 1991; Kokhanovsky, 2001a): $r_\infty = \exp(-4\sqrt{\beta/3(1-g)})$. Thus, the asymmetry parameter needs a special attention. We will consider this parameter in the next section in more detail.

3.1.4. Asymmetry parameter

Let us represent the phase function $p(\theta)$ of a large particle ($x_{ef} \to \infty$, $2x_{ef}(n-1) \to \infty$) as (Kokhanovsky, 2001a)

$$p(\theta) = \frac{\sigma_{sca}^{D} p^{D}(\theta) + \sigma_{sca}^{G} p^{G}(\theta)}{\sigma_{sca}^{D} + \sigma_{sca}^{G}}. \quad (3.31)$$

Here $p^D(\theta)$ is the phase function associated with the Fraunhofer diffraction of light by a droplet; $p^G(\theta)$ is the phase function associated with rays, which penetrate the particle, reflect, and refract inside the droplet; σ_{sca}^G and σ_{sca}^D are scattering coefficients associated with

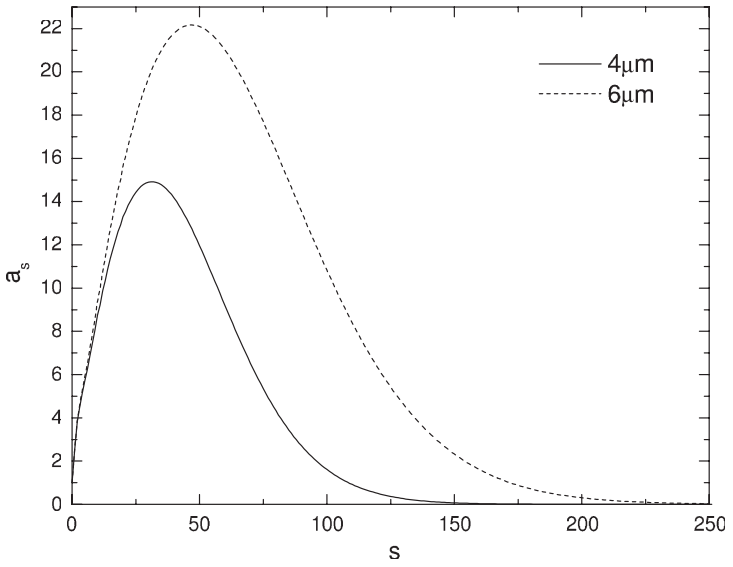

Fig. 8. Coefficients a_s obtained for the same conditions as in Fig. 3. Data for a_{ef} equal to 6 μm are also shown.

these processes. Note that Eq. (3.31) corresponds to the Van de Hulst's (1957) localization principle. It holds only approximately and ignores the possible interference of waves (Glautshing and Chen, 1981) that originate due to separate diffraction and geometrical optics scattering processes.

It follows from Eqs. (3.30) and (3.31)

$$g = \frac{\sigma_{sca}^{D} g^{D} + \sigma_{sca}^{G} g^{G}}{\sigma_{sca}^{D} + \sigma_{sca}^{G}}, \tag{3.32}$$

where

$$g^{D} = \frac{1}{2}\int_{0}^{\pi} p^{D}(\theta)\sin\theta\cos\theta d\theta, \tag{3.33}$$

$$g^{G} = \frac{1}{2}\int_{0}^{\pi} p^{G}(\theta)\sin\theta\cos\theta d\theta. \tag{3.34}$$

One can obtain (Van de Hulst, 1957; Kokhanovsky, 2001a,b) that $g^{D} \approx 1$. Note that the function $p^{G}(\theta)$ does not depend on the size of large nonabsorbing particles (Van de Hulst, 1957; Kokhanovsky and Nakajima, 1998). Thus, g^{G} depends only on the refractive index, n, of water in this case. The value of n does not change considerably in the visible region of the electromagnetic spectrum (see Fig. 1). We will assume that $n = 1.333$. Then it follows that $g^{G} = 0.7686$ (Kokhanovsky, 2001a) and $g = 0.8843$ according to Eq. (3.32), where we accounted for the equality $\sigma_{sca}^{D} = \sigma_{sca}^{G}$, which also holds in the visible region of the electromagnetic spectrum, where absorption can be neglected (Van de Hulst, 1957). The value of asymmetry parameter g of water clouds, in practice, weakly depends on the size of particles and wavelength. This dependence can be approximated by the following equation (Kokhanovsky, 2001a):

$$g = g_0 - \frac{C}{x_{ef}^{2/3}}, \tag{3.35}$$

where C is the constant, which does not depend on the size of droplets (but possibly depends on their shape) and $g_0 \equiv g(x_{ef} \to \infty)$. The integral for g_0 is given by Van de Hulst (1957). It depends only on the refractive index of a particle and equal approximately to 0.8843 at $n = 1.333$, as stated above.

Results of calculations of the value $C = (g_0 - g)x_{ef}^{2/3}$ with Mie theory are presented in Fig. 9 for the particle-size distribution (Eq. (2.3)) at $\mu = 6$, $a_{ef} = 4$ μm, and $\lambda \le 1$ μm. It follows that $C \approx 0.5$. Thus, we

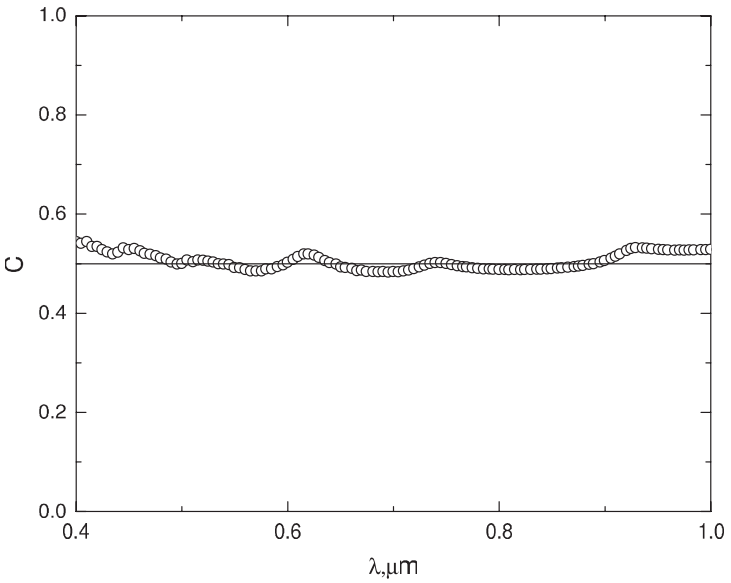

Fig. 9. Spectral dependence $C(\lambda)$ obtained for the same conditions as in Fig. 3.

have from Eq. (3.35) the value of $G=1-g$, which is often called the co-asymmetry parameter:

$$G = 0.12 + \frac{1}{2x_{\mathrm{ef}}^{2/3}}. \tag{3.36}$$

It is the value of G and not g itself which plays an important role in the radiative transport in cloudy media. For instance, values of g equal to 0.75 (typical for ice clouds) and 0.85 (typical for water clouds) are comparatively close to each other, but corresponding values of G (0.25 and 0.15, respectively) differ. This is a noteworthy feature for comparing cloudy media with different values of asymmetry parameters.

It is important to understand the physical meaning of the parameter G. For this, we use the expansion $\cos\theta = 1-(\theta^2/2)+\ldots$ in Eq. (3.30). Then it follows that $G=\langle\theta^2\rangle/2$, where $\langle\theta^2\rangle = \frac{1}{2}\int_0^{\pi}\theta^2 p(\theta)\sin\theta \mathrm{d}\theta$ is the averaged square of the scattering angle. We neglect high-order terms in the expansion of $\cos\theta$ which is possible due to a peaked character of the phase function in Eq. (3.30) (see Fig. 7).

The average value of the squared scattering angle, therefore, governs the radiative transport in cloudy media. In particular, semiinfinite clouds with close values of ratios $\beta/\langle\theta^2\rangle$ also have close values of the total reflectance. Smaller values of $\langle\theta^2\rangle$ mean that photons penetrate to larger depths in cloudy media before their escape back to the free space, where the source of radiation is located. This also makes the total path lengths of photons in cloudy media larger, which in turn produces the larger total absorption of radiation inside clouds with larger values of $\langle\theta^2\rangle$.

The total fraction of radiation absorbed by a semi-infinite cloud is given by the following expression (Kokhanovsky, 2001a):

$$A = 1 - \exp\left\{-4\sqrt{\frac{\beta}{3(1-g)}}\right\}$$

or

$$A = 4\sqrt{\frac{2\beta}{3\langle\theta^2\rangle}}$$

as $\beta \to 0$. Clearly, the ratio

$$\bar{n} = \frac{A}{\beta},$$

can be used as an estimation of the average number of photon-scattering events in a cloud layer. In particular, we get $\bar{n} \to 4\sqrt{\frac{2}{3\beta\langle\theta^2\rangle}}$ as $\beta \to 0$. Smaller values of β and $\langle\theta^2\rangle$ give larger values of $\bar{n}$ as one might expect.

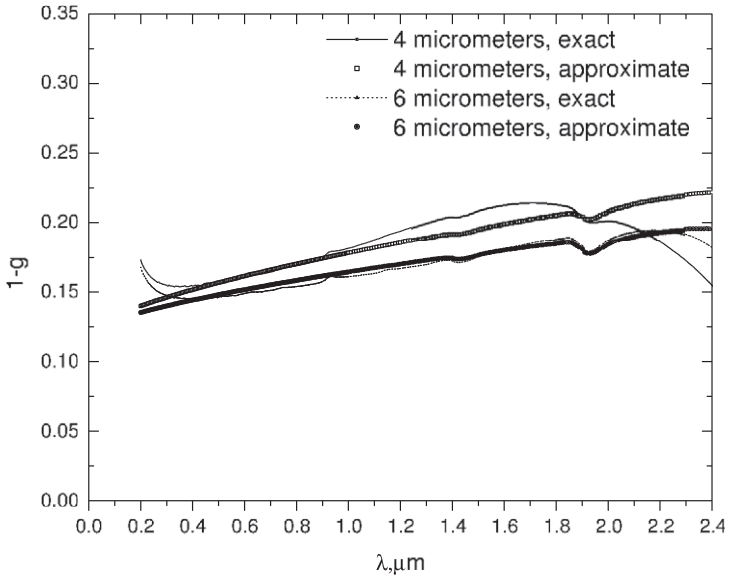

Fig. 10. Asymmetry parameter obtained for the same conditions as in Fig. 3. Results for the effective radius $a_{\mathrm{ef}}=6$ μm are also shown.

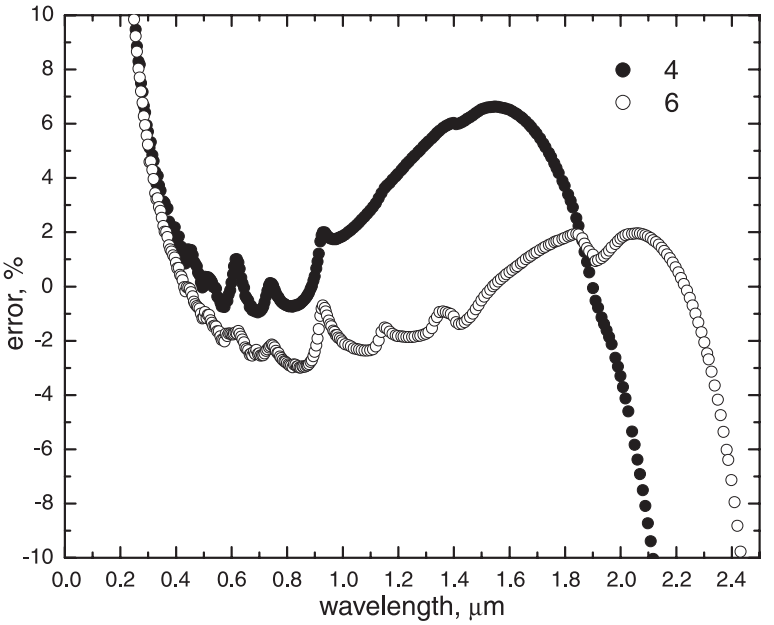

Fig. 11. Error of the geometrical optics approximation for the asymmetry parameter obtained from data presented in Fig. 10 for effective radii 4 and 6 μm.

Eq. (3.36) can be used only for nonabsorbing channels (e.g., in visible). However, it can be modified in a full analogy with Eq. (3.23) to account for light absorption at $\lambda \geq 1$ μm (Kokhanovsky, 2001a):

$$G = 0.12 + \frac{1}{2x_{\mathrm{ef}}^{2/3}} - \varepsilon\alpha a_{\mathrm{ef}}. \qquad (3.37)$$

We obtained fitting Eq. (3.37) to Mie theory results that $\varepsilon = 0.15$. Comparisons of calculations with simple Eq. (3.37) and Mie theory are presented in Fig. 10. They were performed for the particle-size distribution (Eq. (2.3)) at $\mu = 6$, $a_{\mathrm{ef}} = 4$ μm, and $a_{\mathrm{ef}} = 6$ μm for wavelengths, $\lambda \leq 2.4$ μm. It follows that the accuracy of Eq. (3.37) (see Fig. 11) is better than 5% at $a_{\mathrm{ef}} = 6$ μm in visible and near infrared for $\lambda \leq 2.3$ μm. It is also better than 5% for droplets with $a_{\mathrm{ef}} = 4$ μm for values of $\lambda \leq 2.0$ μm.

Another important characteristic of the phase function of a cloudy medium is the probability of light scattering in the backward hemisphere:

$$F = \frac{1}{2}\int_{\pi/2}^{\pi} p(\theta)\sin\theta\cos\theta \mathrm{d}\theta.$$

It was shown (Kokhanovsky et al., 1998a) that it holds approximately for water clouds:

$$F = 0.03 + \frac{1}{5x_{\mathrm{ef}}^{2/3}}.$$

It suggests that approximately 97% of light is scattered by a local volume of a cloudy medium in the range of angles smaller than 90°. The backscattering signal is, therefore, quite low. It increases, however, due to multiple-scattering processes that take place inside a cloud (Bissonnete et al., 1995; Zege et al., 1995, 1998a,b).

3.2. Ice clouds

3.2.1. Extinction coefficient

Local optical characteristics of ice and mixed clouds cannot be calculated so easily as for water clouds. In particular, the Mie theory (Shifrin, 1951) cannot be used due to the complex shape and internal structure of ice crystals (Takano and Liou, 1989; Macke, 1993, 1994; Macke et al., 1996, 1998; Mitchell and Arnott, 1994; Yang and Liou, 1998; Yang et

al., 2000, 2001). Main results obtained in the optics of crystalline clouds were summarized by Volkovitsky et al. (1984) and Liou (1992, 2002).

Ice crystals are usually much larger than the wavelength of the incident radiation. Thus, the extinction cross section, C_{ext}, does not depend on the wavelength and the refractive index of particles (Shifrin, 1951; Van de Hulst, 1957):

$$C_{ext} = 2s, \tag{3.38}$$

where s is the cross section of a particle, projected on the plane perpendicular to the incidence direction. It follows for N identical crystals in a fixed orientation that

$$\sigma_{ext} = 2Ns, \tag{3.39}$$

where N is number concentration of particles and σ_{ext} is the extinction coefficient. However, crystals differ by their shape, size, and orientation; thus, the extinction coefficient can be calculated as

$$\sigma_{ext} = 2N\bar{s}, \tag{3.40}$$

where $\bar{s}$ is the average cross section of particles. This equation can be written as

$$\sigma_{ext} = 2C_v \frac{\bar{s}}{\bar{V}}, \tag{3.41}$$

where C_v is the volumetric concentration of crystals and $\bar{V}$ is the average volume of crystals ($C_v = N\bar{V}$). It follows for convex crystals of the same shape in random orientation (Van de Hulst, 1957) that $\bar{\Sigma} = 4\bar{s}$, where $\bar{\Sigma}$ is the average surface area of particles. Therefore, we get:

$$\sigma_{ext} = \frac{3C_v}{2a_{ef}}, \tag{3.42}$$

where

$$a_{ef} = \frac{3\bar{V}}{\bar{\Sigma}} \tag{3.43}$$

is the effective radius of particles. This result is similar to Eq. (3.7). Only a portion of ice crystals (e.g., hexagonal plates and columns) are convex. For this and other reasons, one should expect that Eq. (3.42) will provide us with only a coarse approximation. It follows from Eq. (3.42) that

$$a_{ef} = \frac{3C_v}{2\sigma_{ext}}. \tag{3.44}$$

Eq. (3.44) suggests a method for indirect determination of the effective radius of particles in complex crystalline cloudy media.

3.2.2. Absorption coefficient

The absorption cross section of a single crystal at small absorption ($\alpha a_{ef} \to 0$) can be found in a full anology with Eq. (3.16):

$$C_{abs} = B\alpha V, \tag{3.45}$$

where V is the volume of a crystal, $\alpha = 4\pi\chi/\lambda$ and B is the coefficient proportionality, which depends on the shape and the real part of the refractive index of particles (Kokhanovsky and Macke, 1997), but not on their size (see Eq. (3.14)).

For an ensemble of crystals of identical shapes:

$$\sigma_{abs} = B\alpha C_v \tag{3.46}$$

and for N distinct shapes of crystals in a cloud:

$$\sigma_{abs} = \alpha \sum_{j=1}^{N} B_j C_{vj}. \tag{3.47}$$

Values of B_j do not depend on the imaginary part of the refractive index and the size of crystals, but only on the real part of the refractive index, n, of crystals and their shapes. The most probable values of $B = (1/C_v)\Sigma_{j=1}^{N} B_j C_{vj}$ in crystalline clouds can be found from experimental measurements of ratios $\sigma_{abs}/C_v\alpha$ in ice clouds of different microstructures.

The probability of photon absorption $\beta = \sigma_{abs}/\sigma_{ext}$ can be found from Eqs. (3.42) and (3.47):

$$\beta = \Xi\alpha a_{ef}, \tag{3.48}$$

where

$$\Xi = \frac{2}{3C_v} \sum_{j=1}^{N} B_j C_{vj}. \tag{3.49}$$

Using the model of fractal particles (Macke, 1994), one can obtain that $\Xi \approx 1.8$. Due to the complexity of crystal shapes in ice clouds, the accurate value of Ξ

cannot be found theoretically. Thus, measurements of this parameter are needed.

It is readily apparent from Eq. (3.48) that the single-scattering albedo

$$w_0 = 1 - \Xi \alpha a_e \tag{3.50}$$

for crystalline media. Note that the formulae presented here are valid only as $\alpha a_{ef} \to 0$. Generalization of these equations for arbitrary light absorption by droplets was given by Kokhanovsky and Macke (1997). Most recent parameterizations were developed by Yang et al. (2000) and McFarquhar et al. (2002).

3.2.3. Phase function

The phase function of ice clouds in the visible is the average over ensemble of phase functions of crystals with different shapes (Takano and Liou, 1995). It depends on the size of crystals in the small-angle scattering region and primarily on shape and structure of crystals at larger scattering angles. The phase function of ice clouds cannot be modelled (Liou and Takano, 1994) by spherical polydispersions. This is in contrast with integral light-scattering and absorption characteristics of crystalline clouds, which in many cases (see, e.g., Eqs. (3.21) and (3.48)) do can be modelled by a collection of spherical particles (Grenfell and Warren, 1999).

The phase function of hexagonal cylindrical crystals outside the diffraction region, presented in Fig. 12, was obtained using the Monte-Carlo ray tracing approach (Macke, 1994) for identical hexagonal ice cylinders of length 0.5 mm in random orientation at wavelength 0.5 μm. The side of the cross section was taken to be equal to 0.08 mm. Dominant features of the phase functions of this type are enhanced scattering at angles of 22° and 46°, corresponding to the so-called halos. Greenler (1980) states that he observes 22° halos in Wisconsin on 70 to 80 days of a typical year. The second halo at 46° is of a rare occurrence in natural conditions due to the presence of crystals of other shapes, which obscure halo phenomena. Both rainbow and glory (Tricker, 1970; Greenler, 1980; Konnen, 1985) are absent for ice clouds.

The backward cross section of hexagonal ice crystals of arbitrary orientation is calculated for visible light by means of a ray-tracing code by Borovoi et al. (2000). It is shown that backscattering of the tilted crystals is caused by a corner reflectorlike effect. A very large peak of backscattering is found for a tilt

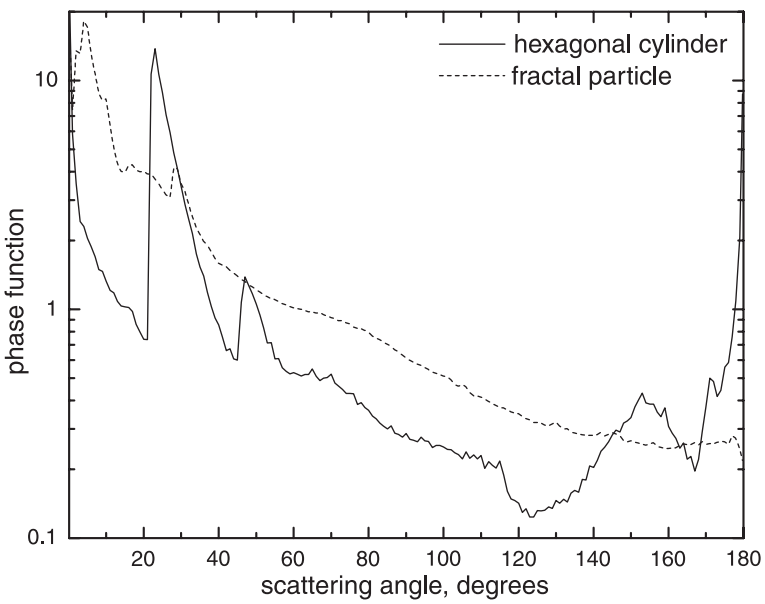

Fig. 12. Phase functions of hexagonal ice cylinders with the aspect ratio(length/size of the side of the hexagonal cross section) of 5.88 and fractal particles in random orientation at the wavelength 0.5 μm. Only the geometrical optics contribution of both phase functions is shown.

angle of 32.5° between the principal particle axis and the incidence direction. This peak is caused by multiple total internal reflections for part of the rays that are incident upon the skewed rectangular faces.

Realistic phase functions of a crystalline cloud that account also for diffraction of light at small angles and size/shape distribution of crystals are tabulated by Takano and Liou (1989) and Liou (1992) and are characterized by an asymmetry parameter equal to 0.75.

Calculation of phase functions of crystals of different shapes can be avoided by introducing the single fictive particle with the phase function similar to the phase function of an ensemble (Kokhanovsky, 2001a, 2003a,b,c). Particles with random stochastic surfaces were studied by Peltoniemi (1993) and Muinonen et al. (1996). The model of a fractal particle was introduced by Macke and Tzschichholz (1992), Macke (1994), and Macke et al. (1996). Depending on the parameters of roughness, these models can quite well describe the phase functions of ice crystals (Macke, 1994; Kokhanovsky, 2003a,b,c) and the mineral fraction of the atmospheric aerosol (Volten et al., 2001; Kokhanovsky, 2003a,b,c).

Phase function of a fractal particle, which may be a better description of complex shapes in crystalline clouds, is presented (along with that of a randomly oriented hexagonal cylinder) in Fig. 12. Data were obtained using the Monte-Carlo ray-tracing code (Macke, 1994; Macke et al., 1996). The fractal phase function is characterized almost the same value of the asymmetry parameter ($g \approx 0.74$) as the phase function of randomly oriented hexagonal crystals given in the same figure.

Linear combinations of functions presented in Figs. 7 and 12 with weights depending on the concentration of spherical particles, hexagonal cylinders and irregularly shaped particles in the cloud can be used to describe natural clouds. Note that other regular shapes, such as plates, can also contribute to the total phase function of an elementary volume of a cloudy medium. Measurements of phase functions of crystalline clouds were presented by Volkovitsky et al. (1984), Gayet (1998), Saunders et al. (1998), Barkey et al. (1999), Baran et al. (2001) and Jourdan et al. (2003).

Horizontal orientation of crystals may complicate the phase function in up to 40% of clouds (Chepfer et al. (1999)). In particular, the phase function of horizontally oriented crystals (e.g., plates) depends on directions of light incidence and observation separately and not on a single parameter (scattering angle) as for spherical or randomly oriented particles. Such clouds belong to a broad class of the so-called anisotropic media. The radiative transfer in ice clouds with horizontally oriented crystals was studied by Liou (2002). This is a major topic of modern cloud optics research. Note that clouds with horizontally oriented crystals are characterized by dichroism and birefringence (Van de Hulst, 1957).

3.2.4. Asymmetry parameter

Asymmetry parameters of crystals depend on the shape, but not on their size in the visible (Macke et al., 1996; Kokhanovsky and Nakajima, 1998), due to large size of ice crystals. Size-dependent wave corrections (see, e.g., Baran and Havemann, 1999), such as given by the second term in Eq. (3.36), can be neglected for crystals as $\lambda \to 0$.

The real part of the refractive index of ice crystals is also important, but it varies only slightly in the visible (see Fig. 1); this dependence can be neglected. The asymmetry parameter for ice clouds will be the average value over an ensemble of particles of different shapes. Macke et al. (1998) found from extensive numerical calculations that the asymmetry parameter, g, is in the range 0.79–0.85 for columns, 0.83–0.94 for plates, and 0.74 for polycrystals, represented by a fictive fractal particle in the visible. It is in the range 0.83–0.87 for spherical droplets. We see, therefore, that the value of g for cloudy media with ice crystals should be somewhere between 0.74 and 0.87. Larger values of g indicate that ice clouds are composed of plates only, which is never the case in natural conditions. We see that the co-asymmetry parameter, $G = 1 - g$, changes from 0.13 for water clouds to 0.26 for irregularly shaped particles. Actual values of g for a given cloud can be found only from direct measurements in natural ice clouds such as were performed by Garett et al. (2001), who found that the value of g is in the range 0.73–0.76, depending on the cloud area under investigation. They obtained values of g from measurements of the phase function inside the ice cloud in the angle range 10–175°. In one case, the value of g reached 0.81, but sublimation was noted, rendering it to be a typical case. The

asymmetry parameter of ice clouds does not vary considerably for visible light and, on average, is equal to 0.745, a value close to that for a fractal fictive particle and to the value for hexagonal crystals, which give the phase function, presented in Fig. 12.

We suggest that an asymmetry parameter value of 0.74 should be used for theoretical modelling of light propagation in crystal clouds. The corresponding value of G is equal to 0.26, which does not depend on the size of crystals because they are large as compared to the wavelength in the visible range of the electromagnetic spectrum. G does not depend on the shape of crystals because for a given cloud, we have a statistical and very broad distribution of shapes, which produce in the end a saturated value of the asymmetry parameter for a completely chaotic scattering. This scattering can be modelled by a single fractal fictive particle (Macke, 1994; Kokhanovsky, 2003a). It should be stressed, however, that the calculation of g involves also averaging over scattering angle (see Eq. (3.30)). Thus, the model of chaotic scattering is more appropriate for the value of g than for the phase function itself. The phase function should be modelled as a combination of light scattering by regular and irregularly shaped particles with different weights, as discussed above (see, e.g., Liou, 2002). Again, such a model can be established only from measurements performed in natural clouds.

Now we consider briefly the case of mixed ice–water clouds for which the value of G is

$$G = G_{\mathrm{i}} + \Upsilon G_{\mathrm{w}}, \tag{3.51}$$

where G_{i} and G_{w} are co-asymmetry parameters of ice and water particles, respectively, and Υ is the fraction of water droplets in a mixed cloud, defined as the ratio of number of droplets to a total number of particles in a mixed cloud. G_{i} and G_{w} do not vary significantly in mixed clouds; thus, in the first approximation, we can assume constant values for them. Measurements by Garett et al. (2001) suggest that $G_{\mathrm{i}} = 0.26$ and $G_{\mathrm{w}} = 0.13$. Then we have from Eq. (3.51):

$$\Upsilon = \frac{G}{0.13} - 2 \tag{3.52}$$

or approximately $\Upsilon = (4\langle\theta^2\rangle) - 2$. The correlation between values of G and Υ was confirmed experimentally (Garett et al., 2001). Therefore, measurements of G (or, alternatively, $\langle\theta^2\rangle$) in mixed clouds can yield the value of a liquid fraction, Υ.

It is evident (Kokhanovsky and Macke, 1997; Kokhanovsky, 2001a) that in the near-infrared range of the electromagnetic spectrum the larger size of crystals generally leads to larger asymmetry parameter. Detailed calculations of optical characteristics of ice crystals in the infrared for different shapes of crystals were performed by Zhang and Xu (1995) and Macke et al. (1998). Parameterization schemes for local optical characteristics of ice clouds were developed by Ebert and Curry (1992), Fu and Liou (1993), Fu (1996), Kokhanovsky and Macke (1997), Yang et al. (2000), Harrington and Olsson (2001), and McFarquhar et al. (2002). Selected parameterizations of cloud local optical characteristics given in this review are summarized in Table 4.

4. Radiative characteristics

4.1. The visible range

Let us consider now the global optical characteristics of clouds such as their reflection and transmission functions (Van de Hulst, 1980). They can be measured remotely by airborne, satellite and ground-based radiometers and spectrometers (Kondratyev and Binenko, 1984; Liou, 2002). The aim of this section is

Table 4
Integral local optical characteristics of clouds in visible and near infrared

LOC	Water cloud	Ice cloud	Range of validity
σ_{abs}	$(5/3)\alpha(1-\alpha a_{\mathrm{ef}})C_{\mathrm{v}}$	$B\alpha C_{\mathrm{v}}$	$\alpha a_{\mathrm{ef}} \to 0$
σ_{ext}	$(3/2a_{\mathrm{ef}})C_{\mathrm{v}}(1+1.1x_{\mathrm{ef}}^{-2/3})$	$(3/2a_{\mathrm{ef}})C_{\mathrm{v}}$	$x_{\mathrm{ef}} \to \infty,\ 2x_{\mathrm{ef}}(n-1) \to \infty$
$1-g$	$0.12+0.5x_{\mathrm{ef}}^{-2/3}-0.15\alpha a_{\mathrm{ef}}$	0.26	$x_{\mathrm{ef}} \to \infty,\ 2x_{\mathrm{ef}}(n-1) \to \infty,\ \alpha a_{\mathrm{ef}} \to 0$

Here $\alpha = 4\pi\chi/\lambda$ and $x_{\mathrm{ef}} = 2\pi a_{\mathrm{ef}}/\lambda$. The parameter B depends on the shape of crystals in a cloud (Kokhanovsky and Macke, 1997). It follows for fractals: $B \times 1.8$.

to introduce simple analytical formulae, which can be used to relate global optical characteristics of clouds to their local optical characteristics discussed in the previous section. This will also mean that we obtain direct relationships between observable quantities, such as cloud reflection and transmission functions, with microphysical parameters of clouds (e.g., the size and refractive index of particles, see Table 4).

We start from the study of the reflection function of a cloudy medium under an assumption that the cloud can be represented as a homogeneous plane-parallel layer. The absorption of light by particles is neglected in this section. This is a standard assumption in the visible range of the electromagnetic spectrum. However, in some cases the absorption of light by water clouds in visible cannot be neglected. This is due to various sources of pollution (Melnikova and Mikhailov, 1994, 2000; Asano et al., 2002; Vasilyev and Melnikova, 2002).

The reflection function of a cloud $R(\vartheta_0,\vartheta,\varphi)$ is defined as the ratio of reflected light intensity $I(\vartheta_0,\vartheta,\varphi)$ for the case of a cloud to that of an ideal Lambertian ideally white reflector

$$R(\vartheta_0,\vartheta,\varphi)=\frac{I(\vartheta_0,\vartheta,\varphi)}{I^*(\vartheta_0)}, \tag{4.1}$$

where

$$I^*(\vartheta_0)=F\cos\vartheta_0 \tag{4.2}$$

is the intensity of light reflected from the ideally white Lambertian reflector, πF is the solar flux on the area perpendicular to the direction of incidence, ϑ_0 is the solar angle, ϑ is the observation angle, and φ is the relative azimuth between solar and observation directions (Minin, 1988). Also, we will use $\mu=|\cos\vartheta|$, $\mu_0=\cos\vartheta_0$. For the Lambertian ideally white reflector from Eq. (4.1), $R\equiv 1$, which, by definition, does not depend on the viewing and observation geometry.

Although clouds are white when looking from space, their reflection function $R(\vartheta_0,\vartheta,\varphi)$ is not equal to one, but depends on the viewing and observation geometry. Results of calculations of the reflection function of an idealized semiinfinite nonabsorbing water cloud $R^0_\infty(\vartheta_0,\vartheta,\varphi)$ at the wavelength, $\lambda=0.65$ μm and the nadir observation are presented in Fig. 13. Calculations were performed for the gamma particle-size distribution, given by Eq. (2.3) at $\mu=6$. Values of effective radius in Fig. 13 were 6 and 16 μm, which cover the typical range for natural water clouds. $R(\vartheta_0,\vartheta,\varphi)$ can be smaller and larger than 1, depending on the incidence angle, which implies that depending on particular viewing geometries, clouds can be even more reflective than the ideally white Lambertian surface. This is mostly due to peculiarities of the phase function of cloudy media [e.g., in the backscattering ($\vartheta\approx\vartheta_0,\varphi\approx\pi$) region]. It follows from Fig. 13 that in the range of solar angles 30–60° and nadir observation, the reflection function of a semi-infinite water cloud is almost equal to the reflection function of an ideally white Lambertian reflector. It differs from 1 not more than by 10% for these geometries (Zege et al., 1991).

The reflection function $R^0_\infty(\vartheta_0,\vartheta,\varphi)$ can be represented by the following simple approximate equation (Kokhanovsky, 2002a):

$$R^0_\infty(\vartheta_0,\vartheta,\varphi)=\frac{b_1+b_2\cos\vartheta\cos\vartheta_0+p(\theta)}{4(\cos\vartheta+\cos\vartheta_0)} \tag{4.5}$$

where $\theta=\arccos(-\cos\vartheta\cos\vartheta_0+\sin\vartheta\sin\vartheta_0\cos\varphi)$ is the scattering angle, $p(\theta)$ is the phase function of a cloudy medium, and b_1 and b_2 are constants. Eq. (4.5) obeys to the reciprocity principle [$R^0_\infty(\vartheta_0,\vartheta,\varphi)=R^0_\infty(\vartheta,\vartheta_0,\varphi)$, see, e.g., Zege et al., 1991].

We found that $b_1=1.48$, $b_2=7.76$ for nadir observations (Kokhanovsky, 2002a). Comparison of the approximation and exact data in Fig. 13 shows that the accuracy of Eq. (4.5) is better than 2% at $\vartheta_0<85°$, $\vartheta=0°$. Constants b_1 and b_2 for other viewing geometries can be found using parametrizations of results obtained from the exact radiative transfer codes (see, e.g., Mishchenko et al., 1999). Approximations for the function $R^0_\infty(\vartheta_0,\vartheta,\varphi)$ at $\vartheta\neq 0°$ were also obtained by Melnikova et al. (2000a,b) and Kokhanovsky (2003c).

Eq. (4.5) can be used to find the reflection function of a finite cloud $R(\mu,\mu_0,\varphi,\tau)$ via the following formula (Germogenova, 1963; Van de Hulst, 1980, Minin, 1988):

$$R(\mu,\mu_0,\varphi,\tau)=R^0_\infty(\mu,\mu_0,\varphi)-t(\tau)K_0(\mu)K_0(\mu_0), \tag{4.6}$$

where

$$t=\frac{1}{0.75\tau(1-g)+\alpha} \tag{4.7}$$

is the global transmittance of a cloud, g is the asymmetry parameter studied above in detail, and $K_0(\mu)$ is

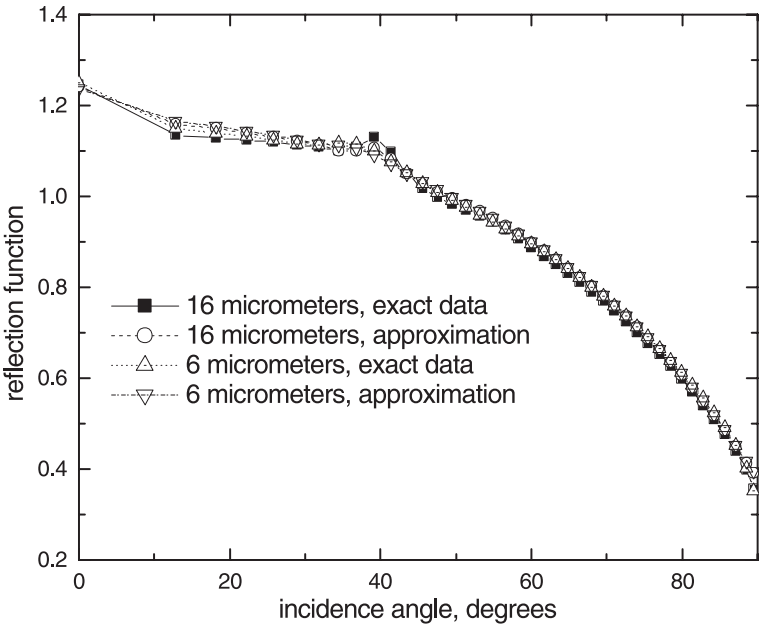

Fig. 13. Reflection function of an idealized semiinfinite nonabsorbing cloud $R^0_\infty(0,\vartheta_0,0)$ obtained from the exact radiative transfer code (Mishchenko et al., 1999) and approximation (4.5) at the wavelength $\lambda=0.65$ μm and the effective radii of droplets $a_{ef}=6$ and 16 μm. It is assumed that particles in a cloud are characterized by the gamma particle-size distribution (Eq. (2.3)) with the parameter $\mu=6$.

the escape function (Van de Hulst, 1980). Eqs. (4.6) and (4.7) are valid only in the absence of light absorption in a cloud. The escape function is defined via the solution of the characteristic integral equation (Van de Hulst, 1980). Note that the parameter α in Eq. (4.7) is defined as follows (Sobolev, 1972):

$$\alpha = 3\int_0^1 K_0(\mu)\mu^2 \mathrm{d}\mu. \tag{4.8}$$

The escape function, $K_0(\mu)$, only weakly depends on the cloud microstructure and can be presented by the following equation (Zege et al., 1991; Kokhanovsky, 2001a):

$$K_0(\mu) = \frac{3}{7}(1+2\mu). \tag{4.9}$$

The function $K_0(\mu_0)$ calculated with exact radiative transfer code with g equal to 0.75, 0.85, and 0.9 in the case of Heney–Greenstein phase function

$$p(\theta) = \sum_{l=0}^{\infty}(2l+1)g^l P_l(\cos\theta), \tag{4.10}$$

where P_l is the Legendre polynomial and, according to Eq. (4.10), is presented in Fig. 14. We see that $K_0(\mu)$ almost does not depend on g at $\mu \geq 0.2$ ($\vartheta < 78°$). This is the case even for $g=0$ and for the Mie-type phase functions (Kokhanovsky, 2001a). There is some dependence of the escape function on the microstructure of the cloud at the range of observation angles $\vartheta = 80–90°$, but the cloud-top inhomogeneity plays a role at such grazing observation angles, preventing use of the idealized plane-parallel layer approximation.

The variability of $K_0(\mu)$ at $\mu=0.2–1.0$ for different values of $g=0.75–0.9$ is well inside the 2% sensitivity range. This coincides with the error of Eq. (4.9) at $\mu \geq 0.2$, being smaller than 2%.

Note that function (4.9) also describes the angular distribution of solar light transmitted by a cloud (Zege et al., 1991; Kokhanovsky, 2001a).

The substitution of Eq. (4.9) into Eq. (4.8) yields:

$$\alpha = \frac{15}{14} \approx 1.07 \tag{4.11}$$

independently of cloud microstructure. The value of α, numerically calculated by King (1987), assuming the

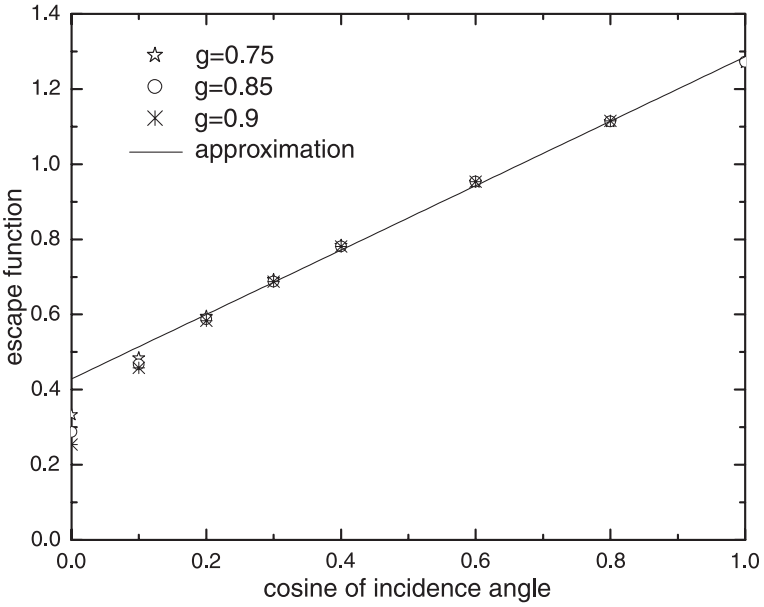

Fig. 14. Escape function, calculated with exact radiative transfer code for the Heyney–Greenstein phase function at $g=0.75$, 0.8 and 0.9 (Yanovitskij, 1997) and with approximation given by Eq. (4.9).

fair weather cumulus cloud model, is given approximately by 1.07 in agreement with our estimation. King (1987) used Mie theory to find the phase function of a cloudy medium for the calculation of $K_0(\mu_0)$ and α via Eq. (4.8). Yanovitskij (1997) found the same value of α for Heney–Greenstein phase functions with asymmetry parameters in the range 0.0–0.9. This supports the approximation of a fixed value of α in Eq. (4.7), given by Eq. (4.11), independently of cloud microphysical parameters.

The error of Eq. (4.6) is smaller than 1% at $\tau \geq 10$ (King, 1987). It rapidly increases with τ. Kokhanovsky and Rozanov (2003) proposed to modify Eq. (4.6) to diminish the error of this equation for smaller τ. In particular, they proposed to use instead of t in Eq. (4.6):

$$t^* = t - \tilde{t}, \qquad \tilde{t} = (4.86 - 13.08\mu\mu_0 + 12.76\mu^2\mu_0^2)/\tau.$$

This modification allows to increase the accuracy of approximate formulae considered for smaller τ (down to $\tau=5$). This range of optical thicknesses is that most frequently observed in water clouds both with satellite and ground-based techniques (see Fig. 15, prepared from data given by Trishchenko et al., 2001). Kokhanovsky and Rozanov (2003) found that the error of the modified reflection function at the nadir observation is smaller than 5% for solar angles smaller than 74°.

Eq. (4.6) is readily modified to account for the Lambertian light reflection from the underlying surface (Sobolev, 1972):

$$\hat{R}(\mu,\mu_0,\varphi,\tau) = R(\mu,\mu_0,\varphi,\tau) + \frac{r_s T(\mu) T(\mu_0)}{1 - r_s r}, \tag{4.12}$$

where $\hat{R}$ is the reflection function of a Lambertian surface-cloud system, r_s is the spherical albedo of the Lambertian surface, which may depend on the wavelength, $R \equiv \hat{R}$ ($r_s=0$),

$$T(\mu) = tK_0(\mu) \tag{4.13}$$

is the diffuse transmittance of a cloud layer (Sobolev, 1972) and $r=1-t$ is the spherical albedo of a non-absorbing cloud.

We have neglected the direct solar light term (Liou, 2002) in Eq. (4.12) due to a large thickness of clouds under consideration.

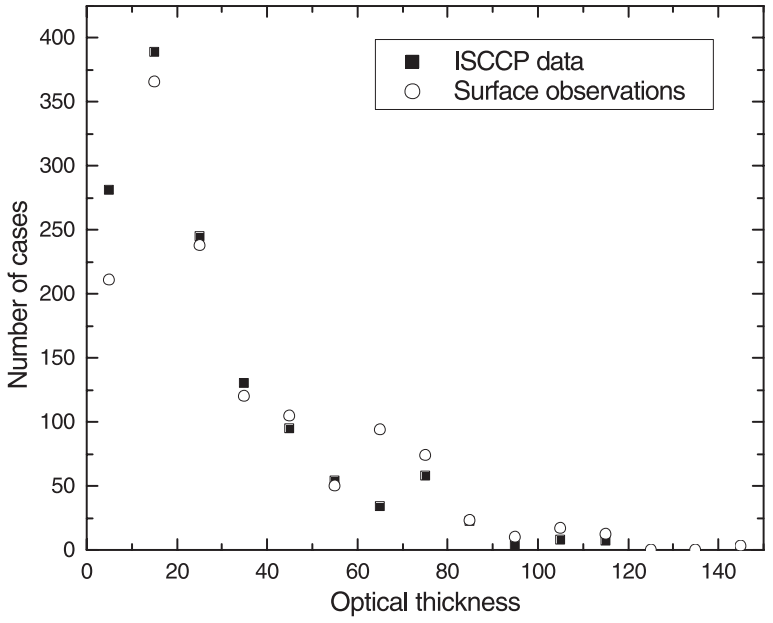

Fig. 15. Frequency of registration of different optical thicknesses of cloudy media obtained from satellite and ground measurements as presented by Trishchenko et al. (2001).

Finally, substituting Eqs. (4.6) and (4.13) into Eq. (4.12), it follows for the reflection function of a Lambertian surface-nonabsorbing cloud system (Kokhanovsky et al., 2003):

$$\hat{R}(\mu,\mu_0,\varphi,\tau) = R^0_\infty(\mu,\mu_0,\varphi) - \frac{t(1-r_s)}{1-r_s(1-t)}K_0(\mu)K_0(\mu_0). \tag{4.14}$$

This formula can be used as a basis for the semi-analytical cloud retrieval algorithm (Kokhanovsky et al., 2003). Note that $\hat{R}(\mu,\mu_0,\varphi,\tau) \equiv R^0_\infty(\mu,\mu_0,\varphi)$ at $r_s = 1$.

4.2. The near-infrared range

Unfortunately, the relatively simple Eq. (4.6) cannot be used to calculate the reflection function of a finite cloud in the near-infrared region of the electromagnetic spectrum due to the presence of absorption bands of liquid water (see Fig. 2). Alternatively, the following formula applies (Germogenova, 1963; Van de Hulst, 1980; King, 1987; Nakajima and King, 1992; Vasilyev and Melnikova, 2002):

$$R(\mu,\mu_0,\varphi,\tau) = R_\infty(\mu,\mu_0,\varphi) - \frac{mle^{-2\gamma\tau}}{1-l^2e^{-2\gamma\tau}}K(\mu)K(\mu_0), \tag{4.15}$$

where γ is the so-called diffusion exponent, $K(\mu)$ and R_∞ are the escape function and the reflection function of an absorbing semiinfinite medium with the same local optical characteristics as a finite layer under study, respectively. Eq. (4.15) accounts for the influence of light absorption on the reflection function of clouds. The reflection function decreases if additional absorbers are present in cloud droplets. Constants l and m are defined by the following integrals (Van de Hulst, 1980):

$$l = 2\int_{-1}^{1} i^2(\eta)\eta d\eta, \tag{4.16}$$

$$m = 2\int_{0}^{1} K(\eta)i(-\eta)\eta d\eta, \tag{4.17}$$

$i(\eta)$ being the angular distribution of light in deep layers of a cloud, defined as the so-called asymptotic regime (Sobolev, 1972).

Functions $R_\infty(\mu,\mu_0,\varphi)$, $K(\mu)$, and constants m and l have the following asymptotic forms when light absorption by droplets is relatively small ($\omega_0 \to 1$) (Van de Hulst, 1980):

$$R_\infty(\mu,\mu_0,\varphi) = R^0_\infty(\mu,\mu_0,\varphi) - 4\sqrt{\frac{1-\omega_0}{3(1-g)}}K_0(\mu)K_0(\mu_0), \quad (4.18)$$

$$K(\mu) = K_0(\mu)\left(1 - 2\alpha\sqrt{\frac{1-\omega_0}{3(1-g)}}\right), \quad (4.19)$$

$$m = 8\sqrt{\frac{1-\omega_0}{3(1-g)}}, \quad (4.20)$$

$$l = 1 - 4\alpha\sqrt{\frac{1-\omega_0}{3(1-g)}}, \quad (4.21)$$

and $\gamma \to \sqrt{3(1-\omega_0)(1-g)}$ as the single-scattering albedo, $\omega_0 \to 1$. Thus, at $\omega_0=1$, $R_\infty = R^0_\infty$, $K(\mu) = K_0(\mu)$, $m = l = 0$, and Eq. (4.15) transforms into Eq. (4.6).

Note that Eqs. (4.18)–(4.21) follow from the asymptotic analysis of the radiative transfer equation (Van de Hulst, 1980). Integration of Eq. (4.18) with respect to all angles yields $r_\infty = 1 - y$, where $y = 4\sqrt{\frac{1-\omega_0}{3(1-g)}}$ and r_∞ is the spherical albedo of a weakly absorbing semiinfinite cloud (Van de Hulst, 1980). Thus, the parameter y can be interpreted as a fraction of photons absorbed in a weakly absorbing semi-infinite cloud. It depends both on the single-scattering albedo and the asymmetry parameter. Larger values of g imply that photon scattering increases at small angles. Thus, the photon path length before its escape from the medium is also increased. As a consequence, this results in increased light absorption in the medium. Clouds having larger values of g, therefore, absorb more light. Media having different values of ω_0 and g, but the same values of y, have the same values of r_∞. The parameter $s = \sqrt{\frac{1-\omega_0}{3(1-\omega_0 g)}}$ is called the similarity parameter in the radiative transfer textbooks (Van de Hulst, 1980). It is a useful parameter, describing the optical properties of clouds. We see that $y \to 4s$ as $\omega_0 \to 1$. Substituting y into Eqs. (4.18)–(4.21) yields:

$$R_\infty(\mu,\mu_0,\varphi) = R^0_\infty(\mu,\mu_0,\varphi) - yK_0(\mu)K_0(\mu_0), \quad (4.22)$$

$$K(\mu) = K_0(\mu)\left(1 - \frac{\alpha y}{2}\right), \quad (4.23)$$

$$m = 2y, \quad (4.24)$$

and

$$l = 1 - \alpha y. \quad (4.25)$$

Eqs. (4.22)–(4.25) were derived assuming that $\omega_0 \to 1$. Alternatively, the right-hand sides of Eqs. (4.22)–(4.25) give us the first terms of the expansion of corresponding functions with respect to y (Minin, 1988). The accuracy of these equations decreases with y quite rapidly. The next terms of the expansions ($\sim y^2$) are given by Minin (1988) and Melnikova et al. (2000b). Still higher terms are not known or quite complex (Minin, 1988), but it has been shown that the following equations account approximately for higher-order terms (Rozenberg, 1962; Zege et al., 1991; Kokhanovsky et al., 1998b, 2003):

$$R_\infty(\mu,\mu_0,\varphi) = R^0_\infty \exp[-yu(\mu,\mu_0,\varphi)], \quad (4.26)$$

$$mK(\mu)K(\mu_0) = [1 - \exp(-2y)]K_0(\mu)K_0(\mu_0), \quad (4.27)$$

$$l = \exp(-\alpha y), \quad (4.28)$$

where a viewing function u is defined by

$$u(\mu,\mu_0,\varphi) = \frac{K_0(\mu)K_0(\mu_0)}{R^0_\infty(\mu,\mu_0,\varphi)} \quad (4.29)$$

and does not depend on ω_0 and τ. The viewing function has only a weak dependence on the microphysical characteristics of clouds (e.g., the droplet-size distribution). This follows from the low sensitivity of the functions $R^0_\infty(\mu,\mu_0,\varphi)$ and $K_0(\mu)$ in Eq. (4.29) to the microphysical characteristics of clouds (see Figs. 13 and 14). The physical sense of the function (4.29) has been discussed by Kokhanovsky (2002b). The accuracy of Eq. (4.26) was studied by Kokhanovsky

(2002c). It is better than 10% at $y \le 0.8$ for the nadir observation and solar angles in the range 0–75°.

Eqs. (4.26)–(4.28) avoid the solution of integral equations (Van de Hulst, 1980; Yanovitskij, 1997) for the determination of functions $R_\infty(\mu,\mu_0,\varphi)$ and $K(\mu)$ in Eq. (4.15). They transform into exact asymptotic results (Eqs. (4.22)–(4.25)) as $y \to 0$.

Substituting Eqs. (4.27) and (4.28) into Eq. (4.15), we have:

$$R(\mu,\mu_0,\varphi,\tau) = R_\infty(\mu,\mu_0,\varphi) - te^{-x-y}K_0(\mu)K_0(\mu_0), \tag{4.30}$$

where $x=\gamma\tau$ and the global transmittance, t, is given by (Kokhanovsky et al., 2003):

$$t = \frac{\sinh y}{\sinh(\alpha y + x)} \tag{4.31}$$

Eq. (4.31) yields Eq. (4.7) at $\omega_0=1$. The value of $\exp(-x)$ describes light attenuation in deep layers of a cloud (Van de Hulst, 1980).

Eq. (4.30) was first proposed by Rozenberg (1962, 1967), but he assumed that $\alpha=1$ in Eq. (4.31), which is not consistent with the exact asymptotic result given by Eq. (4.7).

The range of applicability of Eq. (4.26) with respect to higher values of y can be readily extended using the following correction (Kokhanovsky, 2002c):

$$R_\infty(\mu,\mu_0,\varphi) = R^0_\infty(\mu,\mu_0,\varphi) \times \exp[-y(1-cy)u(\mu,\mu_0,\varphi)]. \tag{4.32}$$

where $c=0.05$. The value of c was obtained by the parameterization of calculations with exact radiative transfer code, developed by Mishchenko et al., 1999. Kokhanovsky (2002c) found that the error of Eq. (4.32) is smaller than 5% at the nadir observation, the solar angle smaller than 75° and $y \le 1.18$.

Detailed studies of accuracy of Eq. (4.30) were performed by Kokhanovsky et al. (1998b). In particular, they found that the error of Eq. (4.30) is smaller than 15% at $\tau \ge 10$ and $\omega_0 > 0.95$. Kokhanovsky and Rozanov (2003) proposed to substitute $t\exp(-x)$ in Eq. (4.30) by $\hat{t}=t\exp(-x)-\tilde{t}$, where $\tilde{t}$ has been introduced in Section 4.1. The accuracy of the modified equation is given in Fig. 16a–d (Kokhanovsky and Rozanov, 2003). It is better than 6% at solar angles smaller than 70° at nadir observation, if $\tau \ge 5$, $\lambda \le 1.5$ μm for the Deirmendjian's Cloud C.1 model with $a_{ef}=6$ μm.

Eq. (4.30) can be used to determine the optical thickness and effective radius from spectral reflection function measurements over extended cloud fields (Kokhanovsky and Zege, 1996; Kokhanovsky et al., 2002).

Surface reflection is accounted for by Eq. (4.12). Substitution of Eq. (4.30) into Eq. (4.12) yields:

$$\hat{R}(\mu,\mu_0,\varphi,\tau) = R_\infty(\mu,\mu_0,\varphi,\tau) - \left[\exp(-x-y) - \frac{tr_s}{1-r_s r}\right]T(\mu,\mu_0), \tag{4.33}$$

where

$$T(\mu,\mu_0) = tK_0(\mu)K_0(\mu_0) \tag{4.34}$$

is the transmittance function of a cloud, r is the total reflectance of a cloud, t is given by Eq. (4.31), and R_∞ is given by Eq. (4.32). It is assumed that $tK(\mu)K(\mu_0) \approx tK_0(\mu)K_0(\mu_0)$. This assumption is valid for single-scattering albedos close to one.

4.3. Total reflectance

Let us find the approximate solution for the total reflectance r in Eq. (4.33). Clearly, the value of $r \neq 1-t$. This is due to light absorption in a cloudy medium.

The total reflectance or the spherical albedo r is defined by (Sobolev, 1972):

$$r = \frac{1}{2\pi}\int_0^{2\pi} d\varphi \int_0^{\pi} d\vartheta \sin 2\vartheta \times \int_0^{\pi} d\vartheta_0 \sin 2\vartheta_0 R(\vartheta_0,\vartheta,\varphi,\tau). \tag{4.35}$$

Let us also introduce the plane albedo

$$\Re(\vartheta_0) = \frac{1}{2\pi}\int_0^{2\pi} d\varphi \int_0^{\pi} d\vartheta \sin 2\vartheta R(\vartheta_0,\vartheta,\varphi,\tau)$$

and the diffuse transmittance

$$T(\vartheta_0) = \frac{1}{2\pi}\int_0^{2\pi} d\varphi \int_0^{\pi} d\vartheta \sin 2\vartheta T(\vartheta_0,\vartheta,\varphi,\tau).$$

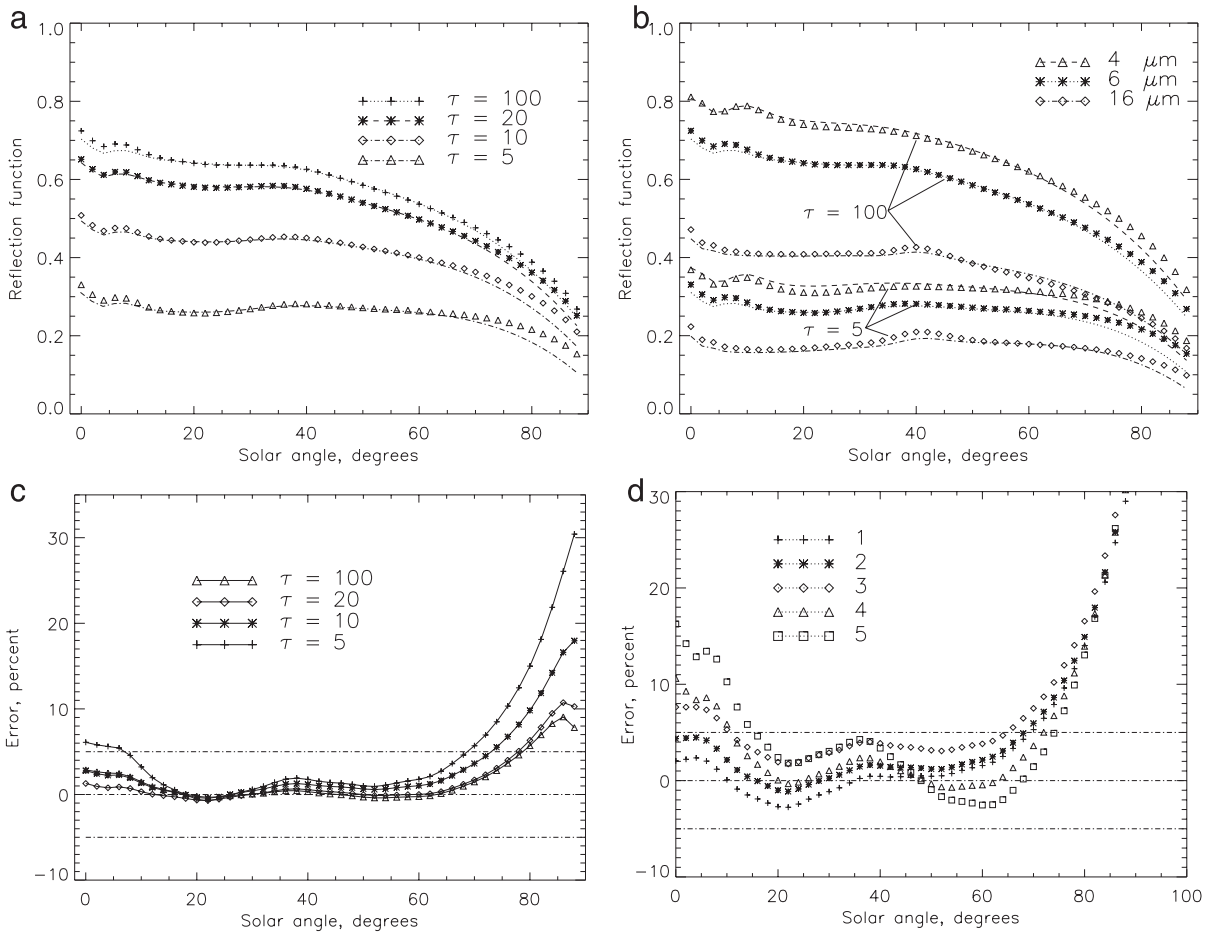

Fig. 16. (a) Dependence of the reflection function of a plane-parallel homogeneous cloud layer with water droplets on the solar zenith angle at nadir observation for different values of the cloud optical thickness at the effective radius of droplets equal to 6 μm, the wavelength equal to 1.55 μm (exact data - symbols, approximation - lines). The droplet-size distribution is given by Eq. (2.3) at μ=6 (Kokhanovsky and Rozanov, 2003). (b) The same as in Fig. 16a but for various effective radii and τ=5, 100 (Kokhanovsky and Rozanov, 2003). (c) The error of approximation obtained using data in Fig. 16a (Kokhanovsky and Rozanov, 2003). (d) The error of approximation for various values of y=0.12 (1), 0.27 (2), 0.37 (3), 0.83 (4), and 1.2 (5) and τ=5 (Kokhanovsky and Rozanov, 2003).

For the case of idealized semiinfinite nonabsorbing clouds (Sobolev, 1972) and as a result of the conservation of energy law,

$$\frac{1}{2\pi}\int_0^{2\pi} d\varphi \int_0^{\pi/2} d\vartheta_0 \sin 2\vartheta_0 \times \int_0^{\pi/2} d\vartheta \sin 2\vartheta R^0_\infty(\vartheta_0,\vartheta,\varphi) = 1 \qquad (4.36)$$

and

$$\frac{1}{2\pi}\int_0^{2\pi} d\varphi \int_0^{\pi/2} d\vartheta \sin 2\vartheta R^0_\infty(\vartheta_0,\vartheta,\varphi) = 1, \qquad (4.37)$$

i.e., all photons injected into a cloudy medium are reflected back in outer space after an infinite travel time. Here $R^0_\infty(\vartheta_0,\vartheta,\varphi)$ is the reflection function of a semiinfinite nonabsorbing cloud. The reflection function $R^0_\infty(\vartheta_0,\vartheta,\varphi)$ of a cloudy medium only weakly

depends on its microstructure (see Fig. 13); by definition, it does not depend on either the optical thickness, $\tau = \sigma_{ext} L$, or the single-scattering albedo, $\omega_0 = \sigma_{sca}/\sigma_{ext}$. Here σ_{ext} is the extinction coefficient and σ_{sca} is the scattering coefficient of a cloudy layer of the geometrical thickness L.

It follows from Eqs. (4.30) and (4.35) for absorbing clouds:

$$r = r_\infty - t\exp(-x-y), \tag{4.38}$$

where

$$r_\infty = \frac{1}{2\pi}\int_0^{2\pi} d\varphi \int_0^{\pi/2} d\vartheta \sin 2\vartheta \times \int_0^{\pi/2} d\vartheta_0 \sin 2\vartheta_0 R_\infty(\vartheta_0, \vartheta, \varphi) \tag{4.39}$$

and we take the normalization condition (Van de Hulst, 1980)

$$2\int_0^1 d\mu \mu K_0(\mu) = 1 \tag{4.40}$$

into account. The approximate formula (4.10) for $K_0(\mu)$ obeys the exact integral relation (4.40). The constant r_∞ represents the total reflectance of a semiinfinite layer. According to the definition (Eq. (4.36)), $r_\infty = 1$ at $\omega_0 = 1$. Eq. (4.39) is not readily analytically integrated at arbitrary values of ω_0, but it follows from Eqs. (4.18) and (4.39) as $\omega_0 \to 1$ (see also the discussion in the previous section) that

$$r_\infty = 1 - y. \tag{4.41}$$

At larger values of y using the same substitution as was used in the derivation of Eq. (4.28) from Eq. (4.25), the integral (Eq. (4.39)) gives approximately

$$r_\infty = \exp(-y) \tag{4.42}$$

or (see Eq. (4.28)) $r_\infty = l^{1/\alpha}$. Similar result for the plane albedo reads (Kokhanovsky, 2001a):

$$\Re_\infty(\mu_0) = \exp[-yK_0(\mu_0)]. \tag{4.43}$$

It easy to show that the diffuse transmittance is given by the following equation (Kokhanovsky, 2001a):

$$T(\mu_0) = tK_0(\mu_0). \tag{4.44}$$

The accuracy of Eq. (4.42) is studied in Fig. 17a,b. We conclude that the accuracy of this formula is better than 5% at $\omega_0 > 0.93$ for crystalline clouds. For water clouds, the accuracy of this formula is better than 5% at $\omega_0 > 0.97$.

Combining Eqs. (4.31), (4.38) and (4.42), we have for the total reflectance of a cloud layer:

$$r = \frac{\sinh(x+\alpha y)\exp(-y) - \sinh(y)\exp(-x-y)}{\sinh(x+\alpha y)}. \tag{4.45}$$

Substitution of Eq. (4.45) into Eq. (4.33) enables the reflection function of a cloud over underlying surface with the spherical albedo r_s to be calculated. Such calculations were performed and presented in a graphical form by Kokhanovsky et al. (1998b).

Total light absorptance in a cloud layer is given by $a = 1 - r - t$, where r is calculated by Eq. (4.42) and t by Eq. (4.31). As a result, we have the following analytical equation for the total light absorbtion inside a plane-parallel cloud having a finite thickness:

$$a = \frac{\sinh(x+\alpha y)[1-\exp(-y)] - \sinh(y)[1-\exp(-x-y)]}{\sinh(x+\alpha y)} \tag{4.46}$$

It follows as $\alpha \equiv 1$:

$$r = \frac{\sinh(x)}{\sinh(x+y)}, \quad t = \frac{\sinh(y)}{\sinh(x+y)}, \quad a = \frac{\sinh(x+y) - \sinh(x) - \sinh(y)}{\sinh(x+y)}, \tag{4.47}$$

which yields the well-known formulae presented elsewhere (see, e.g., Zege et al., 1991).

Overall, the global radiative characteristics of cloudy media are well described by only two parameters, which are called the generalized radiative transfer parameters (Zege et al., 1991):

$$x = \tau\sqrt{3(1-\omega_0)(1-g)}, \quad y = 4\sqrt{\frac{1-\omega_0}{3(1-g)}}. \tag{4.48}$$

The parameter x describes the attenuation of a light field in deep layers of semiinfinite weakly absorbing

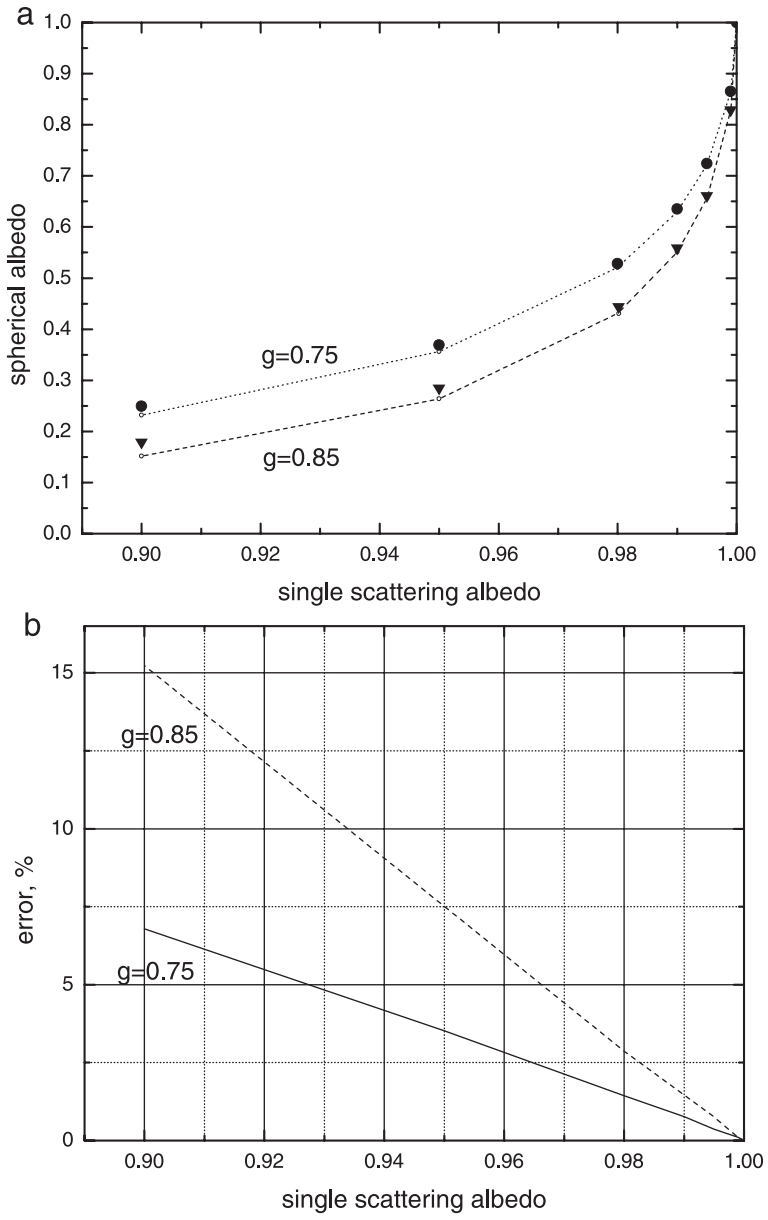

Fig. 17. (a) Cloud spherical albedo calculated with the exact radiative theory (Yanovitskij, 1997) (symbols) and according to approximation (4.42) (lines) at $g=0.75$, 0.8 and various ω_0. In exact calculations, Heney–Greenstein phase function was assumed. (b) Errors of Eq. (4.42) as obtained from data in Fig. 17a.

media. For the light intensity in deep layers, $I(\mu,\tau)=\psi(\mu)\exp(-x)$, where the angular distribution of light field $\psi(\mu)$ does not depend on the optical depth, τ. We see from Eq. (4.42) that $y=\ln(1/r_\infty)$. Thus, the radiative characteristics of optically thick cloud layers are determined by parameters x and y, which govern asymptotic regime and light reflection for semiinfinite cloudy media.

Table 5
Radiative characteristics of cloudy media

Radiative characteristic	Equation
Reflection function	$R(\mu_0,\mu,\varphi)=R_\infty(\mu,\mu_0,\varphi)-t\exp(-x-y)K_0(\mu)K_0(\mu_0)$
Plane albedo	$\Re(\mu_0)=\Re_\infty(\mu_0)-t\exp(-x-y)K_0(\mu_0)$
Spherical albedo	$r=r_\infty-t\exp(-x-y)$
Transmission function	$T(\mu_0,\mu,\varphi)=tK_0(\mu_0)K_0(\mu)$
Diffuse transmittance	$T(\mu_0)=tK_0(\mu_0)$
Global transmittance	$t=\sinh y/\sinh(\alpha y+x)$

Here $R_\infty(\mu_0,\mu,\varphi)=R^0_\infty(\mu_0,\mu,\varphi)\exp[-yu(\mu_0,\mu,\varphi)]$, $u(\mu_0,\mu,\varphi)=K_0(\mu_0)K_0(\mu)/R^0_\infty(\mu_0,\mu,\varphi)$, $\Re_\infty(\mu_0)=\exp[-yK_0(\mu_0)]$, $K_0(\mu_0)=(3/7)(1+2\mu_0)$, $r_\infty=\exp(-y)$, $\alpha=1.07$, and $R^0_\infty(\mu_0,\mu,\varphi)$ is the reflection function of a semiinfinite nonabsorbing cloud medium, $x=\tau\sqrt{3(1-\omega_0)(1-g)}$, $y=4\sqrt{\frac{1-\omega_0}{3(1-g)}}$.

This concludes the consideration of reflection, transmission, and absorption characteristics of cloudy media. For the sake of convenience, we present main equations of this section in Table 5. They can be used for a rapid estimation of radiative characteristics of water clouds, giving that their microphysical or local optical parameters are known. Also they give a convenient formulation and starting point for a semi-analytical solution of the inverse problem, namely, for finding τ and a_{ef} from spectral measurements of reflected light (Kokhanovsky et al., 2003).

For instance, measurements of light fluxes above and below clouds were performed using pyranometers by Asano et al. (2002). They used look-up table approach to retrieve cloud properties. Taking into account that the cloud system studied was optically thick, more simple solutions given here can be equally applied, leading in the decrease in the computational burden.

5. Polarization characteristics

5.1. Introduction

Cloudy media do not only absorb and scatter radiation. They also can be considered as major sources (along with aerosols, gases, and underlying surfaces) of polarized light in the terrestrial atmosphere. Clouds introduce a new property to incoming unpolarized solar light, namely, the preferential direction of oscillation of the electric vector in a light beam (Kokhanovsky, 2003b). Generally speaking, both reflected and transmitted light is elliptically polarized.

The polarization arises mainly due to single scattering of light by a water droplet, an aerosol particle or an ice crystal. Molecular scattering is another source of the polarized light in the terrestrial atmosphere. Multiple scattering, which is of particular importance for clouds, leads to randomization both photons directions and polarization states. This decreases light polarization due to increase in the optical thickness of a cloud. Another effect of multiple scattering is the introduction of ellipticity in scattered light beams. It should be pointed out that the solar light scattered by spherical water droplets becomes partially linearly polarized. This is due to the fact that the ellipticity of singly scattered light is equal to zero for spherical scatterers if the incident light is unpolarized (Van de Hulst, 1957).

Studies of polarization characteristics of solar light transmitted and reflected by cloudy media have a long history (Hovenier, 1971; Hansen, 1971a,b; Hansen and Hovenier, 1974; Gehrels, 1974; Coffeen, 1979; Coulson, 1988; Knibbe, 1997; Kokhanovsky, 2003b). However, the real burst of research in this area was given by a launch of the Polarization and Directionality of Earth Reflectances (POLDER) instrument on board the Japanese ADEOS-I satellite (Deschamps et al., 1994; Chepfer et al., 2001). The POLDER was able to transmit to ground stations a huge amount of information about polarization characteristics of light reflected from cloudy media, aerosols, and underlying surfaces at several wavelengths. Specifically, the first three components of the Stokes vector $\vec{S}_r(I,Q,U,V)$ (Chandrasekhar, 1950) have been measured for wavelengths, λ, equal to 443, 670, and 865 nm. There is no doubt that even more advanced polarimeters (see, e.g., Cairns et al., 1999) with more wide spectral coverage will appear on board different satellites in future, which makes further theoretical studies of polarization characteristics of cloudy media extremely important. This is due to potential possibilities for global retrievals of cloud microphysical parameters (Breon and Goloub, 1998), the shape of particles (Deschamps et al., 1994) and the optical thickness of clouds (Kokhanovsky, 2000) based on polarization measurements.

Of course, similar information can be obtained from the reflected intensity measurements. However, it could well appear that the degree of polarization can be used as a source of additional information about cloud particle-size distributions close to the top of a clouds (Breon and Goloub, 1998). Indeed, the high proportion of photons scattered from a thin upper layer of a cloud in creating light polarization is quite understandable. Multiply scattered light fluxes from deep layers are hardly polarized at all. Radiative characteristics, on the other hand, represent the cloud as a whole. Thus, the effective radius derived from radiative measurements is an average of large ensembles, possibly very different particle-size distributions, present in different parts of cloudy media.

It has been emphasized by Hansen (1971a) that the fact that the polarization data refers to cloud tops may be not a drawback, but an advantage. Indeed, it is easier to interpret observations which do not refer to some average values over the entire cloud depth.

The polarization characteristics of cloudy media can be studied applying numerical codes (Hansen, 1971a; Liou, 1992) based on the vector radiative transfer equation solution. However, one can also use the fact that cloud fields are optically thick in most cases (Kondratyev and Binenko, 1984). This allows application of vector asymptotic analytical relations (Domke, 1978) derived for optically thick disperse media with arbitrary phase functions and absorption. These solutions help clarify physical mechanisms and main features behind the polarization change due to the increase of the size of droplets or the thickness of a cloud. Analytical solutions also provide an important tool for the simplification of the inverse problem. They can be used, e.g., in studies of the information content of polarimetric measurements.

The drawback of well-known vector asymptotic theory for optically thick layers (Domke, 1978) is related to the fact that the main equations of this theory depend on different auxiliary functions and parameters. Calculations of these functions and parameters are rather complex due to their general applicability in terms of the single-scattering albedo.

The special case of weakly absorbing light scattering media was considered by Kokhanovsky (2001a) in the framework of the modified asymptotic theory. Formulae obtained are rather simple and allow for semianalytical solution of the inverse problem (Kokhanovsky and Weichert, 2002). They can be applied to water clouds due to weak absorption of light by water droplets in a broad spectral range (at least up to 2.2 μm, see Fig. 2).

5.2. Reflection and transmission matrices

Let us introduce the reflection $\hat{R}(\mu,\mu_0,\varphi)$ and transmission $\hat{T}(\mu,\mu_0,\varphi)$ matrices of cloudy media. Reflection and transmission matrices depend on the optical thickness, τ, of a cloud, microstructure of a cloud, cosine μ_0 of the solar angle ϑ_0, cosine μ of the viewing angle ϑ, and the relative azimuth $\varphi = \psi - \psi_0$, where ψ_0 and ψ are azimuths of the Sun and observer, respectively. The importance of these matrices is that they can be used for the calculation of the Stokes vector of reflected $\vec{S}_r(I,Q,U,V)$ and transmitted $\vec{S}_t(I',Q',U',V')$ light under arbitrary illumination of a cloudy layer. Namely, it follows for plane-parallel cloudy layers (Hovenier, 1971):

$$\vec{S}_r(\mu,\varphi) = \frac{1}{\pi}\int_0^1 d\mu'\mu'\int_0^{2\pi} d\varphi'\hat{R}(\mu,\mu',\varphi-\varphi') \times \vec{S}_0(\mu',\varphi'), \tag{5.1}$$

$$\vec{S}_t(\mu,\varphi) = \frac{1}{\pi}\int_0^1 d\mu'\mu'\int_0^{2\pi} d\varphi'\hat{T}(\mu,\mu',\varphi-\varphi') \times \vec{S}_0(\mu',\varphi') + \vec{S}_0(\mu,\varphi)\exp\left(-\frac{\tau}{\mu_0}\right), \tag{5.2}$$

where $\vec{S}_0(\mu,\varphi)$ represents the Stokes vector of the incident light beam. The second term in Eq. (5.2) is small for most of cloudy media ($\tau \gg 1$) and can be neglected.

In a good approximation, the Sun is a source of unpolarized light incident from only one direction (μ_0, φ_0). Then it follows:

$$\vec{S}_0(\mu,\varphi) = \frac{1}{\mu_0}\delta(\mu-\mu_0)\delta(\psi-\psi_0)\pi\vec{F}, \tag{5.3}$$

where vector $\vec{F}$ is normalized so that the first element of $\pi\vec{F}$ (namely, πF_1) is the net flux of solar beam per

unit area of a cloud layer. Eqs. (5.1) and (5.2) simplify if one accounts for Eq. (5.3):

$$\vec{S}_r(\mu,\varphi) = \hat{R}(\mu,\mu_0,\psi-\psi_0)\vec{F}, \tag{5.4}$$

$$\vec{S}_t(\mu,\varphi) = \hat{T}(\mu,\mu_0,\psi-\psi_0)\vec{F}, \tag{5.5}$$

where only first element of the column vector

$$\vec{F} = \begin{pmatrix} F_1 \\ F_2 \\ F_3 \\ F_4 \end{pmatrix} \tag{5.6}$$

differs from zero for unpolarized solar radiation. Thus, only elements R_{j1}, T_{j1} ($j=1, 2, 3, 4$) are relevant to studies of solar light propagation, scattering and polarization in terrestrial atmosphere. Other elements are of interest only in the case of polarized (e.g., laser) incident beams.

Knowledge of matrices $\hat{R}$ and $\hat{T}$ is of primary importance for understanding radiative and polarization characteristics of light fluxes, which emerge from a cloud body. They play a role of well-known Mueller matrices (Shurcliff, 1962; Tynes et al., 2001) for multiple-scattering cloudy media. Note that Eq. (5.4) can be written in scalar form for unpolarized illumination:

$$I = R_{11}F_1, \quad Q = R_{21}F_1, \quad U = R_{31}F_1, \quad V = R_{41}F_1 \tag{5.7}$$

and similarly to the transmitted light. Thus, the intensity of the reflected light is determined by the element R_{11} of the reflection matrix. This is the only element of major concern of most cloud optics studies up to date. The degree of polarization is given by

$$P = \sqrt{P_l^2 + P_c^2}, \tag{5.8}$$

where

$$P_l = \frac{\sqrt{R_{21}^2 + R_{31}^2}}{R_{11}} \tag{5.9}$$

is the degree of linear polarization and

$$P_c = \frac{R_{41}}{R_{11}} \tag{5.10}$$

is the degree of circular polarization. One can show (Van de Hulst, 1980) that for particular viewing geometries (e.g., $\mu_0=1$, $\mu=1$, $\varphi=0,\pi$) the values of R_{31} and R_{41} are equal to zero and light is partially linearly polarized. The degree of circular polarization, P_c, is equal to zero in this case.

It is common to use also a different definition of the degree of polarization, namely,

$$P = -\frac{Q}{I} \tag{5.11}$$

for linearly polarized light beams. It follows from Eq. (5.11) at the nadir viewing geometry ($R_{31}=R_{41}=0$) that

$$P = -\frac{R_{21}}{R_{11}}. \tag{5.12}$$

We will use this definition of the degree of polarization in this review. The second component of the Stokes vector, Q, is proportional to the difference $I_l - I_r$, where values of I_l and I_r are intensities of light polarized parallel and perpendicular to a meridional plane, which contains the normal to a layer and a viewing direction. Thus, light polarized perpendicular to the meridional plane is characterized by the positive polarization. Note that the sign of polarization degree strongly depends on the observation geometry. For instance, it is positive in the main rainbow region (Van de Hulst, 1957). It could be both positive and negative in the glory-scattering region.

The degree of polarization of singly scattered light for solar illumination is given in Fig. 18a,b. They were obtained using Mie theory for polydispersions of water droplets at the wavelength, λ, equal to 443 nm. The particle-size distribution was given by Eq. (2.3).

Polarized light scattering by hexagonal crystals were studied by Labonnote et al. (2001) and Liou (2002), the first paper being devoted to a special case of inhomogeneous crystals.

It should be pointed out that the Stokes vector elements I, Q, U, V (see Eq. (5.7)) can be used to determine the polarization ellipse parameters such as

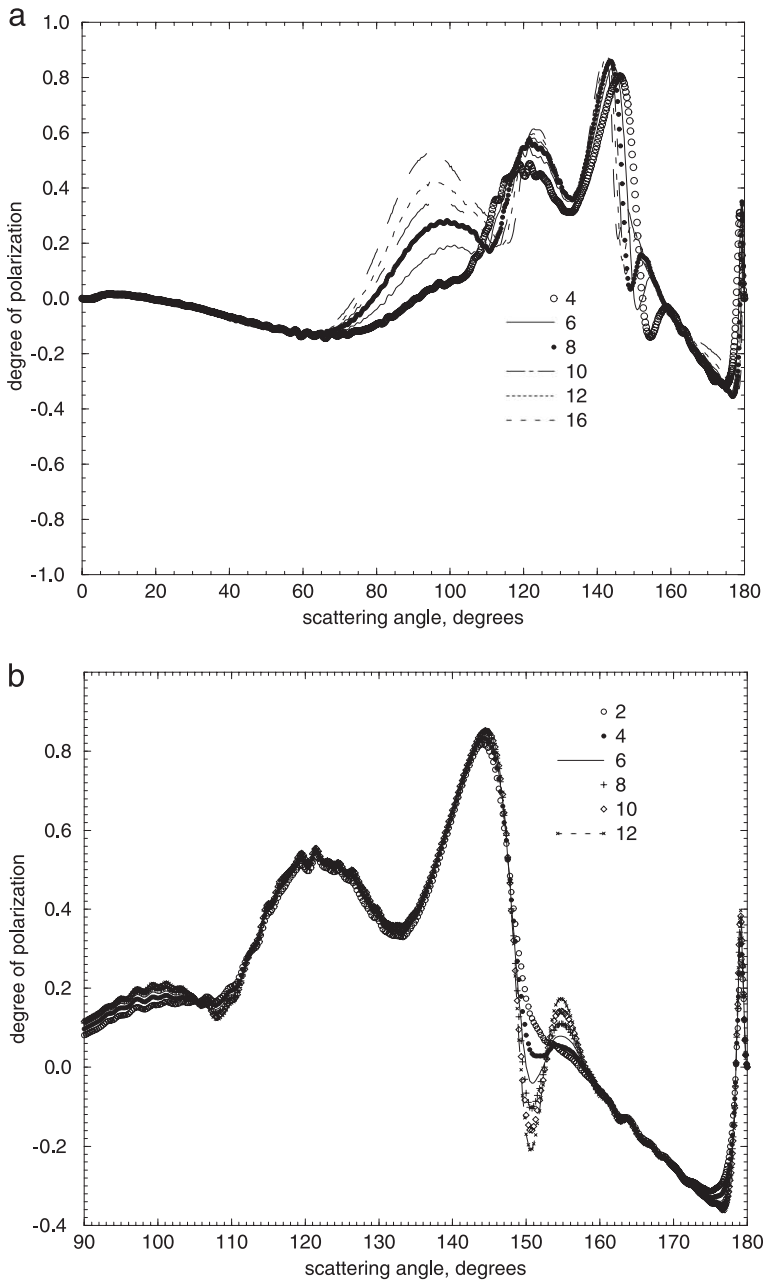

Fig. 18. (a) Degree of polarization of light singly scattered by a polydispersion of spherical water droplets characterized by the gamma particle-size distribution (Eq. (2.3)) with the half-width parameter $\mu = 6$ and the effective radius $a_{ef} = 4$, 6, 8, 10, and 16 μm as the function of the scattering angle at $\lambda = 443$ nm. (b) Same as in Fig. 1a, but at $a_{ef} = 6$ μm and different values of the half-width parameter $\mu = 2$, 4, 6, 8, 10, and 12.

the ellipticity and the angle of preferential oscillations of the electric vector in a light beam (Shurcliff, 1962).

Thus, reflection and transmission matrices allow determination of both intensity and polarization states of reflected and transmitted light

beams under arbitrary illumination of a cloud layer.

5.3. Modified asymptotic theory

5.3.1. General equations

The optical thickness of water clouds is usually large. Some mixed and crystalline clouds are also extended in the vertical direction for many hundred meters and could be optically thick (Uchiyama et al., 1999). Thus, asymptotic vector theory (Domke, 1978; Van de Hulst, 1980) is applicable to cloudy media. Using this theory, the azimuthally averaged reflection matrix $\hat{R}(\mu,\mu_0,\tau)$ and transmission matrix $\hat{T}(\mu,\mu_0,\tau)$ of a homogeneous plane-parallel weakly absorbing turbid layer of a large optical thickness, τ, can be written in the following form as $y\to 0$ (Kokhanovsky, 2001a):

$$\hat{R}(\mu,\mu_0,\tau)=\hat{R}_\infty(\mu,\mu_0)-\hat{T}(\mu,\mu_0,\tau)\exp(-x-y), \tag{5.13}$$

$$\hat{T}(\mu,\mu_0,\tau)=t\vec{K}_0(\mu)\vec{K}_0^T(\mu_0), \tag{5.14}$$

where x and y are given by Eq. (4.46), t is given by Eq. (4.31) and

$$\vec{K}_0(\mu)=\frac{3}{4}\left[\mu+\frac{1}{\pi}\int_0^1 \mathrm{d}\varsigma\varsigma^2\int_0^{2\pi}\mathrm{d}\varphi\hat{R}^0_\infty(\varsigma,\mu,\varphi)\right]\vec{e}, \tag{5.15}$$

where

$$\vec{e}=\begin{pmatrix}1\\ \\0\end{pmatrix}. \tag{5.16}$$

$\hat{R}_\infty(\mu,\mu_0)$ is the azimuthally averaged reflection matrix for a semiinfinite medium with the same local optical properties as a finite medium under study. The vector $\vec{K}^T(\mu_0)$ in Eq. (5.15) is transpose to the vector $\vec{K}(\mu_0)$. The vector $\vec{K}_0(\mu)$ also occurs in the so-called Milne problem (Minin, 1988; Wauben, 1992). It describes the angular dependence and the polarization characteristics of light emerging from semiinfinite nonabsorbing turbid layers with sources of radiation located deep inside the medium.

Eqs. (5.13) and (5.14), derived by Kokhanovsky (2001a) for small probabilities of photon absorption, are much simpler than initial asymptotic formulae obtained by Domke (1978). They allow calculation of the reflection and the transmission matrices of thick weakly absorbing disperse media by simple means if the solution of the problem for a semiinfinite medium with the same phase matrix as for a finite layer under consideration is available (Wauben, 1992; Van de Hulst, 1980). This reduction of a problem to the case of a semiinfinite nonabsorbing medium is of importance for radiative transfer theory, in general, and to cloud optics, in particular.

5.3.2. Nonabsorbing media

It follows from Eqs. (5.12)–(5.14) for the degree of polarization at the nadir observation in the case of nonabsorbing clouds (Kokhanovsky, 2001a) that:

$$P(\mu_0)=\frac{P^0_\infty(\mu_0)}{1-tu(\mu_0)}, \tag{5.17}$$

where

$$u(\mu_0)=\frac{K_0(1)K_0(\mu_0)}{R^0_\infty(1,\mu_0)} \tag{5.18}$$

and t is given by Eq. (4.7). Our calculations show that we have roughly $u\approx 1$ and, therefore (see Eq. 5.17), $P(\mu_0)\approx P^0_\infty(\mu_0)/r$, where we used $r+t=1$ for nonabsorbing clouds. It means that brighter clouds have smaller values of the degree of polarization and vice versa. The degree of polarization for a semiinfinite nonabsorbing cloud at the nadir observation

$$P^0_\infty(\mu_0)=-\frac{R^0_{\infty 21}(1,\mu_0)}{R^0_{\infty 11}(1,\mu_0)} \tag{5.19}$$

depends on the solar angle and the effective radius of particles. Here $R^0_{\infty 11}(1,\mu_0)$ and $R^0_{\infty 21}(1,\mu_0)$ are corresponding elements of the reflection matrix (see Eq. (5.4)) of a nonabsorbing semiinfinite medium. Note that Eq. (5.17) was derived accounting for the equality (Wauben, 1992) $K_{02}(1)=0$. Kokhanovsky and Weichert (2002) proposed the parameterization of this function in terms of a_{ef} at the rainbow-scattering region.

Thus, Eqs. (5.17) reduces the calculation of the degree of polarization of light reflected by a cloud in

the visible to the case of an idealized situation of a nonabsorbing semiinfinite media. Calculations with Eq. (5.17) and exact vector radiative transfer equation are given in Fig. 19 at the rainbow-scattering geometry. The value of $P^0_\infty(\mu_0)$ in Eq. (5.17) was obtained from the exact vector radiative transfer calculations. We see that accuracy of Eq. (5.17) is high. Note also the decrease of the degree of polarization with cloud optical thickness. This can be used for the cloud optical thickness determination at the rainbow-scattering geometry (Kokhanovsky, 2000).

In more general case (see Eqs. (5.13) and (5.14)), the functions $\vec{K}_0(\mu)$ and $\hat{R}^0_\infty(\mu,\mu_0,\varphi)$ for a nonabsorbing semiinfinite light-scattering medium should be found numerically. They depend on the phase matrix of a random medium in question. However, by definition they do not depend on the single-scattering albedo, ω_0, and the optical thickness, τ. Another interesting feature of these functions is their weak dependence on the cloud microphysical parameters (size, shape, and chemical composition of particles) of a medium under study in the broad range of angular parameters. This is due to the randomization of both polarization states and propagation directions of photons in highly scattering nonabsorbing semiinfinite layers irrespective of local optical properties of the medium where they propagate.

5.3.3. Weakly absorbing media

Eq. (5.17) is easily generalized to account for weak absorption of light in a cloudy medium. Namely, it follows from Eqs. (5.12) and (5.13) (Kokhanovsky, 2001b):

$$P(\mu_0) = \frac{P_\infty(\mu_0)}{1 - u^*(\mu_0)t\exp(-x-y)}, \tag{5.20}$$

where the global transmittance, t, is given by Eq. (4.31) and

$$u^*(\mu_0) = \frac{K_0(1)K_0(\mu_0)}{R_\infty(1,\mu_0)}. \tag{5.21}$$

Values of $P_\infty(\mu_0)$ and $R_\infty(1,\mu_0)$ represent the degree of polarization and reflection function of a semiinfinite weakly absorbing cloud at the nadir viewing

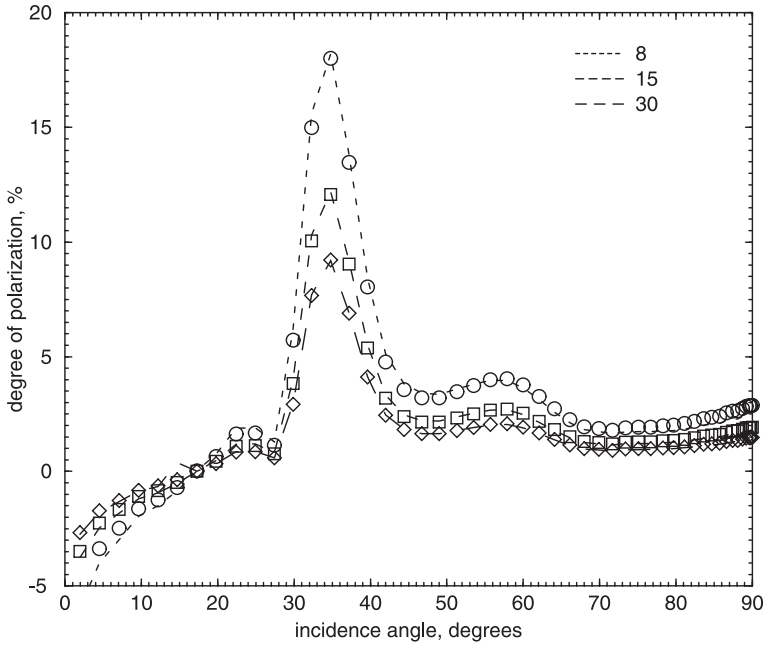

Fig. 19. Dependence of the degree of polarization on the solar angle for cloud optical thickness 8, 15, and 30 at $\lambda = 0.65$ μm, $\vartheta_0 = 37°$, $a_{ef} = 6$ μm, $\mu = 6$ (see Eq. (2.3)) according to the exact radiative transfer calculations (symbols) and Eq. (5.17) (lines).

geometry. They can expressed via the correspondent functions for nonabsorbing media. In particular, Eq. (4.32) can be used to find $R_\infty(1,\mu_0)$. Similar equation holds for $P_\infty(\mu_0)$ (Kokhanovsky, 2002c):

$$P_\infty(\mu_0) = P^0_\infty(\mu_0)\exp[yu(1-0.05y)]. \quad (5.22)$$

Eqs. (4, 32), (5.20)–(5.22) reduce the calculation for a weakly absorbing finite layer to a more simple case of a semiinfinite nonabsorbing medium. The accuracy of these equations has been studied by Kokhanovsky (2001a, 2002c).

Note that the dependence of the degree of polarization of reflected light on the size of droplets has been studied by Hansen (1971a) and Kokhanovsky (2003b).

6. Image transfer

6.1. Introduction

Let us consider now pecularities of image transfer in cloudy media. From vision theory, a cloud is a high-frequency filter. The transmission of high-frequency signals (in time and space domains) is reduced considerably in comparison with low-frequency signals as a result of light scattering. Any diffused source of light can be considered as a superposion of point light sources. Thus, in linear optical systems the image of such an object with intensity $I_0(\vec{r}')$ is a linear superposition of images of point sources (Zege et al., 1991):

$$I(\vec{r}) = \int_{-\infty}^{\infty}\int_{-\infty}^{\infty} \mathrm{d}\vec{r}'\, I_0(\vec{r}')S(\vec{r}',\vec{r})\mathrm{d}\vec{r}', \quad (6.1)$$

where the point spread function (PSF) $S(\vec{r}',\vec{r})$ describes the process of the transformation of the object intensity $I_0(\vec{r}')$ in the initial plane to the image intensity $I(\vec{r})$ in the image plane. The point spread function is a main notion of the image transfer theory. Eq. (6.1) has a more simple form in a frequency domain:

$$I(\vec{\upsilon}) = S(\vec{\upsilon})I_0(\vec{\upsilon}), \quad (6.2)$$

where

$$I(\vec{\upsilon}) = \int_{-\infty}^{\infty}\int_{-\infty}^{\infty} I(\vec{r}')\mathrm{e}^{-i\vec{\upsilon}\vec{r}'}\mathrm{d}\vec{r}', \quad (6.3)$$

$$I_0(\vec{\upsilon}) = \int_{-\infty}^{\infty}\int_{-\infty}^{\infty} I_0(\vec{r}')\mathrm{e}^{-i\vec{\upsilon}\vec{r}'}\mathrm{d}\vec{r}', \quad (6.4)$$

$$S(\vec{\upsilon}) = \int_{-\infty}^{\infty}\int_{-\infty}^{\infty} S(\vec{r}')\mathrm{e}^{-i\vec{\upsilon}\vec{r}'}\mathrm{d}\vec{r}', \quad (6.5)$$

and $\vec{\upsilon}$ is the space frequency. One of the main problems of the image transfer theory is to determine the value of the Fourier transform of the PSF, namely, the optical transfer function (OTF) $S(\vec{\upsilon})$. After that the value of $I(\vec{\upsilon})$ can be determined from Eq. (6.2) and for the light intensity in the image plane, it follows from Eq. (6.3):

$$I(\vec{r}') = \frac{1}{4\pi^2}\int_{-\infty}^{\infty}\int_{-\infty}^{\infty} I(\vec{\upsilon})\mathrm{e}^{i\vec{\upsilon}\vec{r}}\mathrm{d}\vec{\upsilon}. \quad (6.6)$$

The optical transfer function depends on the properties of media between an object and an image (Wells, 1961; Volnistova and Drofa, 1986; Zege et al., 1991). Different methods of calculation of this function and the modulation transfer function (MTF)

$$M(\vec{\upsilon}) = \frac{|S(\vec{\upsilon})|}{|S(0)|}$$

are described by Ishimaru (1978) and Zege et al. (1991).

6.2. Optical transfer function

We will consider here the only case of the image transfer through a cloud with large particles at normal incidence of a light beam. In this case, the OTF is a real function. It does not depend on the azimuth for randomly oriented particles. It was obtained (Zege et al., 1991) that

$$S(\upsilon^*) = \exp[-\tau + \omega_0\tau\eta(\upsilon*)], \quad (6.7)$$

where $\upsilon^* = \upsilon L$ is the dimensionless frequency, L is the geometrical thickness of a layer, $\upsilon = |\vec{\upsilon}|$ and

$$\eta(\upsilon^*) = \int_0^1 P(\upsilon^* v)\mathrm{d}v,$$

$$P(\upsilon^* v) = \frac{1}{2}\int_0^{\infty} p(\theta)J_0(\theta\upsilon^* v)\theta\mathrm{d}\theta. \quad (6.8)$$

Here $J_0(\theta\upsilon^*\nu)$ is the Bessel function. The optical transfer function can be obtained from Eqs. (6.7) and (6.8) if one has information on the optical thickness of a cloud (≤ 7, in the approximations (6.7) and (6.8)), the single-scattering albedo, ω_0, and the phase function $p(\theta)$.

For media with the complex microstructure (e.g., crystal clouds), the crux of the difficulty is that the phase function is not known a priori. In this case, different models to describe this function can be used (see Table 6). For instance, if one supposes that the phase function is described by the Gaussian function:

$$p(\theta) = \frac{2}{b^2}\exp\left[-\frac{\theta^2}{2b^2}\right], \tag{6.9}$$

where b is constant, which is inversely proportional to the effective radius of droplets, and θ is the scattering angle, it follows that

$$P(\upsilon^*\nu) = \exp\left[-\frac{(b\nu\upsilon^*)^2}{2}\right] \tag{6.10}$$

and, therefore,

$$S(\upsilon) = \exp\left[-\tau + \frac{\omega_0\tau}{b\upsilon^*}\sqrt{\frac{\pi}{2}}\mathrm{erf}\left(\frac{b\upsilon^*}{\sqrt{2}}\right)\right], \tag{6.11}$$

where $\mathrm{erf}(b\upsilon^*/\sqrt{2})$ is the probability integral, given by

$$\mathrm{erf}\left(\frac{x}{\sqrt{2}}\right) = \frac{1}{\sqrt{2\pi}}\int_{-x}^{x} \mathrm{e}^{-\frac{t^2}{2}}\mathrm{d}t. \tag{6.12}$$

One can obtain at large values of frequency, υ^*, $\mathrm{erf}(b\upsilon^*/\sqrt{2}) = 1$ and, therefore,

$$S(\upsilon^*) = \exp(-\tau). \tag{6.13}$$

Thus, the OTF is determined by the nonscattered light alone at $\upsilon^* \gg 1$. It follows directly from Eqs. (6.7) and (6.8) as well.

Note that at large optical thickness, the number of nonscattered photons is low. Thus, the value of the OTF is small and the contrast of the image is low. It follows at small values of the frequency, υ^*, that

$$\mathrm{erf}\left(\frac{b\upsilon^*}{\sqrt{2}}\right) = b\upsilon^*\sqrt{\frac{2}{\pi}}\left[1 - \frac{(b\upsilon^*)^2}{6}\right] \tag{6.14}$$

Table 6
Phase functions $p(\theta)$ and their Fourier–Bessel transforms $p(\sigma)$ (Υ is the normalization constant, x is the size parameter) (Zege et al., 1991; Kokhanovsky, 2001a)

$p(\theta)$	$p(\sigma)$
$(2\Upsilon\exp(-\Upsilon\theta))/\theta$	$\dfrac{\Upsilon}{\sqrt{\Upsilon^2+\sigma^2}}$
$2\Upsilon^2\exp(-\Upsilon\theta)$	$\Upsilon^3/(\Upsilon^2+\sigma^2)^{3/2}$
$(2/\Upsilon^2)\exp(-\theta^2/2\Upsilon^2)$	$\exp(-(\Upsilon^2\sigma^2)/2)$
$(4J_1^2(\theta x))/\theta^2$	$\begin{cases}\frac{2}{\pi}\left\{\arccos\left(\frac{\sigma}{2x}\right) - \frac{\sigma}{2x}\sqrt{1-\left(\frac{\sigma}{2x}\right)^2}\right\}, & \sigma \leq 2x \\ 0, & \sigma > 2x\end{cases}$

and, therefore,

$$S(\upsilon^*) = \exp\left\{-\tau\left[1 - \omega_0\left(1 - \frac{(b\upsilon^*)^2}{6}\right)\right]\right\},$$

$$M(\upsilon^*) = \exp\left[-\frac{(b\upsilon^*)^2\tau}{6}\right]. \tag{6.15}$$

In particular, we have at $\upsilon^* = 0$:

$$S(0) = \exp[-\tau(1-\omega_0)], \tag{6.16}$$

which means that $S(0)$ differs from one only due to the light absorption process. Note that the value of b is inversely proportional to the average size of particles. Thus, one can see that the loss of contrast is higher for thicker clouds with larger single-scattering albedos and smaller droplets or crystals.

The dependence of the OTF on the size and refractive index of droplets was studied in detail by Zege and Kokhanovsky (1994), Zuev et al. (1997), and Kokhanovsky (2001a) using the geometrical optical approximation for the phase function $p(\theta)$. This allowed them to obtain analytical relationships between values of OTF and cloud microphysical parameters. Zege and Kokhanovsky (1992) used these relationships for the optical particle sizing problem solution.

Comparisons of calculations the OTF with Eq. (6.7) and Monte-Carlo calculations (Drofa and Usachev, 1980) were performed by Zege and Kokhanovsky (1994). It was found that the accuracy of approximate Eq. (6.7) for cloudy media with an effective radius of water droplets 6 μm and $\tau = 1$ is better than 5% in the visible. The accuracy decreases

with optical thickness, τ, which should be less than 5–7 to apply Eq. (6.7).

7. Satellite remote sensing of cloudy media

7.1. Optical thickness

Equations presented in previous sections can be used for a rapid estimations of the radiative, polarization and image characteristics of cloudy media. They also can be used to check the accuracy of new algorithms using the fact that the numerical solution of the radiative transfer equation (Thomas and Stamnes, 1999) and results presented above for optically thick layers should converge as $\tau \to \infty$ and $\beta \to 0$.

Kokhanovsky and Macke (1999) used approximations, presented in Table 5, to study the influence of the shape of particles on the radiative transfer in clouds. They found that clouds with nonspherical particles are more reflective (larger values of reflectance) as compared to clouds with spherical droplets with the same value of volume to particle surface area ratio. The opposite is true for transmittance. Similar results were obtained by Takano and Liou (1989).

The most important area of the application of asymptotical solutions lies in the field of remote sensing (Rozenberg, 1967; Rozenberg et al., 1978; King, 1981, 1987; Kokhanovsky and Zege, 1996; Kokhanovsky, 2000, 2001a; Kokhanovsky et al., 2003).

In particular, this approach avoids or reduces (if thin clouds are also under consideration) the need for precalculation and storage of the so-called look-up tables, which is a standard technique in passive cloud remote sensing (Arking and Childs, 1985; Rossow et al., 1989; Nakajima and King, 1990).

We have for the global transmittance from Eq. (4.14) after simple algebraic calculations:

$$t = \frac{(1 - r_s)\Lambda}{1 - r_s(1 + \Lambda)}, \tag{7.1}$$

where the function Λ is introduced. It is given by

$$\Lambda \equiv \Lambda(\mu, \mu_0, \varphi) = \frac{R^0_\infty(\mu, \mu_0, \varphi) - \hat{R}(\mu, \mu_0, \varphi, \tau)}{K_0(\mu)K_0(\mu_0)}. \tag{7.2}$$

The analytical results for functions $R^0_\infty(\mu,\mu_0,\varphi)$ and $K_0(\mu)$ have been presented above. Thus, the global transmittance, t, and correspondingly the total reflectance, $r = 1 - t$, can be obtained from Eqs. (7.1) and (7.2) and knowledge of the surface albedo r_s and the measured value $\hat{R}(\mu,\mu_0,\varphi,\tau)$.

For such a retrieval, it is not necessary to know the optical thickness of clouds and the average size of droplets. This is an extremely important point for climate studies, where the global and temporally averaged value of the cloud reflectance, $r = 1 - t$, is an important parameter. Usually, $r < 0.8$ for natural water clouds in the visible (Danielson et al., 1969), which implies that clouds with optical thicknesses larger than 70–100 appear not very often (Trishchenko et al., 2001). The reduced reflectance in visible can be also related to aerosol absorption in clouds (Melnikova and Mikhailov, 1994, 2000) and to the inhomogeneity and finite size of clouds (Stephens and Tsay, 1990).

Using Eq. (7.1), we obtain $t \equiv \Lambda$ at $r_s = 0$, and $t = 0$ and $r = 1$ at $r_s = 1$. This shows that all photons incident on optically thick nonabsorbing clouds over surfaces with $r_s = 1$ survive and return back to outer space. They yield no information about actual cloud thickness. This explains why the retrieval of cloud parameters over bright surfaces (e.g., snow and ice) hardly can be performed in visible (Platnick et al., 2001). The information on the global transmittance, t, can be used to find the scaled optical thickness (Rozenberg et al., 1978; King, 1987), given by

$$\tau^* = \tau(1 - g). \tag{7.3}$$

It follows from Eqs. (7.1) and (7.2) that

$$\tau^* = \frac{4}{3}(t^{-1} - \alpha), \tag{7.4}$$

where t is given by Eq. (7.1). Again, the value of τ^* can be obtained although there is no information about the size of droplets and the actual optical thickness of clouds.

Eq. (7.4) can be used for the retrieval of τ^* from the measurement $\hat{R}(\mu,\mu_0,\varphi,\tau)$ at a single wavelength (King, 1987). Eq. (7.3) is used for the derivation of the optical thickness, τ, (see Eq. (7.3)) if the value of g is known (Rossow, 1989) (approximately 0.74 for ice clouds as previously discussed). However, for warm clouds, the asymmetry parameter g depends on the

size of droplets even for nonabsorbing channels (see Eq. (3.35)). Often, the dependence $g(a_{ef})$ is neglected and it is assumed that $a_{ef}=10$ μm for water clouds (Rossow and Schiffer, 1999). Then it follows from Eq. (3.35) that $g=0.86$ at $\lambda=0.65$ μm and $a_{ef}=10$ μm. Utilizing Eqs. (7.3) and (7.4), this value of g can be used for a crude estimation of the optical thickness of liquid clouds.

Errors can be introduced if one assumes the fixed a priori defined value of g. It follows from Eq. (3.35) at $\lambda=0.65$ μm that $g=0.84-0.87$ at $a_{ef}=4-20$ μm. From Eq. (7.3), we have $\tau=\Im\tau^*$, $\Im\equiv(1-g)^{-1}\approx 6.3-7.6$ and $\tau\in[9.4,11.5]$ at $\tau^*=1.5$, depending on the value of g used. The assumption that $a_{ef}=10$ μm yields $g=0.86$ and $\Im=7.2$, $\tau=10.7$.

This leads to a relative error of 7–14% in the retrieved optical thickness (i.e., a range of possible values from $\tau=9.4$ to $\tau=11.5$ instead of $\tau=10.7$). This uncertainty in the optical thickness can be removed if measurements in the near-infrared region of the electromagnetic spectrum are performed, enabling the size of droplets and, therefore, the asymmetry parameter g to be estimated. For this, however, we should be sure that we have a liquid and not ice or a mixed-phase cloud. Another uncertainty arises due to the possible contamination of clouds by absorbing aerosols (Asano et al., 2001, 2002). Then Eq. (7.1) is not valid.

7.2. Size of droplets

As was specified above for correct estimation of optical thickness of clouds from space, we need to know the effective radius of droplets. The size of droplets can be found if the reflection function in near-infrared region spectrum is measured simultaneously (Nakajima and King, 1990; Kokhanovsky and Zege, 1996). This is due to the fact that the reflection function in the infrared strongly depends on the probability of photon absorption by droplets. This probability is proportional to the effective radius of droplets as was discussed previously (see Eq. (3.21)).

The influence of absorption and scattering of light by molecules and aerosol particles on the measured value $R(\mu,\mu_0,\varphi,\tau)$ is often neglected in the cloud retrieval algorithms. However, correction can be easily taken into account if needed (Wang and King, 1997; Goloub et al., 2000). The influence of surface reflection on the cloud reflection function, assuming that the surface is Lambertian with albedo r_s, is easily taken into account, leading to (see Eqs. (4.14) and (4.33)):

$$\hat{R}_1(a_{ef},w)=R^0_\infty-\frac{t_1(a_{ef},w)[1-r_{s1}]}{1-r_{s1}[1-t_1(a_{ef},w)]}\times K_0(\mu)K_0(\mu_0), \tag{7.5}$$

$$\hat{R}_2(a_{ef},w)=R^0_\infty\exp(-y(a_{ef})(1-cy(a_{ef}))u)-\left\{\exp[-x(a_{ef},w)-y(a_{ef})]-\frac{t_2(a_{ef},w)r_{s2}}{1-r_{s2}r_2(a_{ef},w)}\right\}\times t_2(a_{ef},w)K_0(\mu)K_0(\mu_0). \tag{7.6}$$

The subscripts "1" and "2" refer to wavelengths, λ_1 and λ_2, in visible and near-infrared channels, respectively. The values of r_{s1} and r_{s2} give us the surface albedos in visible and near-infrared respectively. The explicit dependence of functions involved on the parameters a_{ef} and w to be retrieved is introduced in brackets. The liquid water path w is preferred to the optical thickness in retrieval procedures due to the independence of w on the wavelength. The optical thickness is uniquely defined if a_{ef} and w are known.

Eqs. (7.5) and (7.6) form a nonlinear system of two algebraic equations having two unknowns (a_{ef} and w), which can be solved by standard methods and programs. In particular, we can find the value of w from Eq. (7.5) analytically (Kokhanovsky et al., 2003). Substitution of this result in Eq. (7.6) gives us a single transcendent equation for the effective radius of droplets determination (Kokhanovsky et al., 2003). The accuracy of this semianalytical retrieval algorithm has been studied by Kokhanovsky et al. (2003).

7.3. Thermodynamic state of clouds

The discrimination of liquid water from ice clouds is of importance for many applications including flight safety and Earth climate studies. The size and shape of particles in warm and ice clouds are different. This influences the energy transmitted and reflected by a cloud.

This discrimination can be performed, taking into account the difference in angular or spectral distribu-

tion of reflected light. We present results of calculation of the reflection function of cloudy media with liquid and frozen water droplets in Fig. 20. It follows from this figure that minima in the reflection function of ice clouds (e.g., near 1.5 and 2.0 μm) are moved to larger wavelengths as compared to the case of liquid droplets. Of course, this is due to the difference in spectral behaviour of the imaginary parts of the complex refractive index of liquid water and ice (see Fig. 2). Minima for liquid water also moved to larger wavelengths as compared to the absorption bands of water vapour. These different positions of minima can be easily registered with modern spectrometers (see, e.g., Dvoryashin, 2002; Knap et al., 2002).

Another possibility is to consider different angular behaviour of the reflection function for ice and water clouds at specific scattering geometries (e.g., rainbow, glory and halo scattering). In particular, the reflection function of water clouds, as distinct from ice clouds, has a maximum near the rainbow-scattering angle, which also can be easily detected. This feature becomes even more pronounced if the degree of polarization at the rainbow geometry is studied (Goloub et al., 2000; Kokhanovsky, 2003b).

7.4. Cloud-top height and cloud fraction

Another important characteristic of a cloud is its height. It can be retrieved using data from space-borne lidars (Winker and Trepte, 1998). Passive measurements also can be used. For instance, Yamomoto and Wark (1961) proposed the use of the oxygen A band, centred at 0.761 μm. The physical basis of this method depends on a deep minimum around 0.761 μm due to oxygen absorption. This minimum is not shown in Fig. 20 because only scattering and absorption of light by cloud particles was accounted for in the calculation for this figure. The depth of the absorption line will depend on the cloud height. Photons can hardly penetrate thick clouds and be absorbed by the oxygen in the air column below the cloud. This will increase the value of the reflection function at 0.761 μm for the case of clouds at high altitudes. The depth of the absorption line is larger for

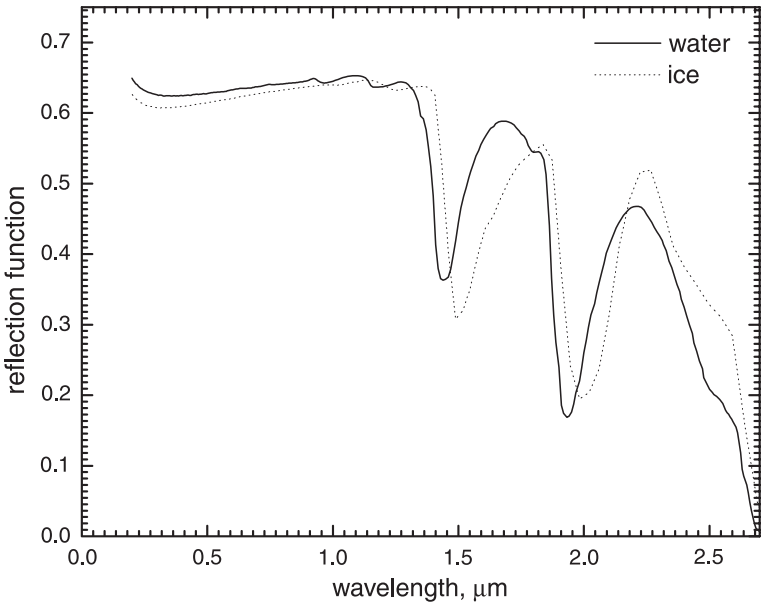

Fig. 20. Spectral dependence of the reflection function of cloudy media for the nadir observation and the solar angle equal to 60°. Clouds are composed of water or ice spherical particles with effective radius 6 μm. It is assumed that particles in a cloud are characterized by the gamma particle-size distribution (Eq. (2.3)) with the parameter $\mu = 6$. The geometrical thickness of cloud is equal to 500 m. The liquid water path is 100 g/m^2, which gives the optical thickness of 27 at the wavelength 0.55 μm. The reflection of light from surface and the scattering and absorption of light by aerosols and gases are neglected.

low clouds. Practical application of the method, however, is not so simple (Kuze and Chance, 1994; Koelemeijer et al., 2001). First of all, the depth of line also depends on the oxygen absorption cross section, which varies with temperature and pressure. Thus, one should use a priori assumptions on the temperature and pressure variation with height in the Earth's atmosphere. The generally unknown surface albedo and cloud geometrical thickness also can influence the retrieval accuracy. Other possible sources of errors are described in detail by Kuze and Chance (1994) and Koelemeijer et al. (2001).

The largest complication arises for pixels that are only partially covered by clouds. Ignoring them will lead to a big reduction of data; hence, to overcome this problem, Koelemeijer et al. (2001) proposed an algorithm that retrieves simultaneously effective cloud-top height/pressure and cloud fraction, assuming that cloud is a Lambertian surface. Such an assumption leads to underestimation of cloud-top heights as compared to in situ measurements.

Global information on cloud fraction/cover, $\mathbb{Q}$, is of a considerable importance by itself (Batey et al., 2000). Usually, the value of $\mathbb{Q}$ varies in the range 0.55–0.85, depending on the exact region under study. Globally, clouds cover around 60% of the atmosphere. This once more underlines the importance of clouds in the radiation balance and atmosphere heating rates studies.

Palle and Butler (2002) state that the global cloud cover increased during the past century. They argue against a dominating role of the solar activity (via galactic cosmic rays) on the cloud formation.

7.5. Remote sensing of crystalline clouds

Remote sensing of optical thicknesses and effective size of droplets in crystalline clouds is complicated by low optical thickness (usually smaller than 5), the high spatial and temporal variability of cloud properties, nonspherical shape of particles and their possible horizontal orientation. If the thickness of a crystalline cloud is high, then the optical thickness can be derived in the same way as was discussed above, assuming an asymmetry parameter of 0.74 (see Eqs. (7.1)–(7.4)). The problem is to find the corresponding reflection function of a semiinfinite medium (see Eq. (7.4)). One possibility is to calculate it beforehand using the phase function of a fractal fictive scatterer. Mie theory should not be used in this case.

For thinner clouds, one should build the precalculated table of reflection functions, which should be compared with experimental data to establish both the optical thickness of clouds and the size/shape of droplets (Masuda et al., 2002). This is not an easy problem. In particular, the model of ice spheres cannot be used for this purpose (Mishchenko et al., 1995, 1996; Chepfer et al., 1998; Rolland et al., 2000; Doutriaux-Bucher et al., 2000).

Yang et al. (2001) considered the influence of vertical variability of ice crystals habits and crystal dimensions on the satellite ice cloud retrieval algorithms. They accounted for the fact that more complex shapes and larger sizes of crystals are more typical for the base of the cloud as compared to its top, where crystals are smaller and more rounded. The authors state that the vertical distribution of optical characteristics of clouds can be neglected if visible channels are used, but the vertical inhomogeneity should be fully accounted for if one is interested in the average size of particles retrievals (e.g., from the measurements of the cloud reflection function at 2.11 μm moderate resolution imaging spectrometer channel (King et al., 1992)). Information on the vertical structure of a crystalline cloud is not known a priori, which complicates the retrieval procedure. We see, therefore, that the creation of a suitable look-up table for reflection functions of crystalline clouds is not at all a trivial problem.

Note that ice clouds are often studied using ground-based systems. This allows us to derive the cloud optical thickness and the effective radius of particles. For this, measurements of direct light and light scattered at small angles usually are performed. The important problem here is to account for multiple light scattering using the radiative transfer equation (Thomas and Stamnes, 1999). For layers with optical thickness smaller than approximately 5, a so-called small-angle approximation (Zege et al., 1991) can be used. The intensity of the diffused light, I_d, is given by a simple integral in this case (Zege et al., 1991; Kokhanovsky, 2001a):

$$I_d(\tau,\vartheta)=\frac{I_0}{2\pi}\int_0^\infty [\Gamma(\tau)-\exp(-\tau)]J_0(\sigma\vartheta)\sigma d\sigma, \tag{7.7}$$

where (see Table 6)

$$\Gamma(\tau) = \exp[-(1 - \omega_0 p(\sigma))\tau] \quad (7.8)$$

is the normalized mutual coherence function for electric fields separated by the distance σ/k for a plane incident wave, where $k = 2\pi/\lambda$; I_0 is the intensity of incident light and it was assumed that a cloud is illuminated along the normal. The function

$$p(\sigma) = \frac{1}{2}\int_0^\infty p(\theta) J_0(\theta\sigma)\theta \mathrm{d}\theta \quad (7.9)$$

is the Fourier–Bessel transform of the phase function $p(\theta)$. The angle ϑ gives the angle that measured transmitted light beam makes with the normal to a cloud layer. Most frequently used functions $p(\theta)$ and their transforms $p(\sigma)$ are given in Table 6. Function (7.8) can be used to study the loss of coherence of optical waves in cloudy media (Zege and Kokhanovsky, 1995).

In conclusion, we note that both ice and water clouds are often studied with lidar techniques (Platt, 1978a,b; Bissonnete et al., 1995; Sassen, 1991, 2001; Winker and Trepte, 1998; Mishchenko and Sassen, 1998; Zege et al., 1998a,b; Winker, 1999; McGill et al., 2002).

8. Inhomogeneous clouds

8.1. Vertical inhomogeneity

Vertical and horizontal inhomogeneity of clouds can be dealt with in the framework of the Monte-Carlo methods of the radiative transfer equation solutions (Schreier and Macke, 2001). This is of considerable importance for crystalline media, as was discussed in the previous section. Unfortunately, Monte-Carlo methods are extremely slow and cannot be applied in the operational satellite cloud retrieval algorithms.

Accounting for the vertical inhomogeneity, however, can be easily done in the framework of the theory of optically thick layers as discussed previously. Corresponding equations are presented by Sobolev (1972) and Yanovitskij (1997). For the sake of simplicity, we consider here only the case of clouds in the visible, where light absorption can be neglected. Then the reflection function of a vertically inhomogeneous optically thick cloud can be presented by Eq. (4.6) as in the case of a homogeneous layer. However, the meaning of parameters in this equation is different in an inhomogeneous case. That is, τ is the optical thickness of a vertically inhomogeneous cloud, R_∞^0 is the reflection function of a semiinfinite cloud with the same vertical distribution of optical characteristics as a finite cloud, and g is the average asymmetry parameter. The value of g does not change considerably with droplet size (see Eq. (3.35) as $x_{\mathrm{ef}} \to \infty$); thus, it can be assumed to be a priori defined value (say, e.g., 0.86; Rossow and Schiffer, 1999). Then accounting also for the weak sensitivity of the reflection function R_∞^0 to the size of droplets (see Fig. 13), we state that Eq. (4.6) can be also applied to the derivation of optical thickness of vertically inhomogeneous clouds. This suggests that one cannot retrieve the vertical distribution of extinction coefficient in a cloud from the reflection function measurements in the visible. Lidar returns, however, can provide this information (Zege et al., 1998a,b).

The situation in the near-infrared is not so simple because the derived size of droplets depends on the average photon penetration depth, which is of course a function of wavelength (Platnick, 2000). It means that the derived effective size of droplets is a function of the wavelength for vertically inhomogeneous clouds. Generally, the absorption increases with wavelength; hence, penetration depth decreases with wavelength.

Thus, we arrive to the conclusion that reflection functions at larger wavelength (e.g., 2.11 μm) will give us values of the droplets radii closer to the cloud tops and reflection functions at smaller wavelengths (e.g., 1.6 μm) give us the radius of droplets deep inside clouds. These different values of radii are considered as a shortcoming of the retrieval method for vertically inhomogeneous clouds. On the other hand, this opens a new possibility to study the vertical distribution of droplets' sizes, analysing spectral reflectances of clouds, obtained both from airborne and satellite platforms.

In conclusion, we note that radii of droplets increase with height (Brenguier et al., 2000). It means that values of radii retrieved at 1.6 μm should be smaller than those obtained from the channel at 2.11 μm. This is also observed experimentally (Platnick et al., 2001).

8.2. Horizontal inhomogeneity

Real cloud fields are horizontally inhomogeneous (Titov, 1998; Marshak et al., 1995, 1998) and have complex shapes, which complicates theoretical modelling (Rogovtsov, 1991, 1999). This also produces unphysical angular dependence of cloud optical thickness for different solar angles (Loeb and Davies, 1996; Loeb and Coakley, 1998) if the model of the horizontally inhomogeneous layer is used in the retrieval procedure for inhomogeneous cloud fields. Fouilloux et al. (2000) found that derived cloud optical thicknesses and effective radii for inhomogeneous clouds depend on the averaging scale. Therefore, they state that comparisons between aircraft measurements and satellite observations are not valid for heterogeneous clouds (which is the case for most clouds). This puts the validation of cloud satellite products with airborne radiometers in question.

Approximations for horizontal photon transport within real-world clouds were developed by Platnick (2001). In particular, he derived analytic approximations for the root-mean-square horizontal displacement of reflected and transmitted photons relative to the incident cloud-top location.

Usually, the influence of horizontal inhomogenity of clouds on their radiative characteristics is studied in the framework of the independent column (or pixel) approximation (Cahalan et al., 1994). This approximation neglects the horizontal photon transport between adjacent columns. Then one can obtain for the reflection function of a pixel in the framework of this approximation (Pinkus and Klein, 2000):

$$\bar{R} = \int_0^\infty R(\tau) f(\tau) \mathrm{d}\tau, \tag{8.1}$$

where $f(\tau)$ is the optical thickness distribution function for a given pixel and $R(\tau)$ is the reflection function for a horizontally homogeneous cloud with a given optical thickness, τ. Cahalan et al. (1994), Fu et al. (2000), and Schreier and Macke (2001) found that this approximation has a high accuracy for the domain-averaged radiative fluxes.

It is known (Cahalan et al., 1994) that $\bar{R} < R(\bar{\tau})$, where $\bar{\tau}$ is the average optical thickness, which means that the values of $\bar{\tau}$ obtained from measurements over horizontally inhomogeneous clouds in the assumption of a horizontally homogeneous plane-parallel clouds are underestimated. Thus, correction of the optical thickness obtained by an empirical factor is needed (Rossow and Schiffer, 1999).

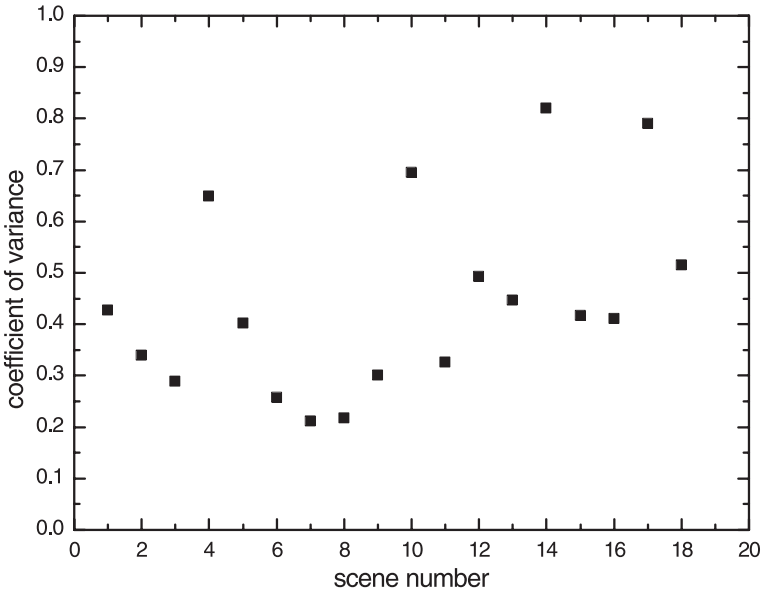

Fig. 21. The coefficient of variance of the cloud optical thickness spatial distribution (Barker et al., 1996).

It is difficult to apply Eq. (8.1) to the radiative transfer problem analysis due to the necessity to perform calculations $R(\tau)$ many times for a given pixel. The problem can be greatly simplified (Kokhanovsky, 2003d) if one uses approximate analytical solutions, which are valid for optically thick clouds (see e.g., Section 4), in combination with analytical forms for the function $f(\tau)$, which is usually given by the gamma (Barker et al., 1996) or the lognormal (Nakajima et al., 1991) distributions. The values of the coefficient of variance of this distribution obtained from experimental measurements over a number of cloud scenes are given in Fig. 21, which was prepared using data of Barker et al. (1996). We see that the coefficient of variance is in the range 20–80%.

The lower limit of integration in Eq. (8.1) should be 10 to allow for the use of Eq. (4.14) in integral (8.1). The integral in the range from 0 to 10 can be estimated using the exact radiative transfer equation. This contribution is small at large values of τ and can be neglected.

9. Summary

The goal of this review was to consider various approaches to calculate local and global optical characteristics of cloudy media. Main tools reviewed are the geometrical optics approximation and the theory of optically thick turbid layers. Both theories can be substituted by exact solutions (the Mie theory for local optical characteristics and the radiative transfer theory for the radiative characteristics) in the case of homogeneous clouds with spherical particles.

However, they appear to be very important in bringing the forward propagation models closer to the reality (e.g., account for nonspherical shape of crystals, effects of cloud inhomogeneity). Approximations developed allow consideration of cases that are difficult or impossible to handle with exact techniques. Another important feature of the approximate methods is the possibility to simplify inverse problems of cloud optics.

The cloud optics studies are far from being completed. Most results of this review are valid only for homogeneous plane parallel clouds, which is a good starting point for cloud optical properties investigations. In reality, most clouds have very complicated shapes and structures. Accounting for these features will be a main topic of cloud optics research for years to come. The progress in respect to the description of local optical characteristics of crystalline clouds with particles of complex shapes is expected due to large efforts currently undertaken in this direction.

Other topics of high priority, which will be developing in a future, are studies of clouds with lidars (e.g., space-based). This will allow provide information on cloud geometrical parameters with a high spatial resolution. Depolarization and polarization techniques will also gain further momentum in cloud optics studies.

All of these developments will allow us to characterize cloud properties and their temporal and spatial variability on a scale that was not possible in the past. In turn, the information obtained will make it possible to understand and describe the influence of clouds on climate and its change, which remains a major unresolved problem of a modern climatology.

Acknowledgements

The author would like to thank A. Macke, K. Masuda and M. Mishchenko for providing their computer codes, which made this research possible. Also, I acknowledge with many thanks important discussions on the cloud optics with J.P. Burrows, M. King, T. Nakajima, S. Platnick, V.V. Rozanov, W. von Hoyningen-Huene, and E. P. Zege. This work was funded by the BMBF via GSF/PT-UKF (07UFE12/8) and by the German Space Agency (50EE0027 and 50EE9901).

References

Ackerman, S.A., Stephens, G.L., 1987. The absorption of solar radiation by cloud droplets: an application of anomalous diffraction theory. J. Atmos. Sci. 44, 1574–1588.

Arking, A., Childs, J.D., 1985. Retrieval of clouds cover parameters from multispectral satellite images. J. Appl. Meteorol. 24, 323–333.

Asano, S., Uchiyama, A., Yamazaki, A., Tanizono, M., 2001. Effects of aerosols on retrieval of the microphysical properties of water clouds from the airborne solar spectral reflectance measurements. Proc. SPIE 4150, 208–216.

Asano, S., Uchiyama, A., Yamazaki, A., Gayet, J.-F., Tanizono, M., 2002. Two case studies of winter continental-type water and

mixed-phase stratocumuli over the sea: 2. Absorption of solar radiation. J. Geophys. Res. 107 (10.1029/2001JD001108).

Auer, A.H., Veal, D.L., 1970. The dimension of ice crystals in natural clouds. J. Atmos. Sci. 27, 919–926.

Ayvazian, G.M., 1991. Propagation of Millimeter and Submillimeter Waves in Clouds. Gidometeoizdat, Leningrad.

Baran, A.J., Havemann, S., 1999. Rapid computation of the optical properties of hexagonal columns using complex angular momentum theory. J. Quant. Spectrosc. Radiat. Transfer 63, 499–519.

Baran, A.J., Francis, P.N., Labonnote, L.-C., Doutriaux-Boucher, M., 2001. A scattering phase function for ice cloud: tests of applicability using aircraft and satellite multi-angle multi-wavelength radiance measurements of cirrus. Q. J. R. Meteorol. Soc. 127, 2395–2416.

Barker, H.W., et al., 1996. A parameterization for computing grid-averaged solar fluxes for inhomogeneous marine boundary layer clouds: II. Validation using satellite data. J. Atmos. Sci. 53, 2304–2316.

Barkey, B., Liou, K.N., Gellerman, W., Sokolsky, P., 1999. An analog light scattering experiment of hexagomal icelike particles: Part II. Experimental and theoretical results. J. Atmos. Sci. 56, 613–625.

Barun, V.V., 1995. Visual perception of retroreflective objects through light scattering media. Proc. SPIE 2410, 470–479.

Barun, V.V., 2000. Influence of cloud aerosol microstructure on the backscattering signal from the object shadow area. Izv. Rus. Acad. Nauk, Atmos. Ocean. Phys. 36, 258–265.

Batey, M., Harshvardhan, Green, R., 2000. Geometrically effective cloud fraction for solar radiation. Atmos. Res. 55, 115–129.

Bissonnete, L.B., et al., 1995. Lidar multiple scattering from clouds. Appl. Phys., B Lasers Opt., B 60, 355–362.

Bohren, C.F., Huffman, D.R., 1983. Absorption and Scattering of Light by Small Particles. Wiley, NY.

Borovoi, A., Grishin, I., Naats, E., Oppel, U., 2000. Backscattering peak of hexagonal ice columns and plates. Opt. Lett. 25, 1388–1392.

Bovensmann, H., Burrows, J.P., Buchwitz, M., Frerick, J., Noel, S., Rozanov, V.V., 1999. SCIAMACHY: mission objectives and measurement modes. J. Atmos. Sci. 56, 127–150.

Brenguier, J.-L., Pawlowska, H., Schüller, L., Preusker, R., Fischer, J., Fouquart, Y., 2000. Radiative properties of boundary layer clouds: droplet effective radius versus number concentration. J. Atmos. Sci. 57, 803–821.

Breon, F.-M., Goloub, P., 1998. Cloud droplet effective radius from spaceborne polarization measurements. Geophys. Res. Lett. 25, 1879–1883.

Cahalan, R.F., Ridgway, W., Wiscombe, W.J., Bell, T.L., 1994. The albedo of fractal stratocumulus clouds. J. Atmos. Sci. 51, 2434–2455.

Cahalan, R.F., Oreopoulos, L., Wen, G., Marshak, A., Tsay, S.-C., DeFelice, T., 2001. Cloud characterization and clear-sky correction from Landsat-7. Remote Sens. Environ. 78, 83–98.

Cairns, B., et al., 1999. The research scanning polarimeter: calibration and ground-based measurements. Proc. SPIE 3754, 186–196.

Chandrasekhar, S., 1950. Radiative Transfer. Oxford Press, Oxford.

Chepfer, H., Brogniez, G., Fouquart, Y., 1998. Cirrus clouds microphysical properties deduced from POLDER observations. J. Quant. Spectrosc. Radiat. Transfer 60, 375–390.

Chepfer, H., Brogniez, G., Goloub, P., Bréon, F.M., Flamant, P.H., 1999. Observations of horizontally oriented ice crystals in cirrus clouds with POLDER-1/ADEOS-1. J. Quant. Spectrosc. Radiat. Transfer 63, 521–543.

Chepfer, H., Goloub, P., Riedi, J., De Haan, J.F., Hovenier, J.W., Flamant, P.H., 2001. Ice crystal shapes in cirrus clouds derived from POLDER/ADEOS-1. J. Geophys. Res., D 106, 7955–7966.

Chylek, P., Lesins, G.B., Videen, G., Wong, J.G.D., Pinnick, R.G., Ngo, D., Klett, J.D., 1996. Black carbon and absorption of solar radiation by clouds. J. Geophys. Res. 1001 (D18), 23365–23371.

Coffeen, D.L., 1979. Polarization and scattering characteristics in the atmospheres of Earth, Venus, and Jupiter. J. Opt. Soc. Am. 69, 1051–1064.

Coulson, K.L., 1988. Polarization and Intensity of Light in Atmosphere. Deepak, Hampton.

Danielson, R.E., Moore, D.R., van de Hulst, H.C., 1969. The transfer of visible radiation through clouds. J. Atmos. Sci. 26, 1078–1087.

Deirmendjian, A., 1969. Electromagnetic Scattering on Spherical Polydispersions. Elsevier, Amsterdam.

Deschamps, P.-Y., Breon, F.-M., Leroy, M., Podaire, A., Bricaud, A., Buriez, J.-C., Seze, G., 1994. The POLDER mission: instrument characteristics and scientific objectives. IEEE Trans. Geosci. Remote Sens. 32, 598–614.

Domke, H., 1978. Linear Fredholm integral equations for radiative transfer problems in finite plane-parallel media: II. Embedding in a semi-infinite medium. Astron. Nachr. 299, 95–102.

Doutriaux-Bucher, M., Buroez, J.-C., Brogniez, G., Labonnote, L.-C., 2000. Sensitivity of retrieved POLDER directional cloud optical thickness to various ice particles models. Geophys. Res. Lett. 27, 113–116.

Drofa, A.S., Usachev, A.L., 1980. On vision in a cloudy medium. Izv. Acad. Nauk SSSR, Fiz. Atmos. Okeana 16, 933–938.

Dvoryashin, S.V., 2002. Remote determination of the ratio between the coefficients of water and ice absorption in clouds in the 2.15–2.35 μm spectral range. Izv. Atmos. Ocean. Phys. 38, 523–528.

Ebert, E.E., Curry, J.A., 1992. A parametrization of ice cloud optical properties for climate studies. J. Geophys. Res. 97, 3831–3836.

Evans, F.K., 1998. The spherical harmonics discrete ordinate method for three-dimensional atmospheric radiative transfer. J. Atmos. Sci. 55, 429–466.

Feigelson, E.M. (Ed.), 1981. Radiation in a Cloudy Atmosphere. Gidrometeoizdat, Leningrad. 280 pp.

Fomin, B.A., Mazin, I.P., 1998. Model for an investigation of radiative transfer in cloudy atmosphere. Atmos. Res. 47–48, 127–153.

Fouilloux, A., Gayet, J.-F., Kriebel, K.-T., 2000. Determination of cloud microphysical properties from AVHRR images: comparisons of three approaches. Atmos. Res. 55, 65–83.

Fu, Q., 1996. An accurate parameterization of the solar radiative

properties of cirrus clouds for climate models. J. Climate 9, 2058–2082.
Fu, Q., Liou, K.N., 1993. Parametrization of the radiative properties of cirrus clouds. J. Atmos. Sci. 50, 2008–2025.
Fu, Q., et al., 2000. Cloud geometry effects on atmospheric solar absorption. J. Atmos. Sci. 57, 1156–1168.
Garett, T.J., 2001. Shortwave, single-scattering properties of arctic ice clouds. J. Geophys. Res. 106 (D14), 15155–15172.
Gayet, J.-F., 1998. In situ measurements of the scattering phase function of stratocumulus, contrails and cirrus. Geophys. Res. Lett. 25, 971–974.
Gehrels, T. (Ed.), 1974. Planets, Stars and Nebulae Studied with Photopolarimetry. University of Arizona Press, Tuscon.
Germogenova, T.A., 1963. Some formulas to solve the transfer equation in the plane layer problem. In: Stepanov, B.I. (Ed.), Spectroscopy of Scattering Media. AN BSSR, Minsk, Minsk, pp. 36–41.
Glautshing, W.J., Chen, S.-H., 1981. Light scattering from water droplets in the geometrical optics approximation. Appl. Opt. 20, 2499–2509.
Goloub, P., Herman, M., Chepfer, H., Riedi, J., Brogniez, G., Couvert, P., Seze, G., 2000. Cloud thermodynamical phase classification from the POLDER spaceborne instrument. J. Geophys. Res. D 105, 14747–14759.
Grandy Jr., W.T. 2000. Scattering of Light from Large Spheres Cambridge Univ. Press, NY.
Greenler, R., 1980. Rainbows, Halos, and Glories. Cambridge Univ. Press, Cambridge.
Grenfell, T.C., Warren, S.G., 1999. Representation of a nonspherical ice particle by a collection of independent spheres for scattering and absorption radiation. J. Geophys. Res. D 104, 31697–31709.
Hale, G.M., Querry, M.R., 1973. Optical contacts of water in the 200-nm to 200-μm wavelength region. Appl. Opt. 12, 555–563.
Han, Q., et al., 1994. Near global survey of effective droplet radii in liquid water clouds using ISCCP data. J. Climate 7, 465–497.
Hansen, J.E., 1971a. Multiple light scattering of polarized light in planetary atmospheres: Part II. Sunlight reflected by terrestrial water clouds. J. Atmos. Sci. 28, 1400–1426.
Hansen, J.E., 1971b. Circular polarization of sunlight reflected by clouds. J. Atmos. Sci. 28, 1515–1516.
Hansen, J.E., Hovenier, J., 1974. Interpretation of the polarization of Venus. J. Atmos. Sci. 31, 1137–1160.
Hansen, J.E., Travis, L.D., 1974. Light scattering in planetary atmospheres. Space Sci. Rev. 16, 527–610.
Harrington, J.Y., Olsson, P.Q., 2001. A method for the parametrization of cloud optical properties in bulk and bin microphysical models. Implications for arctic cloudy boundary layers. Atmos. Res. 57, 51–80.
Hovenier, J.W., 1971. Multiple scattering of polarized light in planetary atmospheres. Astron. Astrophys. 13, 7–29.
Ishimaru, A., 1978. Wave Propagation and Scattering in Random Media. Academic Press, New York.
Jourdan, O., Oshchepkov, S., Gayek, J.F., Scherbakov, V., Tsaka, H., 2003. Statistical analysis of cloud light scattering and microphysical properties obtained from airborne measurements. J. Geophys. Res. 108 (doi:10.1029/2002/D002723).
Katsev, I.L., Zege, E.P., Prikhach, A.S., Polonsky, I.N., 1998. Efficient technique to determine backscattered light power for various atmospheric and oceanic sounding and imaging systems. J. Opt. Soc. Am., A 14, 1338–1346.
Kerker, M., 1969. The Scattering of Light and Other Electromagnetic Radiation. Academic Press, NY.
Khrgian, A.H., Mazin, I.P., 1952. On droplet size distribution in clouds. Pap. Cent. Aerol. Obs., N 7, 56–61 (Moscow).
King, M.D., 1981. A method for determining the single scattering albedo of clouds through observation of the internal scattered radiation field. J. Atmos. Sci. 38, 2031–2044.
King, M.D., 1987. Determination of the scaled optical thickness of clouds from reflected solar radiation measurements. J. Atmos. Sci. 44, 1734–1751.
King, M.D., et al., 1992. Remote sensing of cloud, aerosol, and water vapour properties from the moderate resolution imaging spectrometer (MODIS). IEEE Trans. Geosci. Remote Sens. 30, 2–27.
Knap, W.H., et al., 2002. Cloud thermodynamic-phase determination from near-infrared spectra of reflected light. J. Atmos. Sci. 59, 83–96.
Knibbe, W.J.J., 1997. Analysis of Satellite Polarization Observations of Cloudy Atmospheres. PhD thesis, Free University of Amsterdam, Amsterdam, Netherlands.
Koelemeijer, R.B., Stammes, P., Hovenier, J.W., de Haan, J.F., 2001. A fast method for retrieval of cloud parameters using oxygen A band measurements from the global ozone monitoring experiments. J. Geophys. Res. 106 (D4), 3475–3490.
Kokhanovsky, A.A., 1989. The geometrical optics approximation for the absorption cross section of a layered sphere. Atmos. Opt. 2, 908–912.
Kokhanovsky, A.A., 1997. Expansion of a phase function of large particles on Legandre polynomials. Izv. Rus. Acad. Sci., Atmos. Ocean. Phys. 33, 692–696.
Kokhanovsky, A.A., 2000. Determination of the effective radius of drops in water clouds from polarization measurements. Phys. Chem. Earth, Part B 5–6, 471–474.
Kokhanovsky, A.A., 2001a. Light Scattering Media Optics: Problems and Solutions. Praxis-Springer, Chichester.
Kokhanovsky, A.A., 2001b. Reflection and transmission of polarized light by optically thick weakly absorbing random media. J. Opt. Soc. Am. A 18, 883–887.
Kokhanovsky, A.A., 2002a. A simple approximate formula for the reflection function of a homogeneous semi-infinite turbid medium. JOSA, A 19, 957–960.
Kokhanovsky, A.A., 2002b. Statistical properties of a photon gas in random media. Phys. Rev., E 66 (037601).
Kokhanovsky, A.A., 2002c. Reflection and polarization of light by semi-infinite turbid media: simple approximations. J. Colloid Interface Sci. 251, 429–431.
Kokhanovsky, A.A., 2003a. Optical properties of irregularly shaped particles. J. Phys. D 36, 915–923.
Kokhanovsky, A.A., 2003b. Polarization Optics of Random Media. Springer-Praxis, Berlin.
Kokhanovsky, A.A., 2003c. Reflection of light from nonabsorbing

semi-infinite cloudy media: a simple approximation. J. Quant. Spectrosc. Radiat. Transfer 81, 125–140.

Kokhanovsky, A.A., 2003d. The influence of horizontal inhomogeneity on radioactive characteristics of clouds: an asymptotic case study. IEEE Trans. Geosci. Remote Sens. 41, 61–70.

Kokhanovsky, A.A., Macke, A., 1997. Integral light scattering and absorption characteristics of large nonspherical particles. Appl. Opt. 36, 8785–8790.

Kokhanovsky, A.A., Macke, A., 1999. The dependence of the radiative characteristics of optically thick media on the shape of particles. J. Quant. Spectrosc. Radiat. Transfer 63, 393–407.

Kokhanovsky, A.A., Nakajima, T.Y., 1998. The dependence of phase functions of large transparent particles on their refractive index and shape. J. Phys. D 31, 1329–1335.

Kokhanovsky, A.A., Rozanov, V.V., 2003. The reflection function of optically thick weakly absorbing turbid layers: a simple approximation. J. Quant. Spectrosc. Radiat. Transfer 77, 165–175.

Kokhanovsky, A.A., Weichert, R., 2002. The determination of the droplet effective size and optical depth of cloudy media from polarimetric measurements. Appl. Opt. 41, 3650–3658.

Kokhanovsky, A.A., Zege, E.P., 1995. Local optical parameters of spherical polydispersions: simple approximations. Appl. Opt. 34, 5513–5519.

Kokhanovsky, A.A., Zege, E.P., 1996. The determination of the effective radius of drops and liquid water path of water clouds from satellite measurements. Earth Res. Space 2, 33–44.

Kokhanovsky, A.A., Zege, E.P., 1997a. Optical properties of aerosol particles: a review of approximate analytical solutions. J. Aerosol Sci. 28, 1–21.

Kokhanovsky, A.A., Zege, E.P., 1997b. Physical parametrization of local optical characteristics of cloudy media. Izv. RAN, Fiz. Atmos. Okeana 33, 209–218.

Kokhanovsky, A.A., Babenko, V.A., Barun, V.V., 1998a. On asymptotic values of light fluxes scattered by large spherical particles between two angles. J. Phys. D 31, 1817–1822.

Kokhanovsky, A.A., Nakajima, T., Zege, E.P., 1998b. Physically-based parametrizations of the shortwave radiative characteristics of weakly absorbing optically thick media: application to liquid water clouds. Appl. Opt. 37, 9750–9757.

Kokhanovsky, A.A., et al., 2003. A semi-analytical cloud retrieval algorithm using backscattering radiation in 04.–2.4 μm spectral range. J. Geophys. Res. D 108, 12 (10.1029/2001JD001543).

Kondratyev, K.Ya., Binenko, V.I., 1984. Impact of Cloudiness on Radiation and Climate. Gidrometeoizdat, Leningrad.

Konnen, G.P., 1985. Polarized Light in Nature. Cambridge Univ. Press, Cambridge.

Kuo, L., Labrie, D., Chylek, P., 1993. Refractive indices of water and ice in the 0.65- to 2.5-μm spectral range. Appl. Opt. 32, 3531–3540.

Kuze, A., Chance, K.V., 1994. Analysis of cloud top height and cloud coverage from satellites using the O_2 *A* and *B* bands. J. Geophys. Res. 99, 14481–14491.

Labonnote, L.C., Brogniez, G., Buriez, J.-C., Doutriaux-Boucher, M., Gayet, J.-F., Macke, A., 2001. Polarized light scattering by inhomogeneous hexagonal crystals. J. Geophys. Res., D 106, 12139–12153.

Landolt-Bernstein, L., 1988. Numerical data and functional relationships in science and technology. In: Fischer, G. (Ed.), Group V: Geophysics and Space Research. V.5: Meteorology. Subvolume b. Physical and Chemical Properties of the Air. Springer-Verlag, Berlin. 570 pp.

Liou, K.N., 1992. Radiation and Cloud Processes in the Atmosphere. Oxford Univ. Press, Oxford.

Liou, K.N., 2002. Introduction to Atmospheric Radiation. Academic Press, NY.

Liou, K.N., Hansen, J., 1971. Intensity and polarization for single scattering by polydisperse spheres: a comparison of ray optics and Mie theory. J. Atmos. Sci. 28, 995–1004.

Liou, K.N., Takano, Y., 1994. Light scattering by nonspherical particles: remote sensing and climate implications. Atmos. Res. 31, 271–298.

Liu, L., Mishchenko, M.I., Menon, S., Macke, A., Lacis, A.A., 2002. The effect of black carbon on scattering and absorption of solar radiation by cloud droplets. J. Quant. Spectrosc. Radiat. Transfer 74 (2), 195–204.

Loeb, N.G., Coakley Jr., J.A. 1998. Inference of marine stratus cloud optical depths from satellite measurements: does 1D theory apply? J. Atmos. Sci. 11, 215–233.

Loeb, N.G., Davies, R., 1996. Observational evidence of plane parallel model biases: apparent dependence of cloud optical depth on solar zenith angle. J. Geophys. Res. 101, 1621–1634.

Macke, A., 1993. Scattering of light by polyhedral ice crystals. Appl. Opt. 32, 2780–2788.

Macke, A., 1994. Modellierung der Optischen Eigenschaften von Cirruswolken. PhD thesis, University of Hamburg.

Macke, A., Grossklaus, M., 1998. Light scattering by nonspherical raindrops: implications for lidar remote sensing of rain rates. J. Quant. Spectrosc. Radiat. Transfer 60, 355–363.

Macke, A., Tzschichholz, F., 1992. Scattering of light by fractal particles: a qualitative estimate exemplary for two-dimensional triadic Koch island. Physica A 191, 159–170.

Macke, A., Mueller, J., Raschke, E., 1996. Scattering properties of atmospheric ice crystals. J. Atmos. Sci. 53, 2813–2825.

Macke, A., Francis, P., McFarquhar, G.M., Kinne, S., 1998. The role of ice particle shapes and size distributions in the single scattering properties of Cirrus clouds. J. Atmos. Sci. 55, 2874–2883.

Macke, A., Mitchell, D.L., Bremen, L.V., 1999. Monte Carlo radiative transfer calculations for inhomogeneous mixed phase clouds. Phys. Chem. Earth, Part B 24, 237–241.

Magano, C., Lee, C.V., 1966. Meteorological classification of natural snow crystals. J. Fac. Sci., Hokkaido Univ. 7, 321–362.

Markel, V.A., 2002. The effects of averaging on the enhancement factor for absorption of light by carbon particles in microdroplets of water. J. Quant. Spectrosc. Radiat. Transfer 72, 765–774.

Marsh, N.D., Swensmark, H., 2000. Cosmic rays, clouds and climate. Phys. Rev. Lett. 85, 5004–5007.

Marshak, A., et al., 1995. Radiative smoothing in fractal clouds. J. Geophys. Res., D 100, 26247–26261.

Marshak, A., Davis, A., Wiscombe, W., Cahalan, R., 1998. Radiative effects of sub-mean free path liquid water variability in stratoform clouds. J. Geophys. Res., D 103, 19557–19567.

Mason, B.J., 1975. Clouds, Rain and Rainmaking. Cambridge Univ. Press, Cambridge.

Masuda, K., Ishimoto, H., Takashima, T., 2002. Retrieval of cirrus optical thickness and ice-shape information using total and polarized reflectance from satellite measurements. JQSRT 75, 39–51.

Masunaga, H., Nakajima, T.Y., Nakajima, T., Kachi, M., Suzuki, K., 2002. Physical properties of maritime low clouds as retrieved by combined use of Tropical Rainfall Measuring Mission (TRMM) Microwave Imager and Visible/Infrared Scanner: 2. Climatology of warm clouds and rain. J. Geophys. Res. 107 (10.1029/2001JD001269).

McFarquhar, G.M., Yang, P., Macke, A., Baran, A.J., 2002. A new parameterization of single scattering solar radiative properties for tropical anvils using observed ice crystal size and shape distributions. J. Atmos. Sci. 59, 2458–2478.

McGill, M.J., Hlavka, D., Hart, W., Scott, V.S., Spinhirne, J., Schmid, B., 2002. The cloud physics lidar: instrument description and initial measurement results. Appl. Opt. 41, 3725–3733.

McGraw, R., Nemesure, S., Schwartz, S.E., 1998. Properties and evolution of aerosols with size distributions having identical moments. J. Aerosol Sci. 29, 761–772.

Melnikova, I.N., Mikhailov, V.V., 1994. Spectral scattering and absorption coefficients in strati derived from aircraft measurements. J. Atmos. Sci. 51, 925–931.

Melnikova, I.N., Mikhailov, V.V., 2000. Vertical profile of spectral optical parameters of stratus clouds from airborne radiative measurements. J. Geophys. Res. 105 (D), 23255–23272.

Melnikova, I.N., Dlugach, Zh.K., Nakajima, T., Kawamoto, K., 2000a. Calculation of the reflection function of an optically thick scattering layer for a Heney–Greenstein phase function. Appl. Opt. 39, 4195–4204.

Melnikova, I.N., Domnin, P.I., Mikhailov, V.V., Radionov, V.F., 2000b. Optical characteristics of clouds derived from measurements of reflected or transmitted solar radiation. J. Atmos. Sci. 57, 2135–2143.

Menon, S., Saxena, V.K., Durkee, P., Wenny, B.N., Nielsen, K., 2002. Role of sulfate aerosol in modifying the cloud albedo: a closure experiment. Atmos. Res. 61, 169–187.

Minin, I.N., 1988. Radiative Transfer Theory in Planetary Atmospheres. Nauka, Moscow.

Mishchenko, M.I., Sassen, K., 1998. Depolarization of lidar returns by small ice crystals. Geophys. Res. Lett. 25, 309–312.

Mishchenko, M.I., et al., 1995. Effect of particle nonsphericity on bidirectional reflectance of Cirrus clouds. Proc. of the 1995 ARM Science Meeting, San Diego, CA, March 19–23.

Mishchenko, M.I., Rossow, W.B., Macke, A., Lacis, A.A., 1996. Sensitivity of cirrus cloud albedo, bidirectional reflectance and optical thickness retrieval accuracy to ice particle shape. J. Geophys. Res. D 101, 16973–16985.

Mishchenko, M.I., Dlugach, J.M., Yanovitskij, E.G., Zakharova, N.T., 1999. Bidirectional reflectance of flat, optically thick particulate layers: an efficient radiative transfer solution and applications to snow and soil surfaces. J. Quant. Spectrosc. Radiat. Transfer 63, 409–432.

Mishchenko, M.I., Hovenier, J.W., Travis, L.D. (Eds.), 2000. Light Scattering by Nonspherical Particles: Theory, Measurements, and Applications. Academic Press, New York.

Mishchenko, M.I., Travis, L.D., Lacis, A.A., 2002. Scattering, Absorption, and Emission of Light by Small Particles. Cambridge Univ. Press, Cambridge.

Mitchell, D.L., 2000. Parametrization of the Mie extinction and absorption coefficients for water clouds. J. Atmos. Sci. 57, 1311–1326.

Mitchell, D.L., Arnott, W.P., 1994. A model predicting the evolution of ice particle spectra and radiative properties of cirrus clouds: II. Dependence of absorption and extinction on ice crystal morphology. J. Atmos. Sci. 51, 817–832.

Muinonen, K., Nousiainen, T., Fast, P., Lumme, K., Peltoniemi, J.I., 1996. Light scattering by Gaussian random particles: ray optics approximation. J. Quant. Spectrosc. Radiat. Transfer 55, 577–601.

Nakajima, T., King, M.D., 1990. Determination of the optical thickness and effective particle radius of clouds from reflected solar radiation measurements. Part 1. Theory. J. Atmos. Sci. 47, 1878–1893.

Nakajima, T., King, M.D., 1992. Asymptotic theory for optically thick layers: application to the discrete ordinates method. Appl. Opt. 31, 7669–7683.

Nakajima, T., King, M.D., Spinhirne, J.D., Radke, L.F., 1991. Determination of the optical thickness and effective particle radius of clouds from reflected solar radiation measurements. Part II. Marine stratocumulus observations. J. Atmos. Sci. 48, 728–750.

Nussenzveig, H.M., 1992. Diffraction Effects in Semiclassical Scattering. Cambridge Univ. Press, London.

Okada, K., Heintzenberg, J., Kai, K., Qin, Y., 2001. Shape of atmospheric mineral particles collected in three Chinese arid-regions. Geophys. Res. Lett. 28, 3123–3126.

Palle, E., Butler, C.J., 2002. The proposed connection between clouds and cosmic rays: cloud behaviour during the past 50–120 years. J. Atmos. Sol.-Terr. Phys. 64, 327–337.

Paul, S.K., 2000. Cloud drop spectra at different levels and with respect to cloud thickness and rain. Atmos. Res. 52, 303–314.

Peltoniemi, J.I., 1993. Light scattering in planetary regolits and cloudy atmospheres. PhD thesis, University of Helsinki.

Peltoniemi, J.I., Lumme, K., Muinonen, K., Irvine, W.M., 1989. Scattering of light by stochastically rough particles. Appl. Opt. 28, 4088–4095.

Pinkus, R., Klein, S.A., 2000. Unresolved spatial variability and microphysical process rates in large-scale models. J. Geophys. Res. 105 (D22), 27059–27065.

Pinsky, M.B., Khain, A.P., 2002. Effects of in-cloud nucleation and turbulence on droplet spectrum formation in cumulus clouds. Q. J. R. Meteorol. Soc. 128, 501–534.

Platt, C.M.R., 1978a. Lidar backscattering from horizontally oriented ice crystals. J. Appl. Meteorol. 17, 482–488.

Platt, C.M.R., 1978b. Some microphysical properties of an ice cloud from lidar observations of horizontally oriented crystals. J. Appl. Meteorol. 17, 1220–1224.

Platnick, S., 2000. Vertical photon transport in cloud remote sensing problems. J. Geophys. Res. 105 (D18), 22919–22935.

Platnick, S., 2001. Approximations for horizontal photon transport

in cloud remote sensing problems. J. Quant. Spectrosc. Radiat. Transfer 68, 75–99.
Platnick, S., Li, J.Y., King, M.D., Gerber, H., Hobbs, P.V., 2001. A solar reflectance method for retrieving the optical thickness and droplet size of liquid water clouds over snow and ice surfaces. J. Geophys. Res. 106 (D14), 15185–15199.
Prishivalko, A.P., Babenko, V.A., Kuzmin, V.N., 1984. Scattering and Absorption of Light by Inhomogeneous and Anisotropic Spherical Particles. Nauka i Tekhnika, Minsk.
Pruppacher, H.P., Klett, J.D., 1978. Microphysics of Clouds and Precipitation. D. Reidel Publ., Dordrecht.
Rogovtsov, N.N., 1991. Radiative transfer in scattering media of different configurations. In: Ivanov, A.P. (Ed.), Scattering and Absorption of Light in Natural and Artificial Dispersed Media. Nauka I Tekhnika, Minsk, pp. 58–81.
Rogovtsov, N.N., 1999. Properties and Principles of Invariance Belarussian Polytechnical Academy, Minsk.
Rolland, P., Liou, K.N., King, M.D., Tsay, S.C., McFarquhar, G.M., 2000. Remote sensing of optical and microphysical properties of cirrus clouds using moderate-resolution imaging spectroradiometer channels: methodology and sensitivity to physical assumptions. J. Geophys. Res., D 105, 11721–11738.
Rossow, W.B., 1989. Measuring cloud properties from space: a review. J. Climate 2, 419–458.
Rossow, W.B., Schiffer, R.A., 1999. Advances in understanding clouds from ISCCP. Bull. Am. Meteorol. Soc. 80, 2261–2287.
Rossow, W.B., Garder, L.C., Lacis, A.A., 1989. Global, seasonal cloud variations from satellite radiance measurements: Part I. Sensitivity of analysis. J. Climate 2, 419–458.
Rozenberg, G.V., 1962. Optical characteristics of thick weakly absorbing scattering layers. Dokl. AN SSSR 145, 775–777.
Rozenberg, G.V., 1967. Physical foundations of light scattering media spectroscopy. Sov. Phys., Usp. 91, 569–608.
Rozenberg, G.V., Malkevitch, M.S., Malkova, V.S., Syachinov, V.I., 1978. The determination of optical characteristics of clouds from measurements of the reflected solar radiation using data from the Sputnik "KOSMOS-320". Izv. Acad. Sci. USSR, Fiz. Atmos. Okeana 10, 14–24.
Sassen, K., 1991. The polarization lidar technique for cloud research. Bull. Am. Meteorol. Soc. 78, 1885–1903.
Sassen, K., 2001. Cloud and aerosol research capabilities at FARS. Bull. Am. Meteorol. Soc., 82, 1119–1138, 1885–1903.
Saunders, C., Rimmer, J., Jonas, P., Arathoon, J., Liu, C., 1998. Preliminary laboratory studies of the optical scattering properties of the crystal clouds. Ann. Geophys. 16, 618–627.
Schreier, R., 2001. Solarer Stralungstransport in der inhomogenen Atmosphare. PhD thesis, Institute fur Meereskunde, Kiel.
Schreier, R., Macke, A., 2001. On the accuracy of the independent column approximation in calculating the downward fluxes in the UVA, UVB, and PAR spectral regions. J. Geophys. Res. 106 (D13), 14301–14312.
Schuller, L., Armbruster, W., Fischer, J., 2000. Retrieval of cloud optical and microphysical properties from multispectral radiances. Atmos. Res. 55, 35–45.
Shifrin, K.S., 1951. Scattering of Light in a Turbid Media Gostekhteorizdat, Moscow English translation: NASA Tech. Trans. TT F-447, 1968, NASA, Washinghton, DC.
Shifrin, K.S., Tonna, G., 1993. Inverse problems related to light scattering in the atmosphere and ocean. Adv. Geophys. 34, 175–252.
Shurcliff, W.A., 1962. Polarized Light. Harvard Univ. Press, Cambridge.
Sobolev, V.V., 1972. Light Scattering in Planetary Atmospheres. Nauka, Moscow.
Spinhirne, J.D., Nakajima, T., 1994. Glory of clouds in the near infrared. Appl. Opt. 33, 4652–4662.
Stephens, G.L., Tsay, S.-C., 1990. On the cloud absorption anomaly. Q. J. R. Meteorol. Soc. 116, 671–704.
Swensmark, H., 1998. Influence of cosmic rays on Earth's climate. Phys. Rev. Lett. 81, 5027–5030.
Swensmark, H., Friis-Christensen, E., 1997. Variations of cosmic ray flux and global cloud coverage. A missing link in solar-climate relationships. J. Atmos. Sol.-Terr. Phys. 59, 1225–1232.
Takano, Y., Liou, K.-N., 1989. Solar radiative transfer in cirrus clouds: 1. Single scattering and optical properties of hexagonal ice crystals. J. Atmos. Sci. 46, 3–19.
Takano, Y., Liou, K.-N., 1995. Solar radiative transfer in cirrus clouds: 1. Light scattering by irregular ice crystals. J. Atmos. Sci. 452, 818–837.
Thomas, G., Stamnes, K., 1999. Radiative Transfer in Atmosphere and Ocean. Cambridge Univ. Press, Cambridge.
Titov, G.A., 1998. Radiative horizontal transport and absorption in stratocumulus clouds. J. Atmos. Sci. 55, 2549–2560.
Tricker, R.A.R., 1970. Introduction to Meteorological Optics. Elsevier, London.
Trishchenko, A.P., Li, Z., Chang, F.-L., Barker, H., 2001. Cloud optical depth and TOA fluxes: comparison between satellite and surface retrievals from multiple platforms. Geophys. Res. Lett. 28, 979–982.
Twomey, S., 1977. Atmospheric Aerosols. Elsevier, London.
Tynes, H.H., Kattawar, G.W., Zege, E.P., Katsev, I.L., Prikhach, A.S., Chaikovskaya, L.I., 2001. Mueller matrix for multiple light scattering in turbid media: comparison of two independent methods. Appl. Opt. 40, 400–412.
Uchiyama, A., Asano, S., Shiobara, M., Fukabori, M., 1999. Ground-based Cirrus observations: I. Observation system and results of frontal Cirrostratus Clouds on June 22 and 30, 1989. J. Meteorol. Soc. Jpn. 77, 522–551.
Van de Hulst, H.C., 1957. Light Scattering by Small Particles. Wiley, NY.
Van de Hulst, H.C., 1980. Multiple Light Scattering: Tables, Formulas and Applications. Academic Press, New York.
Vasilyev, A.V., Melnikova, I.N., 2002. Short-Wave Solar Radiation in the Earth Atmosphere, Calculation. Observation. Interpretation. St. Petersburg State University, St. Petersburg.
Volkovitsky, O.A., Pavlova, L.N., Petrushin, A.G., 1984. Optical Properties of the Ice Clouds. Gidrometeoizdat, Leningrad.
Volnistova, L.P., Drofa, A.S., 1986. Quality of image transfer through light scattering media. Opt. Spectrosc. 61, 116–121.
Volten, H., Muñoz, O., Rol, E., de Haan, J.F., Vassen, W., Hovenier, J.W., Muinonen, K., Nousiainen, T., 2001. Scattering matrices of mineral aerosol particles at 441.6 and 632.8 nm. J. Geophys. Res. 106 (D15), 17375–17401.
Wang, M., King, M.D., 1997. Correction of Rayleigh scattering

effects in cloud optical thickness retrievals. J. Geophys. Res. 102 (D22), 25915–25926.
Warner, J., 1973. The microstructure of cumulus clouds: Part IV. The effect on the droplet spectrum of mixing between cloud and environment. J. Atmos. Sci. 30, 256–261.
Warren, S.G., 1984. Optical constants of ice from the ultraviolet to the microwave. Appl. Opt. 23, 1206–1225.
Wauben, W.M.F., 1992. Multiple Scattering of Polarized Radiation in Planetary Atmospheres. PhD thesis, Free University of Amsterdam.
Wells, W.H., 1961. Loss of resolution in water as a result of multiple small-angle scattering. J. Opt. Soc. Am. 59, 686–691.
Winker, D.M., 1999. Global observations of aerosols and clouds from combined lidar and passive instruments to improve radiation budget and climate studies. Proc. AMS 10th Conference on Atmospheric Radiation, 290–293.
Winker, D.M., Trepte, C.R., 1998. Laminar cirrus observed near the tropical tropopause by LITE. Geophys. Res. Lett. 25, 3351–3354.
Yamomoto, G., Wark, D.Q., 1961. Discussion of the letter by R.A. Hanel, 'Determination of cloud altitude from a satellite'. J. Geophys. Res. 66, 3596.
Yang, P., Liou, K.N., 1998. Single-scattering properties of complex ice crystals in terrestrial atmosphere. Contrib. Atmos. Phys. 71, 223–248.
Yang, P., Liou, K.N., Wyser, K., Mitchell, D., 2000. Parameterization of the scattering and absorption parameters of individual ice crystals. J. Geophys. Res. 105, 4699–4718.
Yang, P., et al., 2001. Sensitivity of cirrus bidirectional reflectance to vertical inhomogenity of ice crystal habits and size distributions for two moderate-resolution imaging spectroradiometer (MODIS) bands. J. Geophys. Res. 106 (D15), 17267–17291.
Yanovitskij, E.G., 1997. Light Scattering in Inhomogeneous Atmospheres. Springer-Verlag, NY.
Yum, S.S., Hudson, J.G., 2001. Microphysical relationships in warm clouds. Atmos. Res. 57, 81–104.
Zege, E.P., Kokhanovsky, A.A., 1992. On sizing of big particles under multiple light scattering in a medium. Opt. Spectrosc. 72, 220–226.
Zege, E.P., Kokhanovsky, A.A., 1994. Analytical solution for optical transfer function of a light scattering medium with large particles. Appl. Opt. 33, 6547–6554.
Zege, E.P., Kokhanovsky, A.A., 1995. Influence of parameters of coarse aerosols on properties of light fields and optical transfer functions: analytical solutions. Izv. Acad. Nauk, Atmos. Ocean. Phys. 30, 777–783.
Zege, E.P., Ivanov, A.P., Katsev, I.L., 1991. Image Transfer Through a Scattering Medium. Springer-Verlag, New York.
Zege, E.P., Katsev, I.L., Polonsky, I.N., 1993. Multicomponent approach to light propagation in clouds and mists. Appl. Opt. 32, 2803–2812.
Zege, E.P., Katsev, I.L., Polonsky, I.N., 1995. Analytical solution to lidar return signals from clouds with regard to multiple scattering. J. Appl. Phys. B 60, 345–353.
Zege, E.P., Katsev, I.L., Polonsky, I.N., 1998a. Effects of multiple scattering in laser sounding of a stratified scattering medium: 1. General theory. Izv. Atmos. Ocean. Phys. 34, 36–40.
Zege, E.P., Katsev, I.L., Polonsky, I.N., 1998b. Effects of multiple scattering in laser sounding of a stratified scattering medium: 2. Peculiarities of sounding of the atmosphere from space. Izv. Atmos. Ocean. Phys. 34, 227–234.
Zege, E.P., Kokhanovsky, A., Katsev, I.L., Polonsky, I.N., Prikhach, A.S., 1998. The retrieval of the effective radius of snow grains and control of snow pollution with GLI data. In: Mishchenko, M.I., Travis, L.D., Hovenier, J.W. (Eds.), Conference on Light Scattering by Nonspherical Particles: Theory, Measurements, and Applications, Amer. Meteor. Soc., Boston, MA, pp. 288–290.
Zhang, J., Xu, L., 1995. Light scattering by absorbing hexagonal ice crystals in cirrus clouds. Appl. Opt. 34, 5867–5874.
Zuev, V.E., Belov, V.V., Veretennikov, V.V., 1997. Linear Systems Theory in Optics of Disperse Media. Sibirian Brunch of the Russian Academy of Sciences Publishing, Tomsk.